Brixen 12-15 February 2018

Elastic properties of minerals: theory and practice

Paola Comodi
DIPARTIMENTO DI FISICA E GEOLOGIA
UNIIVERSITA' DI PERUGIA

SUMMARY

- ELASTIC PROPERTIES DEFINITIONS
- BULK MODULUS
- EQUATION OF STATE
- PHASE TRANSITION
- METHODS
- SOFTWARES DATA TREATMENTS
- EXAMPLES FROM EARTH SCIENCES
- ESAMPLES FROM MATERIAL SCIENCES

Knowledge on the elastic constants enables us to realize the elastic and mechanical properties of the crystals.

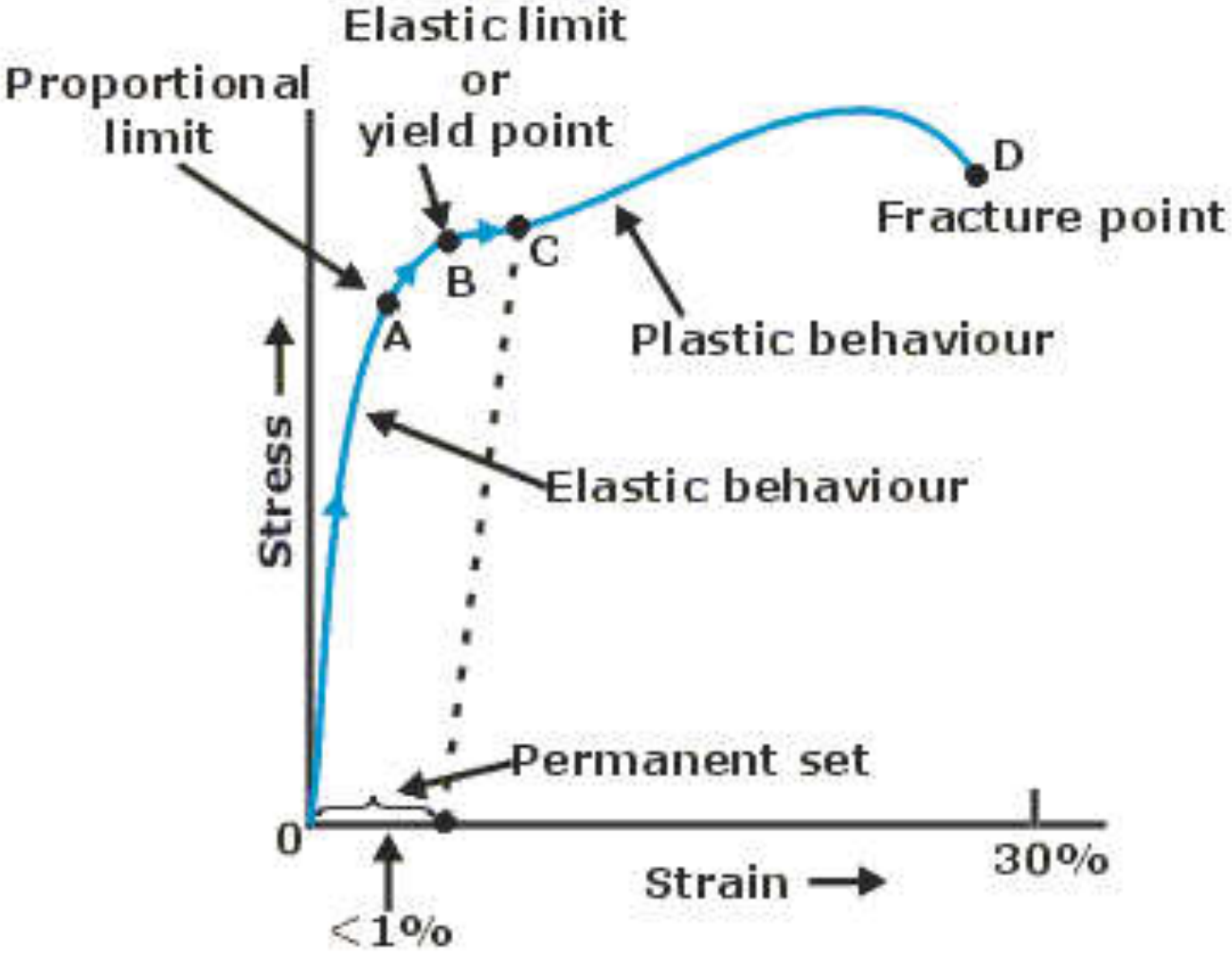

A typical stress-strain curve for a ductile metal

From https://www.tutorvista.com/content/physics/physics-iii/solids-and-fluids/elasticity-modulus.php#young's-modulus-of-elasticity

EoS: basic definitions

An equation of state can be expressed as a P-V relationship

EQUATION OF STATE = RELATIONSHIP BETWEEN THE VOLUME OF A BODY AND THE PRESSURE TO WHICH IT IS SUBJECTED.

Characterised by Volume V and pressure P

- Bulk modulus $$K = -V\,\partial P/\partial V$$
- Bulk modulus derivative (curvature) $$K' = \partial K/\partial P$$
- Bulk modulus derivatives $$K'' = \partial^2 K/\partial P^2$$

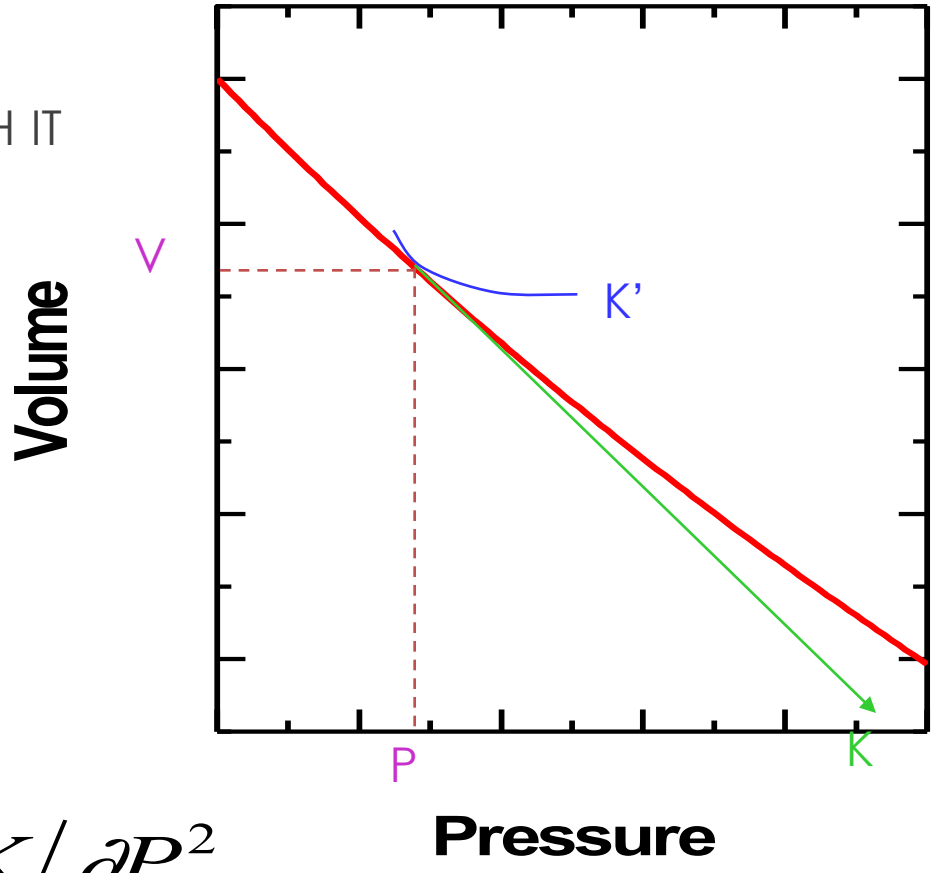

From Angel, R.J. (2000) Equations of state. In: R.M. Hazen and R.T. Downs (Eds.) *High-temperature and high-pressure crystal chemistry*, Reviews in Mineralogy and Geochemistry, 41, 35-60.

BULK MODULUS AND EOS

- EOS MURNAGHAN = 1944 = the more a solid is compressed, the more difficult it is to compress further.

- VALID IF V/V0 < 90%
- P(V) = K0/K'0[(V/V0)EXP-K0' -1]
- K AND K' = BULK MODULUS AND ITS PRESSURE DERIVATIVE
- HOW TO DETERMINE K AND K'

Equations of state: Murnaghan

- can be derived by assuming K is linear with P

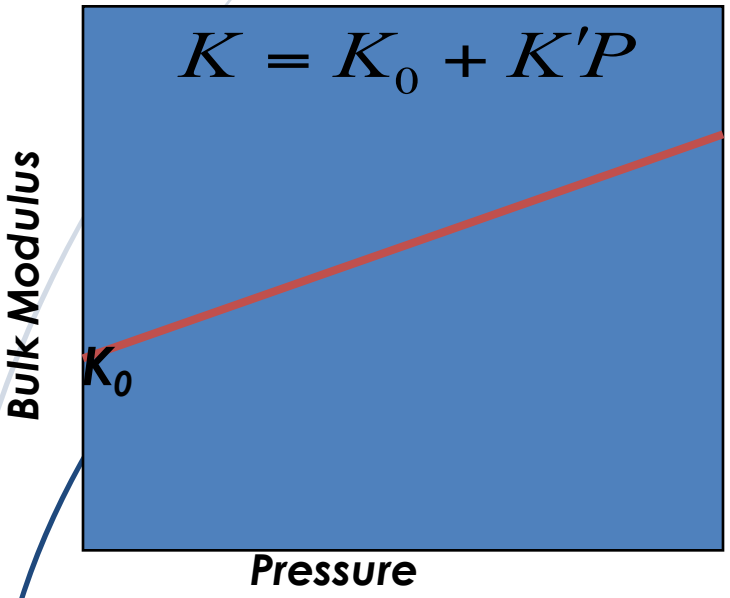

$$-V\frac{\partial P}{\partial V} = K_0 + K'P$$

$$V = V_0\left(1 + \frac{K'P}{K_0}\right)^{-1/K'}$$

$$P = \frac{K_0}{K'}\left[\left(\frac{V_0}{V}\right)^{K'} - 1\right]$$

- Advantages
  - Can be inverted, easily integrated
  - …great for thermo databases
- Disadvantages
  - Does not fit P-V data for $V/V_0 < 0.9$
  - It is OK for volume reduction < 10%

From Angel, R.J. (2000) Equations of state. In: R.M. Hazen and R.T. Downs (Eds.) *High-temperature and high-pressure crystal chemistry*, Reviews in Mineralogy and Geochemistry, 41, 35-60.

Birch-Murnaghan EoS

- Finite strain EoS
  - Assumes strain energy is a polynomial in *f* = *Eulerian strain*

$$f_E = \frac{\left[\left(\frac{V_0}{V}\right)^{2/3} - 1\right]}{2}$$

$$P = 3K_0 f_E (1 + 2f_E)^{5/2}\left(1 + \frac{3}{2}(K' - 4)f_E + \frac{3}{2}\left(K_0 K'' + (K' - 4)(K' - 3) + \frac{35}{9}\right)f_E^2\right)$$

If it is trunked at second term f_e = 0 and K' = 4

If it is trunked at third term f^2_e = 0 and K" = -1/K_0 (3-K')(4-K')+35/9

From Angel, R.J. (2000) Equations of state. In: R.M. Hazen and R.T. Downs (Eds.) *High-temperature and high-pressure crystal chemistry*, Reviews in Mineralogy and Geochemistry, 41, 35-60.

Birch-Murnaghan EoS

$$P = 3K_0 f_E (1+2f_E)^{5/2}\left(1+\frac{3}{2}(K'-4)f_E+\frac{3}{2}\left(K_0K''+(K'-4)(K'-3)+\frac{35}{9}\right)f_E^2\right)$$

$$v_p = a(M_{\mathrm{avg}}) + b\rho,$$

Birch's Law

Truncation:

- 2nd order (in energy)
  - Coefficient of f_E must be zero
  - V_0 and K_0 refined
  - K' = 4
- 3rd order (in energy)
  - Coefficient of f^2_E must be zero
  - V_0 K_0 K' refined
- 4th order (in energy)
  - Coefficient of f^2_E non-zero
  - V_0 K_0 K' K'' refined

$$K'' = \frac{-1}{K_0}\left[(3-K')(4-K')+\frac{35}{9}\right]$$

From Angel, R.J. (2000) Equations of state. In: R.M. Hazen and R.T. Downs (Eds.) *High-temperature and high-pressure crystal chemistry*, Reviews in Mineralogy and Geochemistry, 41, 35-60.

- How we can decide the order of BM EoS?
- F- f plot

f-F plots

- Rearrange BM4 Eos:

$$P = 3K_0 f_E (1+2f_E)^{5/2}\left(1+\frac{3}{2}(K'-4)f_E+\frac{3}{2}\left(K_0K''+(K'-4)(K'-3)+\frac{35}{9}\right)f_E^2\right)$$

Becomes a simple polynomial

$$F_E = K_0 + \left(\frac{3K_0}{2}\right)(K_0'-4)f_E + \left(\frac{3K_0}{2}\right)\left[K_0K''+(K'-4)(K'-3)+\left(\frac{35}{9}\right)\right]f_E^2+\ldots$$

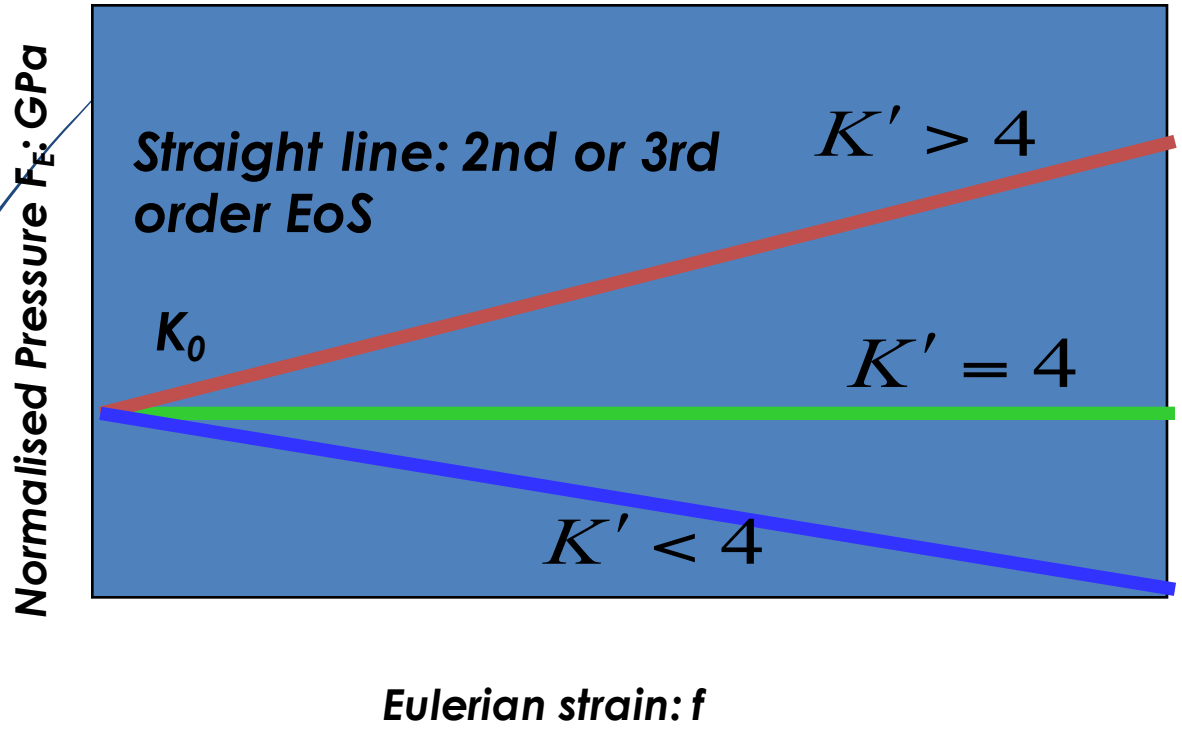

$$f_E = \frac{\left[\left(\frac{V_0}{V}\right)^{2/3}-1\right]}{2}$$

$$F_E = \frac{P}{3f(1+2f_E)^{5/2}}$$

From Angel, R.J. (2000) Equations of state. In: R.M. Hazen and R.T. Downs (Eds.) *High-temperature and high-pressure crystal chemistry*, Reviews in Mineralogy and Geochemistry, 41, 35-60.

- Vinet or Universal EoS
  - Derived from general inter-atomic potential

$$f_V = \left(\frac{V}{V_0}\right)^{1/3}$$ Vinet strain

$$P = 3K_0\left(\frac{1-f_V}{f_V^2}\right)\exp\left[\frac{3}{2}(K'-1)(1-f_V)\right]$$

- It is valid also with very high pressure and V/Vo < 0.6
- with K' = 1 and $K'' = \frac{-1}{K_0}\left[\left(\frac{K'}{2}\right)^2 + \left(\frac{K'}{2}\right) - \frac{19}{36}\right]$

.

From Angel, R.J. (2000) Equations of state. In: R.M. Hazen and R.T. Downs (Eds.) *High-temperature and high-pressure crystal chemistry*, Reviews in Mineralogy and Geochemistry, 41, 35-60.

Thermal Equation of State

The simplest isobaric EOS for a solid is just the definition for the thermal expansion coefficient, a.

$$\alpha = \frac{1}{V}\frac{\Delta V}{\Delta T} = \frac{\Delta \ln V}{\Delta T}$$

A thermal EoS describes a material's reaction to temperature changes.
When a material is heated, the thermal pressure in the system changes and results in thermal expansion.

High-temperature Birch-Murnaghan EoS

Thermal expansion coefficient and bulk modulus are assumed to vary linearly with temperature,

,

where T_0 is the reference temperature (298 K).

$$K(T)=K_0(T_0)+\left(\frac{\Delta K}{\Delta T}\right)_P (T-T_0)$$

Phase transitions @ HP

Polyhedral tilting
polyhedron regularization
Increase of coordination numbers
High spin – low spin transition
H-bond evolution

Structural deformation @ HP

Rule of thumb of HP crystalchemistry

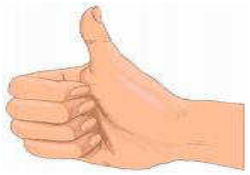

Usually the largest deformation interest

Si-O-Si angle
Then
O-Si-O angle
Then Si-O

Polyhedral tilting

Mineralogical Magazine, 2014, Vol. 78(2), pp. 267–291

OPEN ACCESS

Zeolites at high pressure: A review

G. D. Gatta[1,*] and Y. Lee[2]

[1] Dipartimento di Scienze della Terra, Università degli Studi di Milano, Via Botticelli 23, I-20133 Milano, Italy
[2] Department of Earth System Sciences, Yonsei University, Seoul 120749, Korea

[*Received 17 May 2013; Accepted 8 September 2013; Associate Editor: F. C. Hawthorne*]

ABSTRACT

This is a review of the elastic behaviour and pressure (*P*)-induced structural evolution of zeolites and presents a comparative analysis of the deformation mechanisms of the Si/Al-framework and the rearrangement of the extra-framework species in response to applied pressure. The interaction between *P*-transmitting fluids and zeolites, which can lead to phenomena such as '*P*-induced over-hydration', is described. The comparative elastic analysis and the high-*P* structural data of zeolites reported so far allow us to make some generalizations: (1) The range of compressibility among this class of open-framework silicates is large, with bulk moduli ranging between 15 and 70 GPa; (2) Microporosity does not necessarily imply high compressibility, as several zeolites are less compressible than other non-zeolitic rock-forming minerals; (3) Compressibilities of zeolites do not seem to be directly related to microporosity, at least if we model microporosity with the 'framework density'; (4) The flexibility observed in zeolites under hydrostatic compression is mainly governed by tilting of rigid tetrahedra around O atoms that behave as hinges within the framework. Pressure-induced tilting commonly leads to continuous rearrangement of the framework without any phase transition. More rarely, tilting induces displacive phase transitions and isothermal *P*-induced reconstructive phase transitions (i.e. with change in framework topology), have not been reported in this class of materials; (5) Deformation mechanisms in response to applied pressure are generally dictated by the topological configuration of the framework rather than the Si/Al-distribution or the extra-framework content. The channel content governs the compressibility of the cavities, leading to different unit-cell-volume compressibilities in isotypic structures.

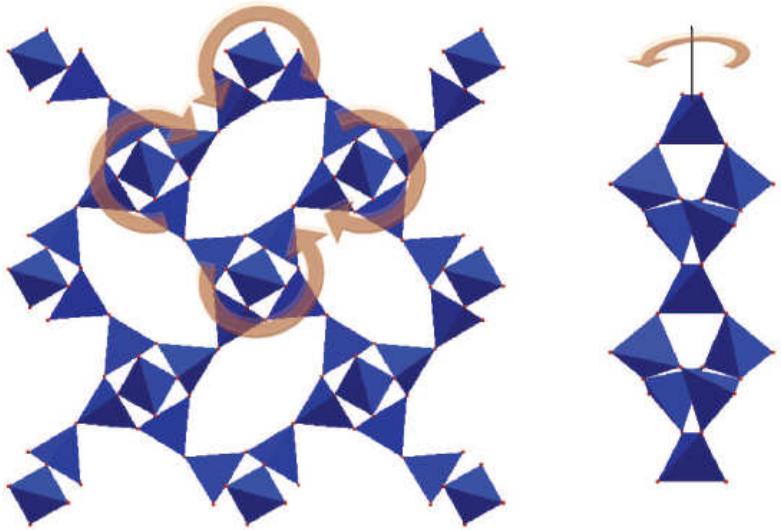

Fig. 1. EDI framework type: SBU chains extend along [001] and undergo cooperative anti-rotation in response to applied pressure. The deformation mechanism leads to compression of the channels of eight-membered rings parallel to [001].

Pressure induce change in coordination number

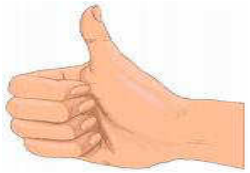

With pressure the reduction of anionic radius (oxygen for example) is larger than that of cation (silicon)

As a consequence the ratio :cation radius/anion radius increas And so increase the coordination number

The increase of coordination number produce an increase in packing efficiency

High pressure crystal-chemical paradox

	SiO_4(quartz)	SiO_6(stishovite)
Ionic character	low	high
Si-O	**1.62**	**1.78**
O-O	**2.63**	**2.51**

Increase of packing efficiency

Both anions and cations increase the coordination number with pressure

XYO_3

- $^{6}Mg^{4}Si^{3}O_{2}{}^{4}O$ Enstatite

  $^{8}Mg_{3}{}^{6}(MgSi)^{4}Si_{3}{}^{4}O_{12}$ Majorite
- $^{6}Mg^{6}Si^{4}O_{3}$ Ilmenite
- $^{8}Mg^{6}Si^{4}O^{5}O_{2}$ Si-Perovskite

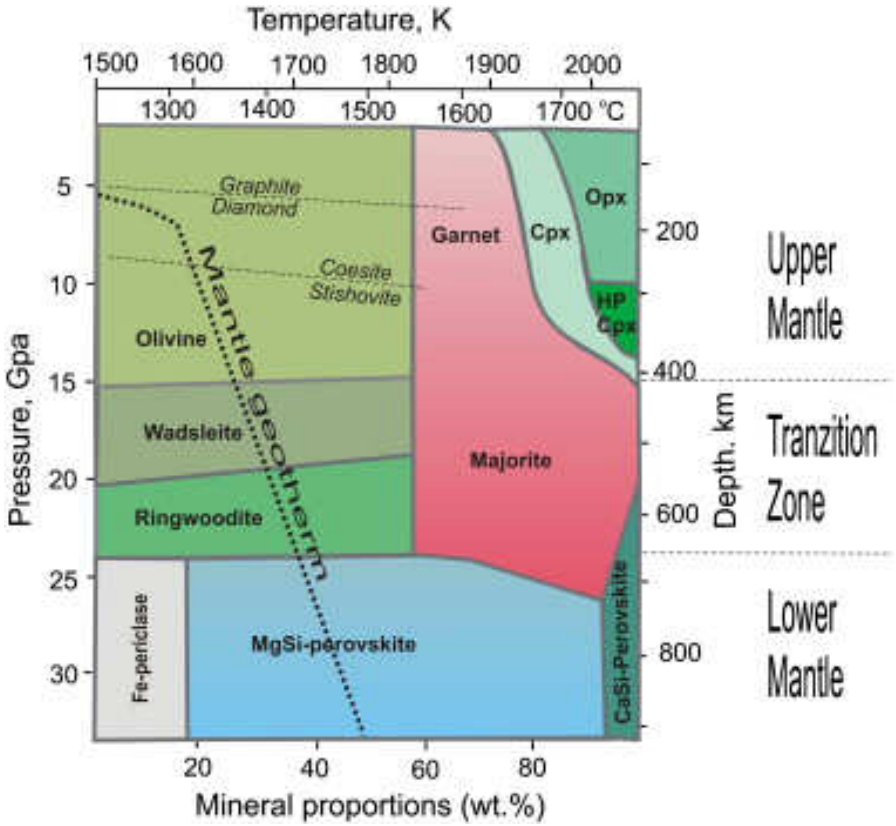

From https://doi.org/10.1016/j.earscirev.2011.10.005

MINERALOGY

Discovery of bridgmanite, the most abundant mineral in Earth, in a shocked meteorite

Oliver Tschauner,[1*] Chi Ma,[2] John R. Beckett,[2] Clemens Prescher,[3] Vitali B. Prakapenka,[3] George R. Rossman[2]

Meteorites exposed to high pressures and temperatures during impact-induced shock often contain minerals whose occurrence and stability normally confine them to the deeper portions of Earth's mantle. One exception has been $MgSiO_3$ in the perovskite structure, which is the most abundant solid phase in Earth. Here we report the discovery of this important phase as a mineral in the Tenham L6 chondrite and approved by the International Mineralogical Association (specimen IMA 2014-017). $MgSiO_3$-perovskite is now called bridgmanite. The associated phase assemblage constrains peak shock conditions to ~ 24 gigapascals and 2300 kelvin. The discovery concludes a half century of efforts to find, identify, and characterize a natural specimen of this important mineral.

In the geosciences, the complexity of compositions and histories of naturally occurring minerals and rocks provides an important ground truth against which experiment and theory are measured. One of the most glaring omissions in the study of Earth's mantle has been the inability to find naturally occurring specimens of what we believe to be Earth's most abundant rock-forming phase, $(Mg,Fe)SiO_3$ in an orthorhombic ABO_3 perovskite structure. Despite appearing for decades in numerous experimental and theoretical studies (*1–5*), characterizations of possible natural samples have not been sufficient to meet International Mineralogical Association criteria for naming a new mineral (*6*). Consequently, any detailed chemical, structural, and petrographic analysis of natural $(Mg,Fe)SiO_3$-perovskite has remained impossible. In addition, having a formal mineral name for a phase that is so important is important in itself. Various ambiguous or incorrect terms such as "silicate perovskite" and "perovskite" have been used for describing this phase, but they convey ambiguity to the description of research findings. We put this ambiguity to rest by describing the natural occurrence of bridgmanite: $MgSiO_3$ in the orthorhombic ABO_3 perovskite structure. The name bridgmanite honors Percy W. Bridgman (1882–1961), the 1946 Nobel laureate in Physics, for his fundamental contributions to high-pressure mineralogy in particular, and to high-pressure research in general.

The importance of bridgmanite in the lower mantle of Earth has long been recognized: Several lines of evidence show that it forms through a

[1]Department of Geoscience and High Pressure Science and Engineering Center, University of Nevada, Las Vegas, NV 89134, USA. [2]Division of Geology and Planetary Science, California Institute of Technology, Pasadena, CA 91125, USA. [3]Center of Advanced Radiation Sources, University of Chicago, Chicago, IL 60632, USA.
*Corresponding author. E-mail: olivert@physics.unlv.edu

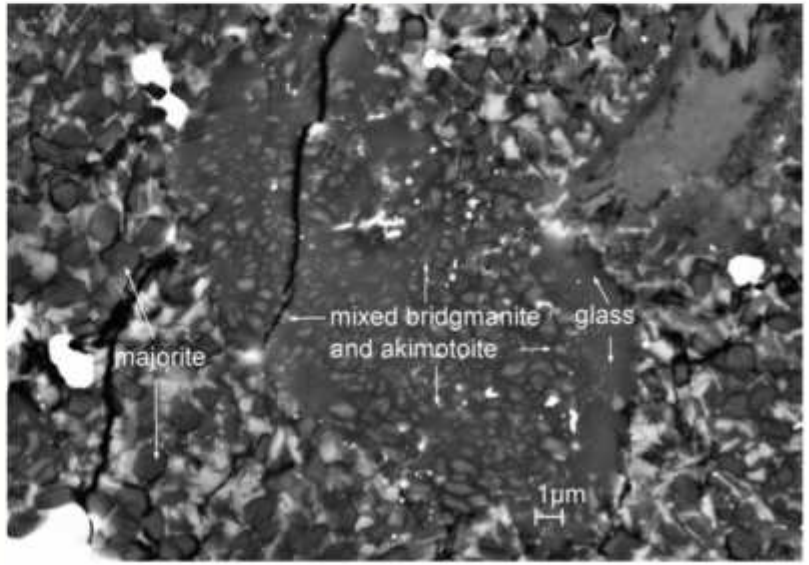

Fig. 1. Scanning electron microscope image of a bridgmanite-akimotoite aggregate. The backscatter electron image reveals an aggregate of submicrometer-sized crystals of bridgmanite and akimotoite enclosed in $(Mg,Fe)SiO_3$ glass and within a Tenham shock-melt vein. Majorite is found in the vein matrix. The bridgmanite-akimotoite clast is a pseudomorph after pyroxene that was trapped in the melt. This observation is consistent with an earlier report about the possible occurrence of bridgmanite with akimotoite in Tenham (*16*).

Brigman (1882-1961) Nobel 1946

high pressure study 100000 kg/cm^2

Tenham L6 chondrite and approved by the International Mineralogical Association (specimen IMA 2014-017). $MgSiO_3$-perovskite is now called bridgmanite. The associated phase assemblage constrains peak shock conditions to ~ 24 GPa and 2300 K.

The discovery concludes a half century of efforts to find, identify, and characterize a natural specimen of this important mineral.

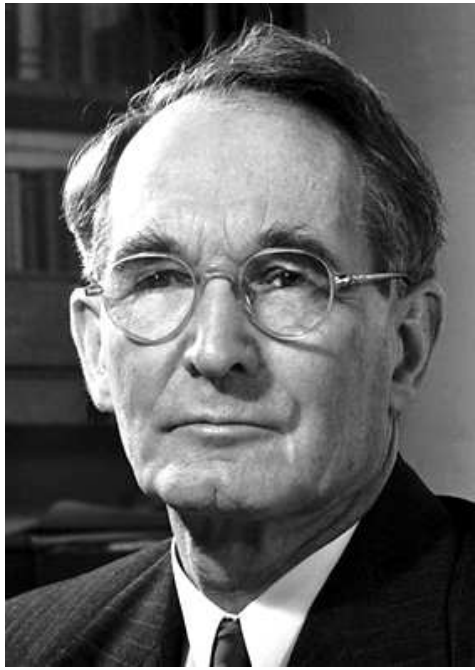

Si-Perowskite- post-Si-perowskite

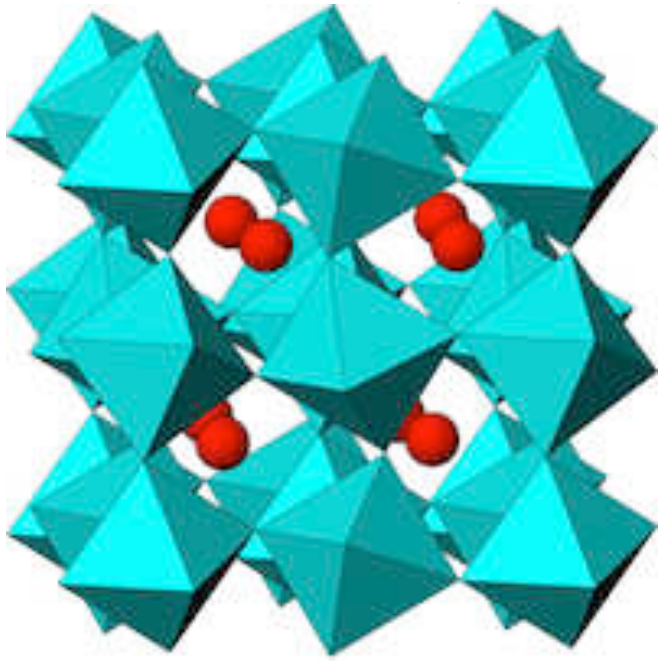

Crystal structure of mantle silicate perovskite. The red spheres are Mg atoms in the dodecahedral sites and the light blue octahedra are SiO6 units

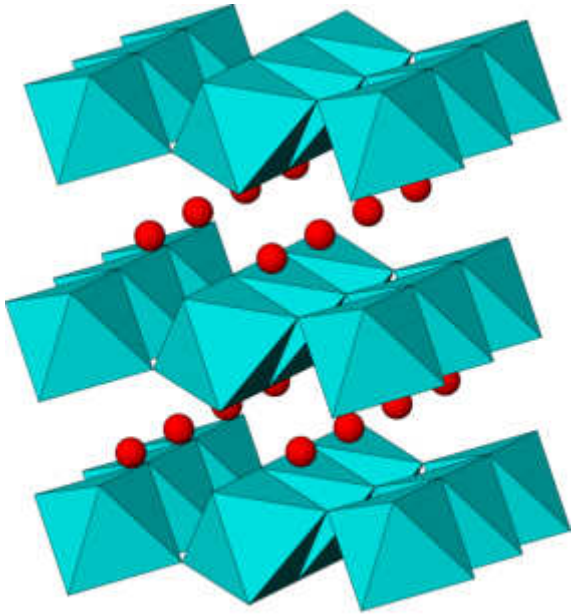

Crystal structure of mantle silicate post-perovskite. The red spheres are Mg atoms in the dodecahedral sites and the light blue octahedra are SiO6 units

From http://www.public.asu.edu/~sshim5/images/mantle_minerals.html

From Post-Perovskite Phase Transition in $MgSiO_3$

Motohiko Murakami1,*, Kei Hirose1,*, Katsuyuki Kawamura1, NagayoshiSata2, Yasuo Ohishi3

Science 07 May 2004:
Vol. 304, Issue 5672, pp. 855-858
DOI: 10.1126/science.1095932

Drastic change in X-ray diffraction pattern around 125 GPa and 2500 K

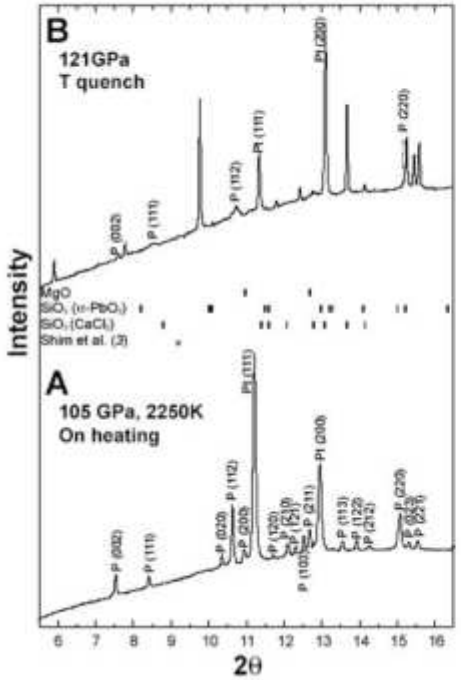

UNKNOWN PHASE

***Pbnm* Perovskite**

(M. Murakami and K. Hirose, private communication)

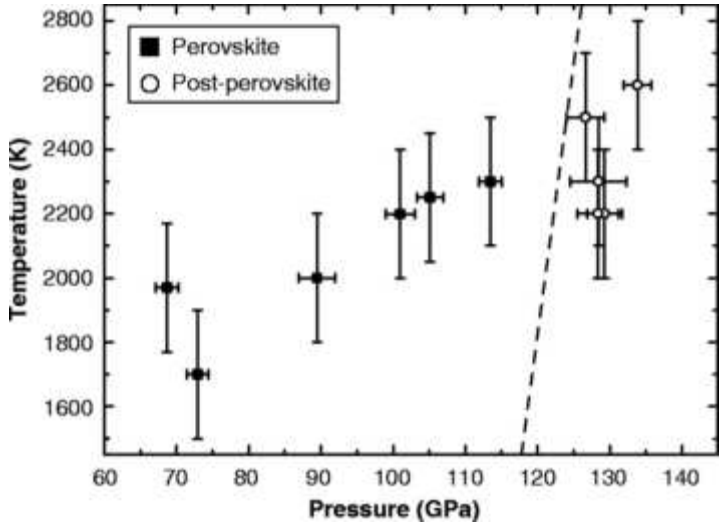

(from http://www.edu.pe.ca/southernkings/compositionch.htm)

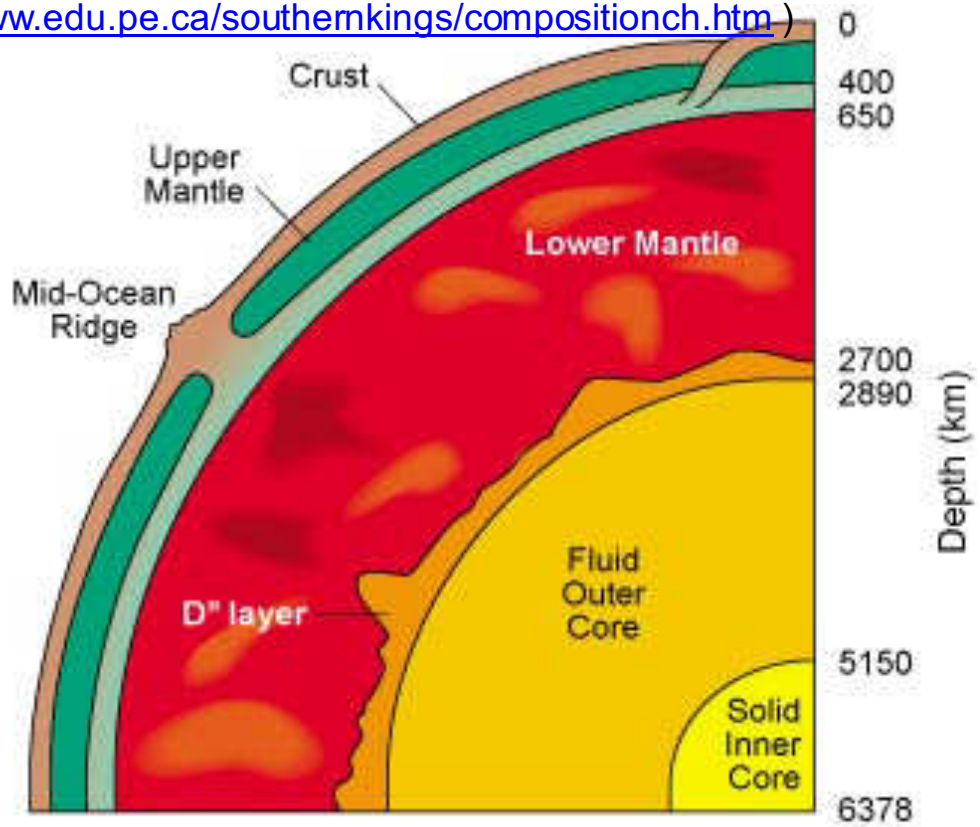

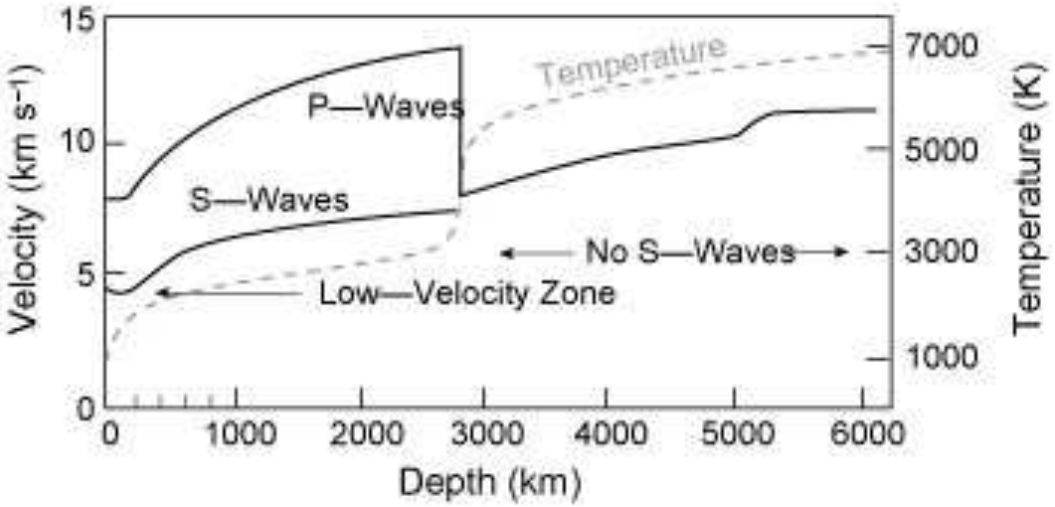

Perowskite to post-perowskite phase transition associated to D'' layer

From http://www.iitaka.org/Post-perovskite.html

High spin - low spin transition @ HP

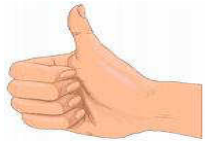

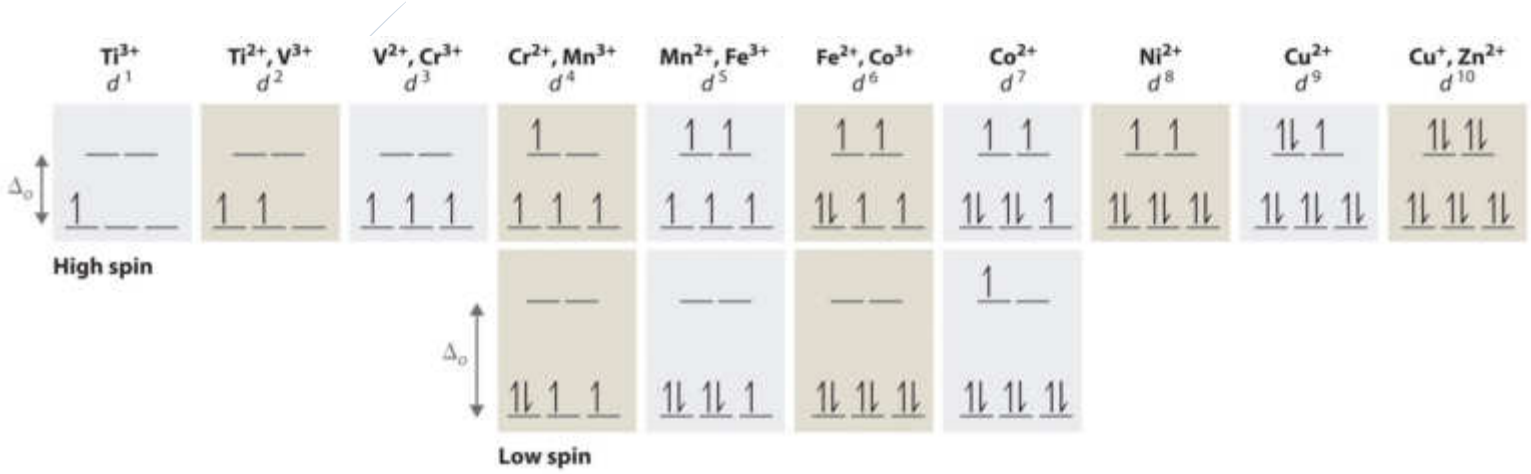

Nei metalli di transizione il passaggio high spin – low spin riduce di circa il 10 % il raggio del metallo e quindi la transizione riduce il volume molare e riduce la compressibilità

https://2012books.lardbucket.org/books/principles-of-general-chemistry-v1.0/s27-05-crystal-field-theory.html

Ionic radii[edit]

The spin state of the complex also affects an atom's ionic radius.[21]

d^4

Octahedral high spin: Cr^{2+}, 64.5 pm.
Octahedral low spin: Mn^{3+}58 pm.

d^5

Octahedral high spin: Fe^{3+}, the ionic radius is 64.5 pm.
Octahedral low spin: Fe^{3+}, the ionic radius is 55 pm.

d^6

Octahedral high spin: Fe^{2+}, the ionic radius is 78 pm, Co^{3+} ionic radius 61 pm.
Octahedral low spin: Includes Fe^{2+} ionic radius 62 pm, Co^{3+} ionic radius 54.5 pm, Ni^{4+} ionic radius 48 pm.

d^7

Octahedral high spin: Co^{2+} ionic radius 74.5 pm, Ni^{3+} ionic radius 60 pm.
Octahedral low spin: Co^{2+} ionic radius 65 pm, Ni^{3+} ionic radius 56 pm.

d^8

Octahedral high spin: Ni^{2+} ionic radius 69 pm.
Square planar low-spin: Ni^{2+} ionic radius 49 pm.

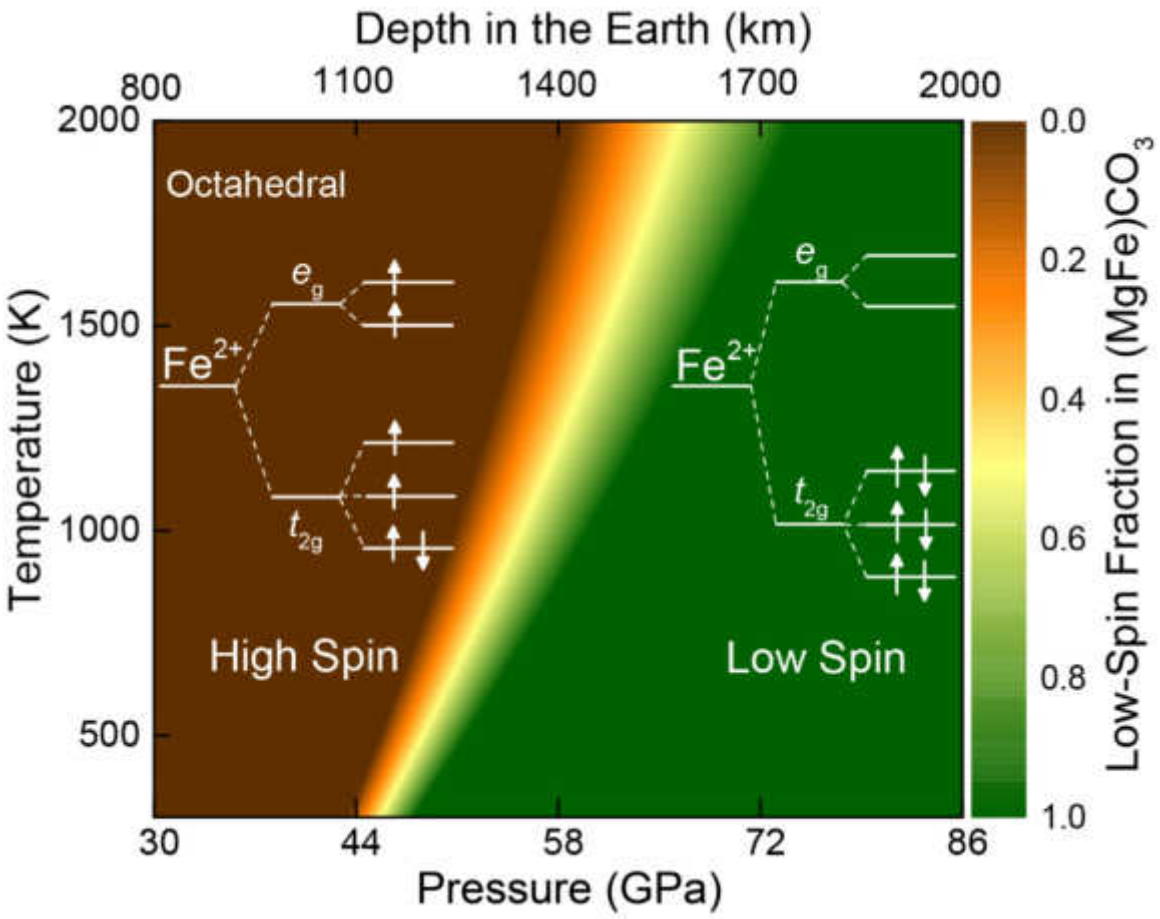

From Liu J, Lin J-F, Mao Z, Prakapenka VB (2014) Thermal equation of state and spin transition of magnesiosiderite at high pressure and temperature. American Mineralogist 99:84-93.

The image depicts spin crossover of **ferromagnesite** at HP and HT . The col on the right represents the fraction of the low-s state of iron in the sample.

cross-over @HP

SCIENTIFIC REPORTS

OPEN

SUBJECT AREAS:
MINERALOGY
GEOCHEMISTRY

Received
20 June 2014

Accepted
3 December 2014

Published
6 January 2015

Correspondence and requests for materials should be addressed to J.L (jinliu@utexas.edu)

High-Pressure Orthorhombic Ferromagnesite as a Potential Deep-Mantle Carbon Carrier

Jin Liu[1], Jung-Fu Lin[1,2] & Vitali B. Prakapenka[3]

[1]Department of Geological Sciences, Jackson School of Geosciences, The University of Texas at Austin, Austin, TX 7
[2]Center for High Pressure Science and Technology Advanced Research (HPSTAR), Shanghai 201203, People's Rep
[3]Consortium for Advanced Radiation Sources, The University of Chicago, Chicago, IL 60637, USA.

Knowledge of the physical and chemical properties of candidate deep-carbon carriers such as fer
[(Mg,Fe)CO_3] at high pressure and temperature of the deep mantle is necessary for our unders
deep-carbon storage as well as the global carbon cycle of the planet. Previous studies have repo
different scenarios for the (Mg,Fe)CO_3 system at deep-mantle conditions including the chemical
to (Mg,Fe)O+CO_2, the occurrence of the tetrahedrally-coordinated carbonates based on CO_4 s
units, and various high-pressure phase transitions. Here we have studied the phase stability an
compressional behavior of (Mg,Fe)CO_3 carbonates up to relevant lower-mantle conditions of ap
120 GPa and 2400 K. Our experimental results show that the rhombohedral siderite (Phase I) tr
an orthorhombic phase (Phase II with *Pmm*2 space group) at approximately 50 GPa and 1400
structural transition is likely driven by the spin transition of iron accompanied by a volume col
Fe-rich (Mg,Fe)CO_3 phases; the spin transition stabilizes the high-pressure phase II at much lov
conditions than its Mg-rich counterpart. It is conceivable that the low-spin ferromagnesite phase
a major deep-carbon carrier at the deeper parts of the lower mantle below 1900 km in depth.

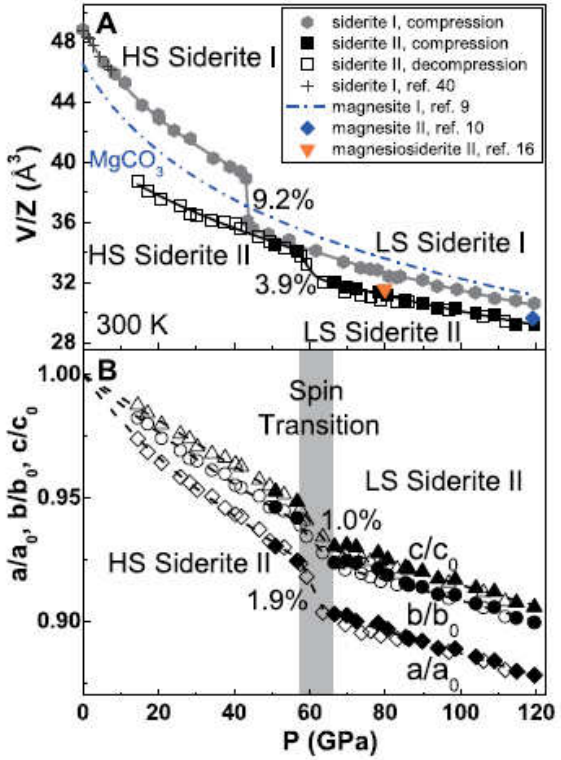

Figure 4 | Comparison of the pressure-volume relations in the (Mg,Fe)CO_3 phases. (*A*) Unit cell volume of siderite I and II phases as a function of pressure at ambient temperature. The vertical axis is plotted as the unit cell volume per formula unit (*V*/*Z*). The number of molecules per unit cell (*Z*) is 6 for siderite I and 12 for siderite II. HS: high-spin state; LS: low-spin state. Solid curves: modeled BM EoS fits of the experimental results. The volume collapse of 9.2 (±0.5)% and 3.9 (±0.4)% for siderite I and II can be associated with their respective spin transition at high pressures. Solid diamond: *V*/*Z* of magnesite II re-calculated from Isshiki et al.[10] (Table S5); Solid triangle: *V*/*Z* of the high-pressure phase of magnesiosiderite [$(Mg_{0.25}Fe_{0.75})CO_3$] re-calculated from Boulard et al.[16] (Table S6). (*B*) Lattice parameters of the siderite II as a function of pressure at 300 K. The lattice collapse in siderite II is 1.9%, 1.0%, and 1.0% for a/a_0, b/b_0, and c/c_0, respectively, at approximately 60 GPa. Filled symbols:

Stable intermediate-spin ferrous iron in lower-mantle perovskite

C. McCAMMON[1]*, I. KANTOR[1†], O. NARYGINA[1], J. ROUQUETTE[1†], U. PONKRATZ[2], I. SERGUEEV[2], M. MEZOUAR[2], V. PRAKAPENKA[3] AND L. DUBROVINSKY[1]

[1]Bayerisches Geoinstitut, Universität Bayreuth, D-95440 Bayreuth, Germany
[2]European Synchrotron Radiation Facility, BP 220, F-38043 Grenoble Cedex, France
[3]Center for Advanced Radiation Sources, University of Chicago, Chicago, Illinois 60637, USA
[†]Present address: University of Chicago, CARS, Building 434A, 9700 S. Cass Avenue, Argonne, Illinois 60439, USA (I.K.); Institut Charles Gerhardt UMR CNRS 5253, Equipe PMOF, University Montpellier II, Place Eugene Bataillon, cc1504, 34095 Montpellier cedex 5, France (J.R.)
*e-mail: catherine.mccammon@uni-bayreuth.de

The lower mantle is dominated by a magnesium- and iron-bearing mineral with the perovskite structure. Iron has the ability to adopt different electronic configurations, and transitions in its spin state in the lower mantle can significantly influence mantle properties and dynamics. However, previous studies aimed at understanding these transitions have provided conflicting results[1–4]. Here we report the results of high-pressure (up to 110 GPa) and high-temperature (up to 1,000 K) experiments aimed at understanding spin transitions of iron in perovskite at lower-mantle conditions . Our Mössbauer and nuclear forward scattering data for two lower-mantle perovskite compositions demonstrate that the transition of ferrous iron from the high-spin to the intermediate-spin state occurs at approximately 30 GPa, and that high temperatures favour the stability of the intermediate-spin state. We therefore infer that ferrous iron adopts the intermediate-spin state throughout the bulk of the lower mantle. Our X-ray data show significant anisotropic compression of lower-mantle perovskite containing intermediate-spin ferrous iron, which correlates strongly with the spin transition. We predict spin-state heterogeneities in the uppermost part of the lower mantle associated with sinking slabs and regions of upwelling. These may affect local properties, including thermal and electrical conductivity, deformation (viscosity) and chemical behaviour, and thereby affect mantle dynamics.

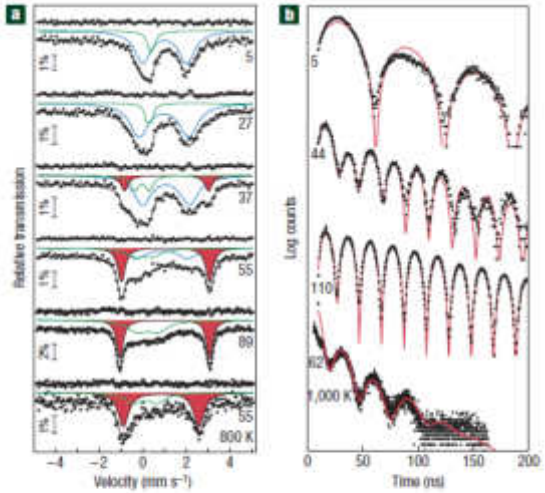

Figure 1 High-pressure ^{57}Fe spectra of $Mg_{0.88}Fe_{0.12}SiO_3$ perovskite. **a**, Mössbauer spectra collected at room temperature (top five spectra) and high temperature (bottom spectrum). Pressures are given in GPa and quadrupole doublets are coloured as follows: HS Fe^{2+}, blue; high-QS Fe^{2+}, red; minor component including Fe^{3+}, green. **b**, NFS spectra collected at room temperature (top three spectra) and high temperature (bottom spectrum). Pressures are given in GPa.

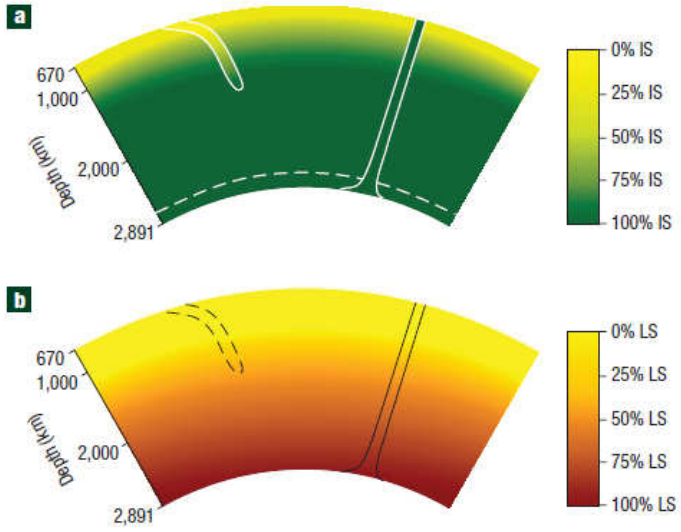

Figure 3 Estimated Fe^{2+} spin-state distribution in the lower mantle. a, Silicate perovskite variation estimated from our data, previous XES data[1,2] and current thermal models[17–19]. The greatest contrast occurs in the uppermost region, and no spin transition is expected at the base of the mantle in the postperovskite phase[10]. **b**, (Mg,Fe)O variation on the basis of previous data[26] shows the greatest contrast in spin state to occur in the middle part of the lower mantle. Slab mineralogy excludes (Mg,Fe)O and the temperature effect is small in the uppermost and lowermost regions of the lower mantle[26].

Phase	E_0/f.u. (eV)	V_0/f.u. (Å^3)	K_0 (GPa)	K_0'
FIM-SP	−40.71	120.8	56.6	3.8
FM-SP	−39.92	116.5	48.0	5.4
AFM-SP	−40.30	120.4	43.2	5.3
FIM -CT	−39.62	113.9	55.1	3.5
FM -CT	−39.21	112.5	41.7	5.2
AFM-CT	−39.74	117.7	44.6	3.7
FIM -CM	−39.62	113.7	56.3	3.4
FM -CM	−39.22	112.6	41.8	5.1
AFM-CM	−39.75	117.8	45.0	3.7
FIM -CF	−39.47	113.1	76.3	3.6
FM -CF	−39.39	114.8	37.5	3.3
AFM-CF	−39.65	113.5	57.0	3.5
FIM -CS	−40.48	110.2	46.6	3.9
FM1-CS	−40.07	98.7	86.9	5.0
FM2-CS	−39.64	92.7	118.6	5.0
AFM1-CS	−40.34	116.1	53.7	4.0
AFM2-CS	−40.22	114.5	30.0	7.2
AFM3-CS	−40.28	112.9	43.3	4 (fixed)
NM -CS	−39.58	92.8	117.1	4.9

Table 1. The calculated parameters of the third-order Birch-Murnaghan Equation of State (energy per formula unit E_0, volume per formula unit V_0, bulk modulus K_0, its pressure derivative K_0' at zero pressure) of different Fe_3S_4 phases.

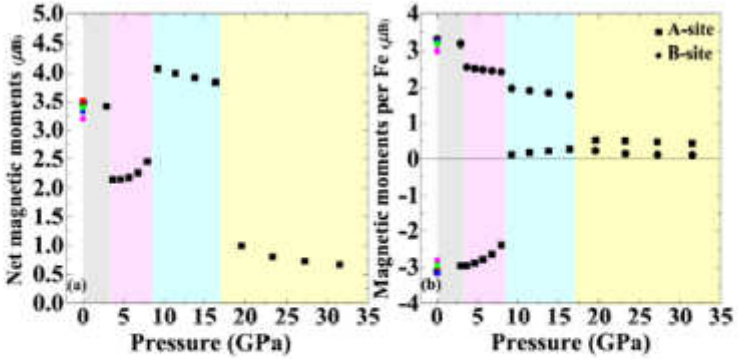

Figure 2. Calculated net magnetic moments (**a**) and sub-lattice magnetic moments per Fe of A-site and B-site (**b**) as a function of pressure. The magnetic moments of Fe on the B-site are defined as positive and therefore those of Fe on the A-site in the FIM-SP and FIM-CS phases are negative. The grey, pink, blue and yellow regions represent FIM-SP, FIM-CS, FM1-CS and FM2-CS phases, respectively. The previous data marked with red (experimental results, Exp.), blue (Exp.), green (theoretical calculations, The.) and pink (The.) points are extracted from refs 38,40 and 42, respectively for comparison.

www.nature.com/scientificreports

SCIENTIFIC REPORTS

OPEN

Pressure-induced structural and spin transitions of Fe_3S_4

Shengxuan Huang[1], Duan Kang[1], Xiang Wu[2], Jingjing Niu[1] & Shan Qin[1]

Received: 28 September 2016
Accepted: 15 March 2017
Published: 12 April 2017

Greigite (Fe_3S_4), isostructural with Fe_3O_4 has recently attracted great scientific interests from material science to geology due to its complicated structure and electronic and magnetic configurations. Here, an investigation into the structural, magnetic and electronic properties of Fe_3S_4 under high pressure has been conducted by first-principle calculations based on density functional theory. The results show that a first-order phase transition of Fe_3S_4 would occur from the inverse spinel (SP) structure to the Cr_3S_4-type (CS) structure at 3.4 GPa, accompanied by a collapse of 9.7% in the volume, a redistribution of iron cations, and a half-metal to metal transition. In the CS-Fe_3S_4, Fe^{2+} located at octahedral environment firstly undergoes a transition from high-spin (HS) state to low-spin (LS) state at 8.5 GPa and Fe^{3+} subsequently does at 17 GPa. The Equation of State for different phases of Fe_3S_4 are also determined. Our results not only give some clues to explore novel materials by utilizing Fe_3S_4 but also shed light on the fundamental information of Fe_3O_4, as well as those of other SP-AB_2X_4 compounds.

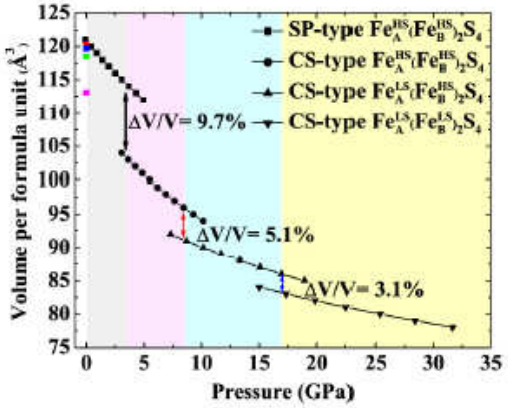

Figure 5. Calculated results of volume per formula unit of different Fe_3S_4 phases as a function of pressure. The solid lines segments are fitted by the third-order Birch-Murnaghan Equation of State. The volume collapse of each phase transition is marked. HS and LS represent high-spin and low-spin states, respectively. The previous data marked with red (Exp.), blue (Exp.), green (The.) and pink (The.) points are extracted from refs 38,40 and 42, respectively for comparison.

How to determine EoS and structural evolution @ HP?

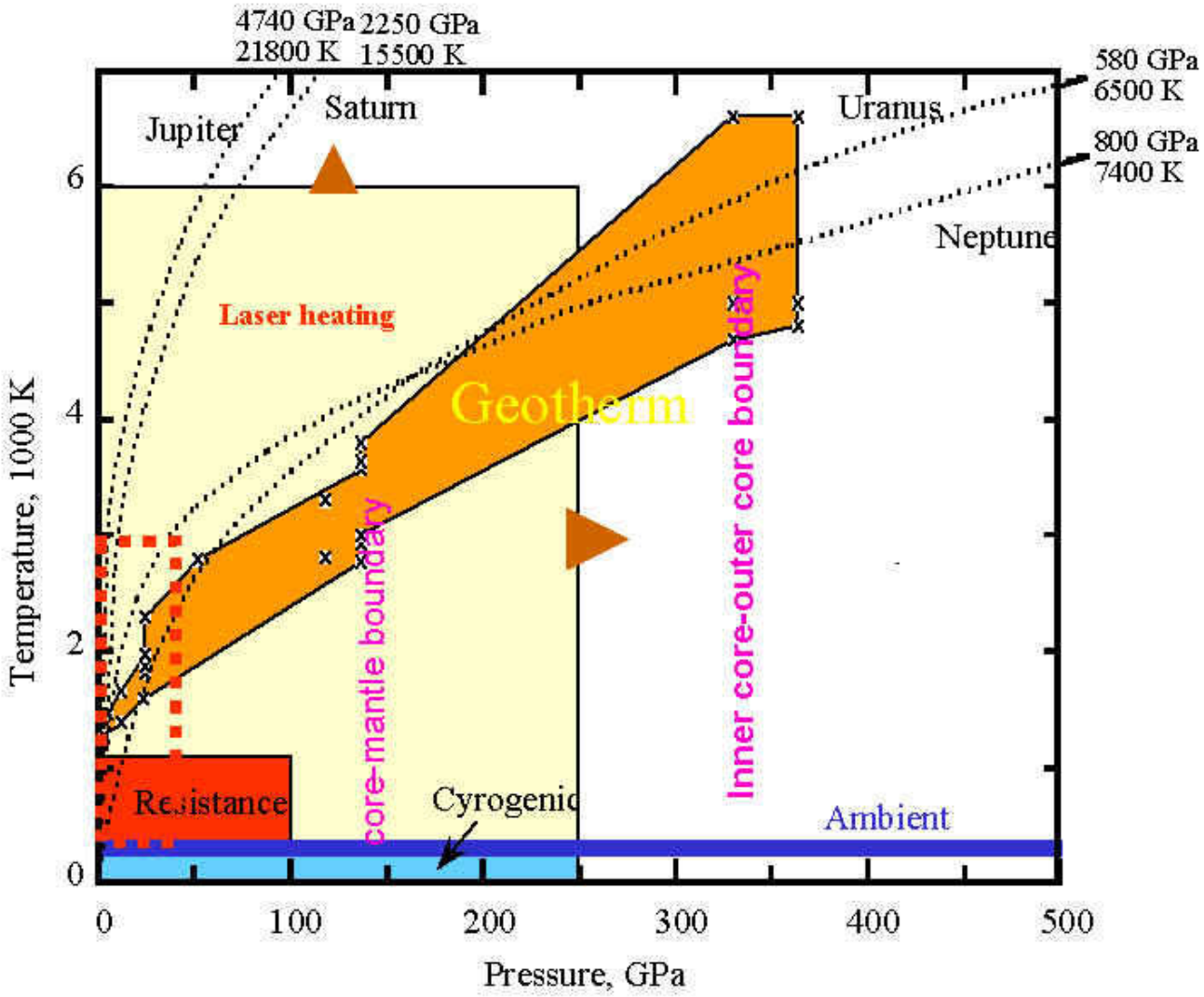

Pressure-temperature range for diamond cell experiments. A: Ambient;
C: Cryogenic (not shown
R: External Resistance Heating;
L: Laser Heating;
Geotherm: Temperature range in Earth's interior.
Dotted curves indicate estimated P-T in Jovian planetary interiors, with the conditions of the center shown at the end of each curve.

From GSECARS, APS web page

Diamond Anvil Cell

P = F/s

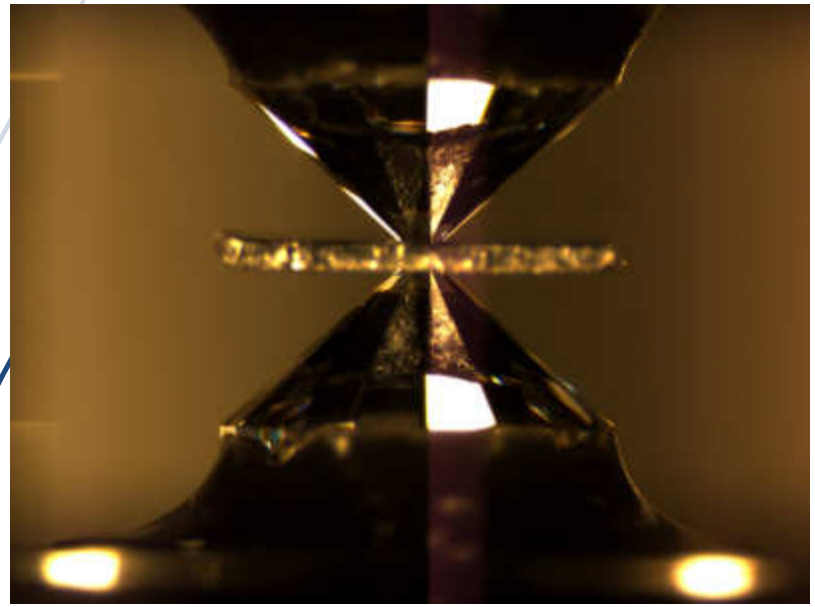

https://serc.carleton.edu/NAGTWorkshops/mineralogy/mineral_physics/diamond_anvil.html

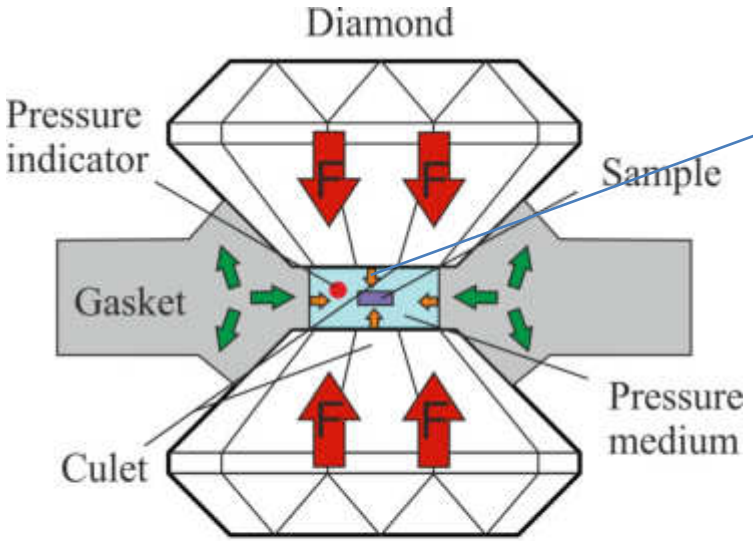

$$\text{Pressure} = \frac{\text{Force}}{\text{Area}}$$

Schematic view of DAC from Waeselmann, Naemi. (2012). Structural transformations in complex perovskite-type relaxor and relaxor-based ferroelectrics at high pressures and temperatures.

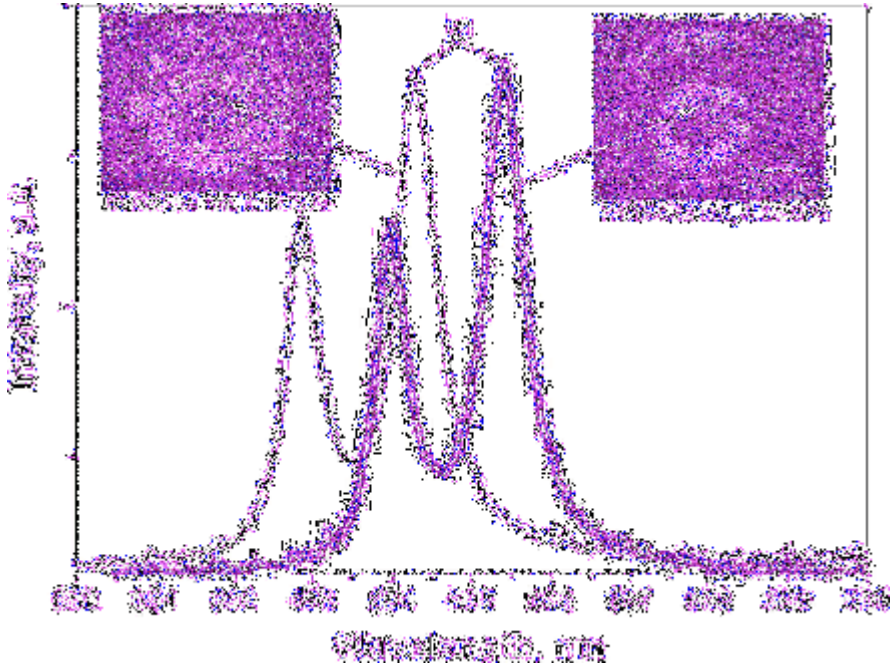

Apollo, Manuel. (2016). X-ray Raman scattering on a carbonatitic glass.

10.13140/RG.2.2.24343.47522.

Pressure transmitting media

	Previous max "Hydro Pressure"	*Diffraction broadening (GPa)*
Methanol:Ethanol	10.4	10.1
Isopropanol	4.3	3.9
Silicone oil	5-7	< 2.0
Nitrogen	13.0	3
Argon	9	2
Fluorinert	5-10	1

Froam Angel, Ross & Bujak, Maciej & Zhao, Jing & Diego Gatta, G & Jacobsen, Steven. (2007). Effective Hydrostatic Limits of Pressure Media for High-Pressure Crystallographic Studies. J. Appl. Cryst. 40. 26-32. 10.1107/S0021889806045523.

Optical view trough the DAC

Gypsum at 4.0 GPa

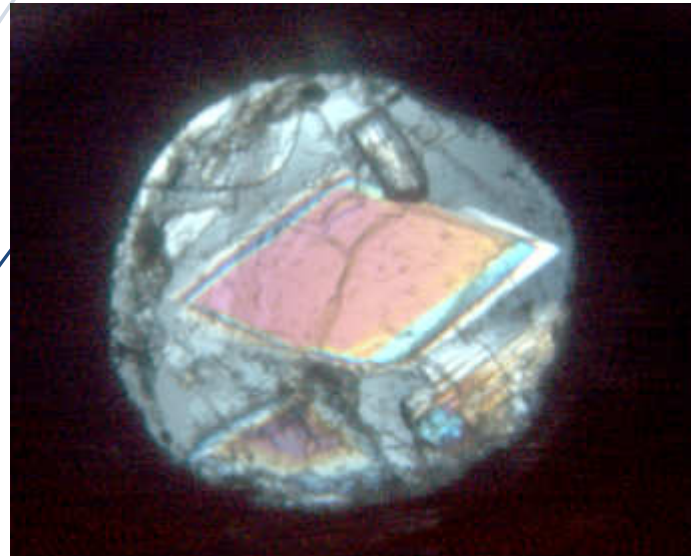

Gypsum at 4.8 GPa

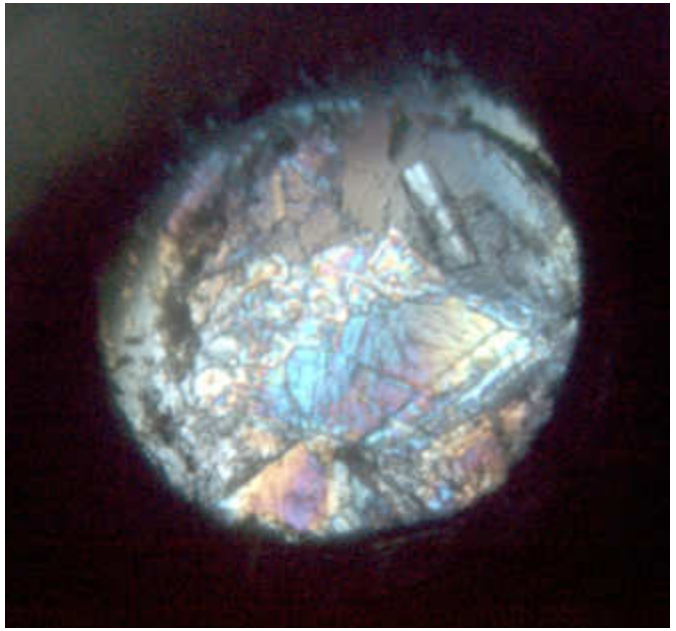

HP – microraman spectroscopy

Ar^+ = 514.5 nm (green laser)
He/Ne = 632.8 nm (red laser)

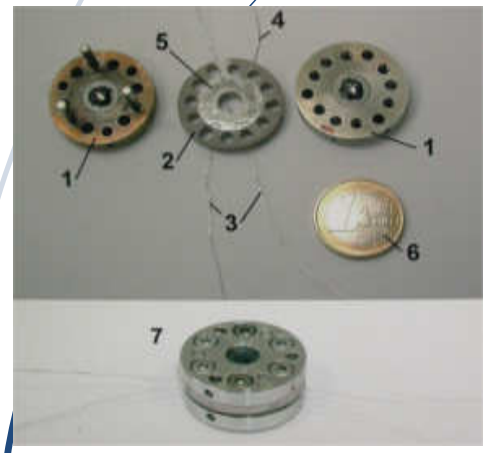

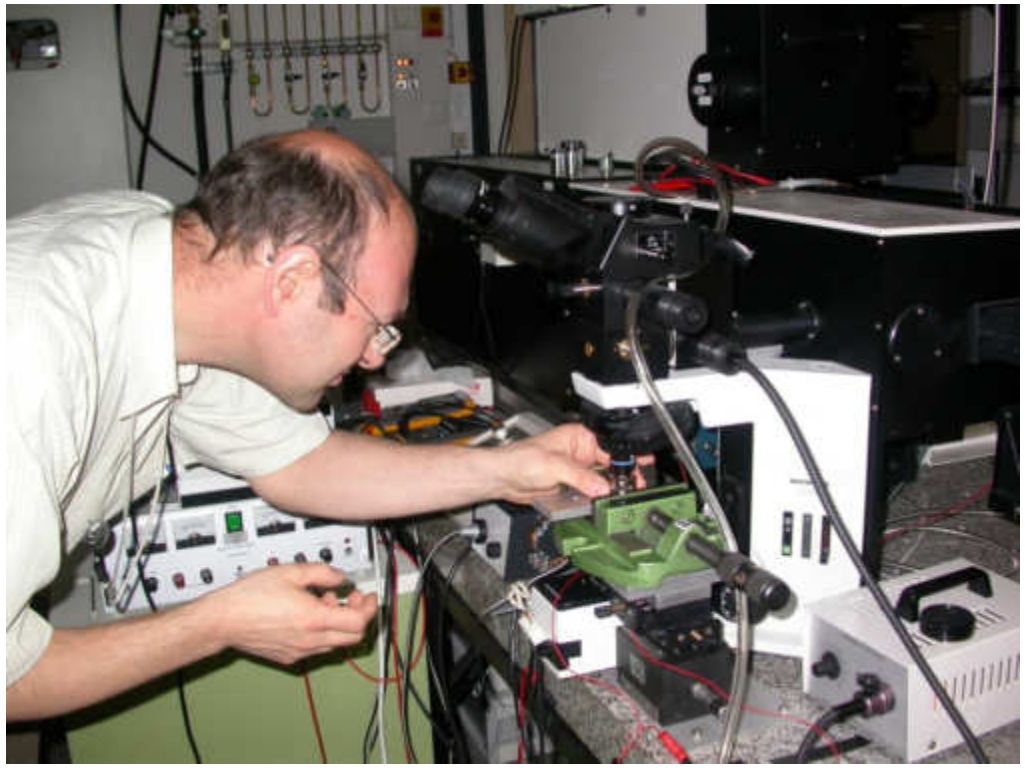

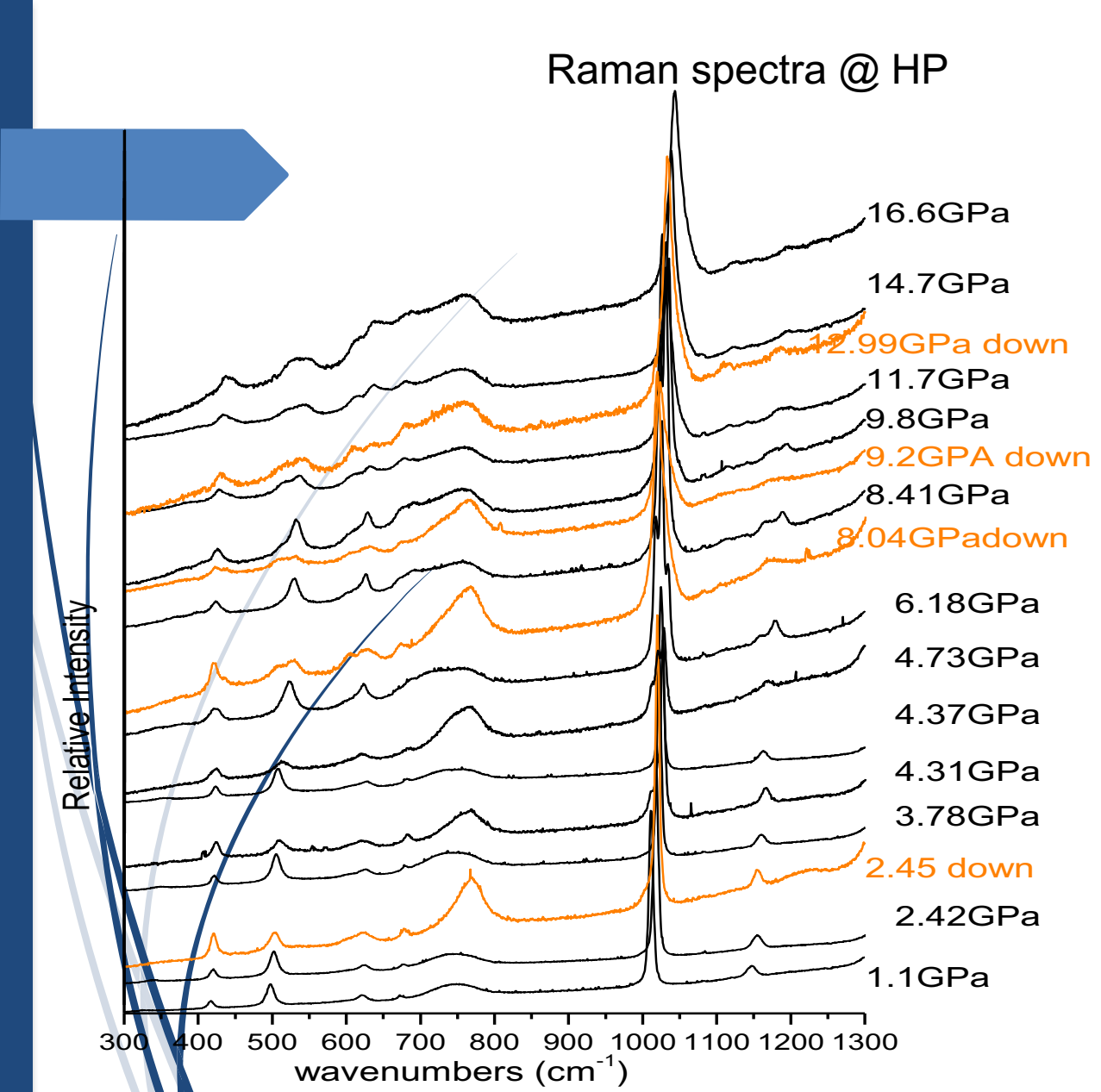

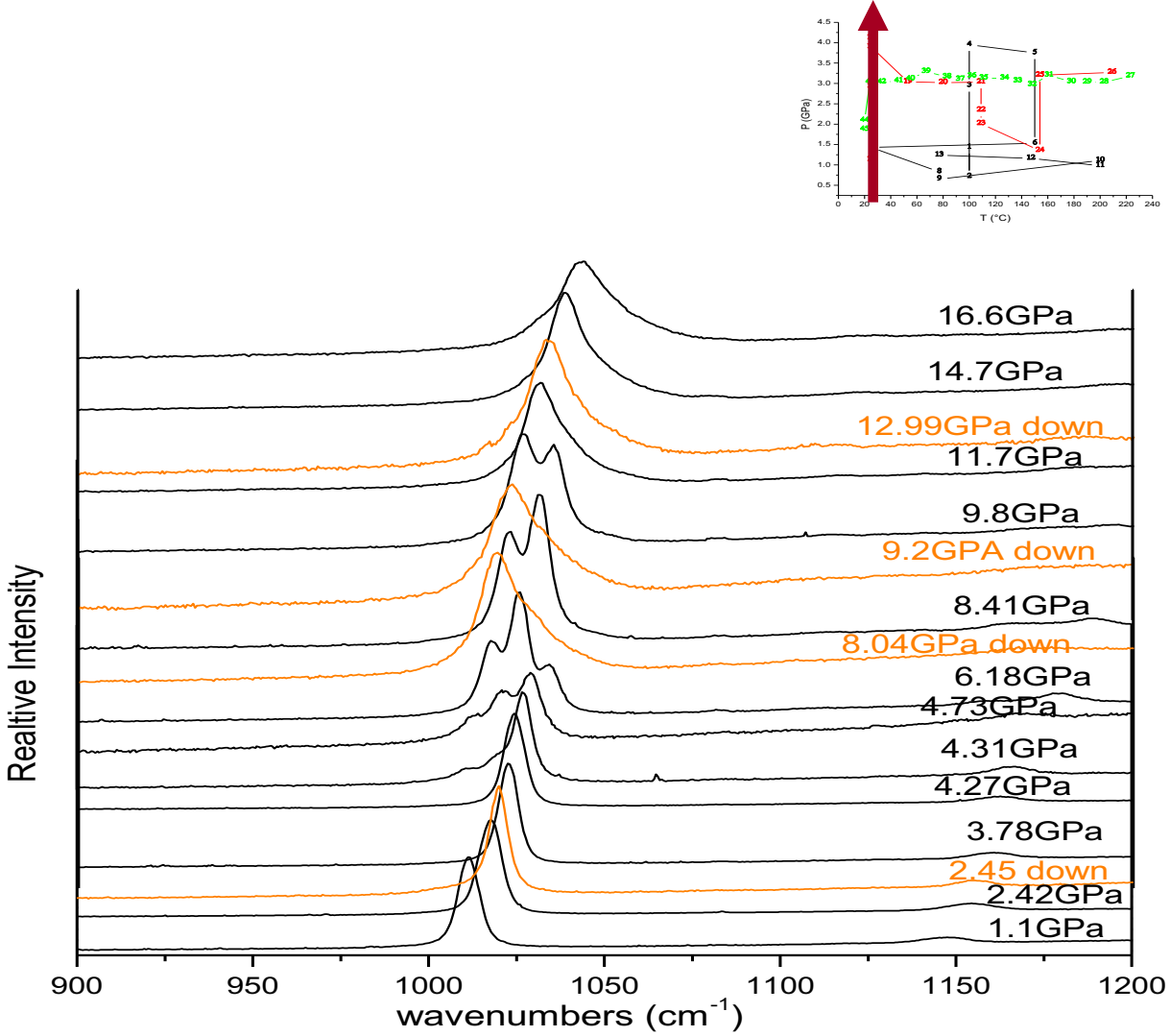

Splitting of v_1 of sulphate at the transition

HP- single crystal X-ray diffraction

Xcalibur single crystal diffractometer (Oxford instrument) @ Dipartimento Scienze della Terra, Perugia, Italy

Point detector = lattice parameters at different P up to 5 GPa

CCD = structural data collection

At different P up to 4 GPa

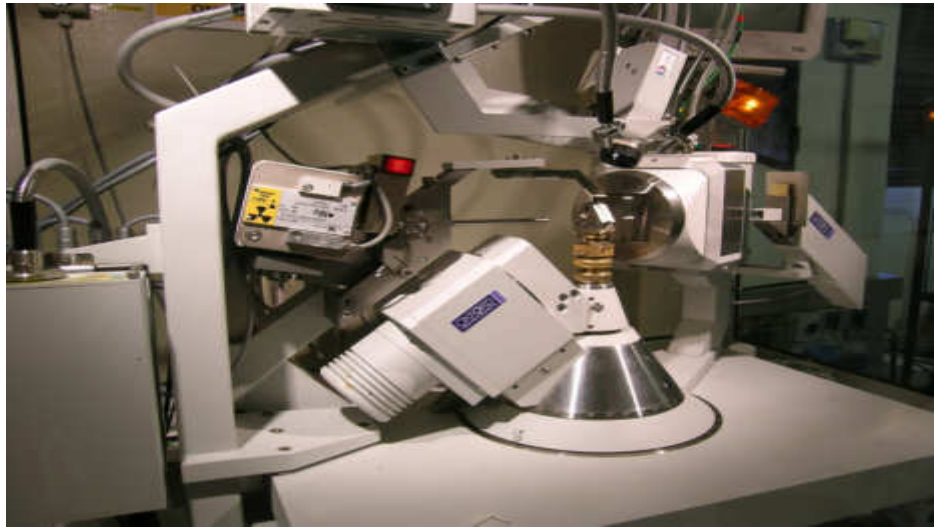

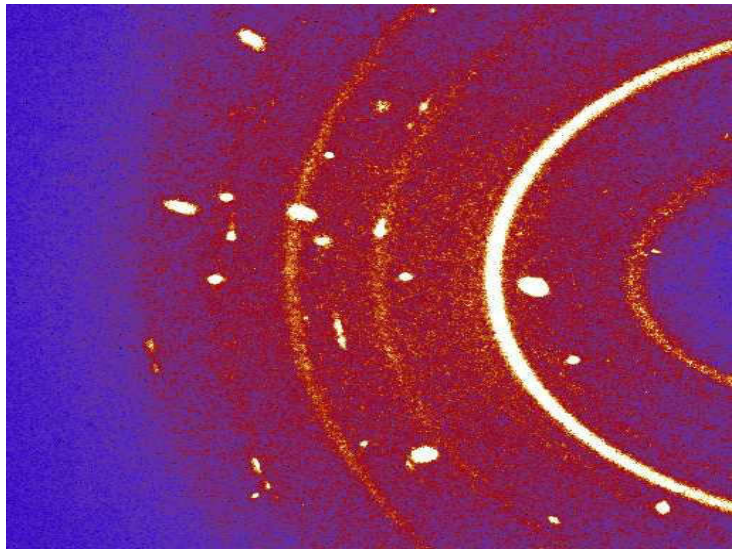

- Limited access = limited part of recripocal lattice can be measured
- Low signal (about one half with respect to signal with crystal in air, due to the absorption of the diamonds)
- Absorption by cell components
- Several phases contemporanearly in diffraction (diamond, beryllium, quartz, ruby)

HP-X-ray diffraction at synchrotrons

Argonne NATIONAL LABORATORY

ESRF
The European Synchrotron

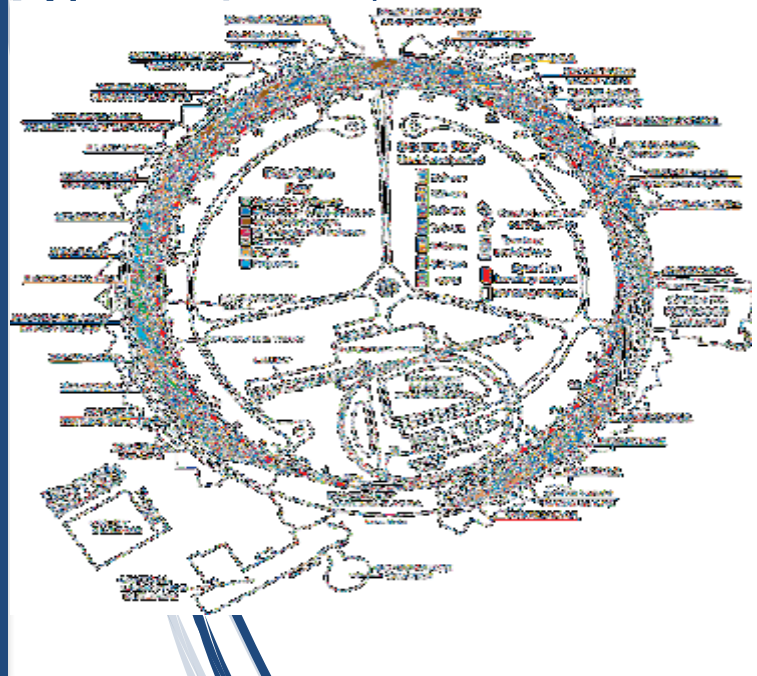

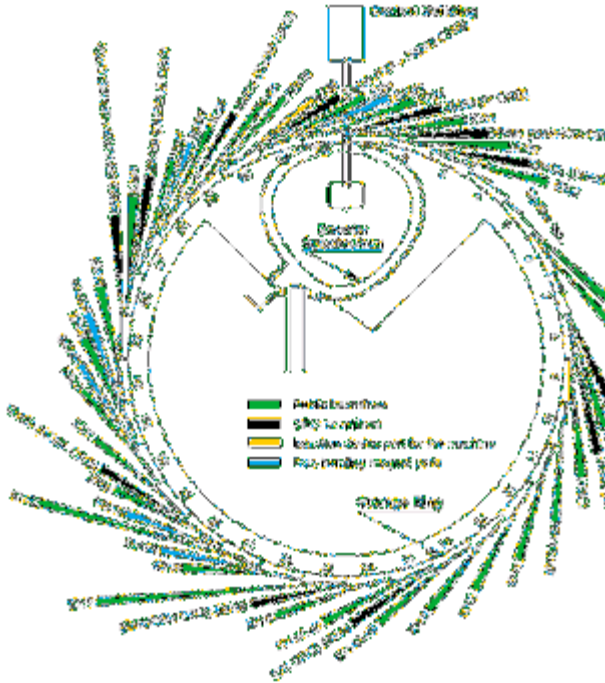

beamline 13BM-C (GSECARS) at the Advanced Photon Source (APS) synchrotron (Argonne National Laboratory, USA)

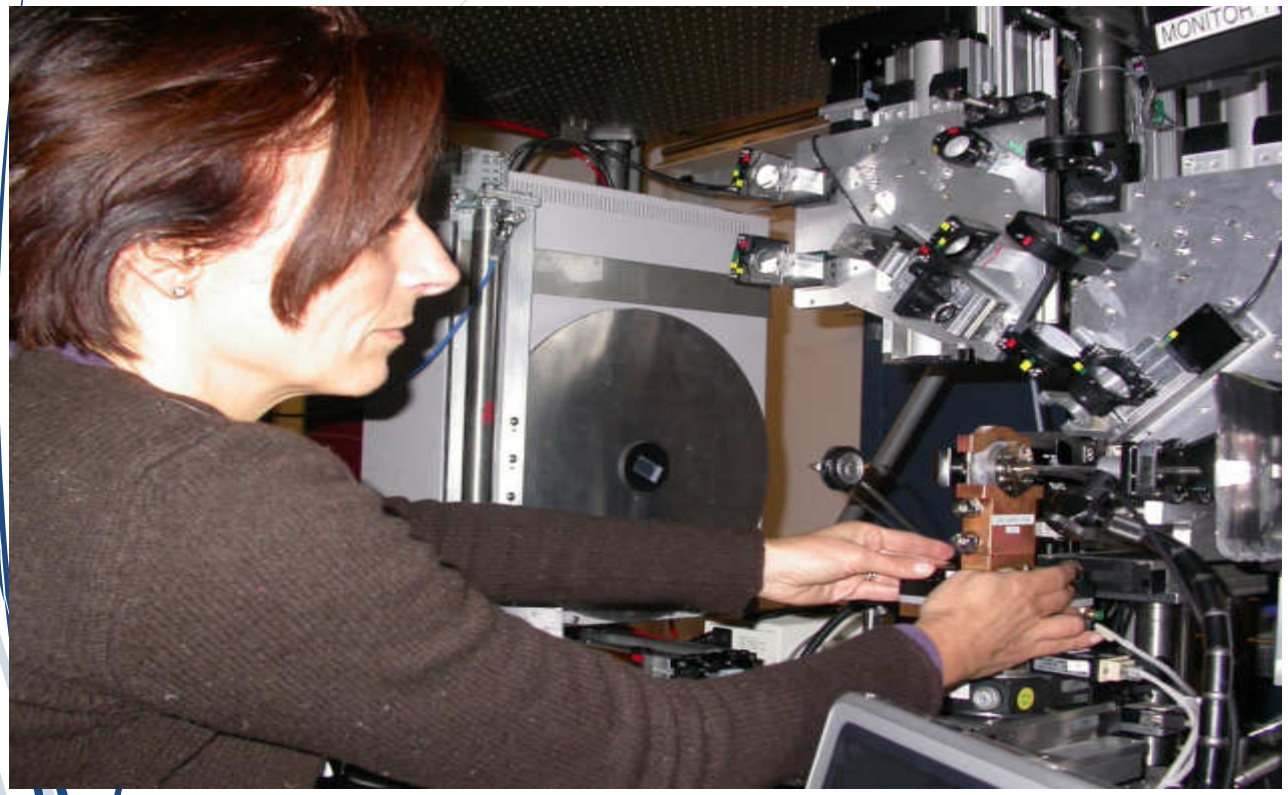

Source	Bending Magnet
Monochromator Type	Si 111
Energy Range	10-10 keV
Resolution (ΔE/E)	5×10^{-5}
Flux (photons/sec)	1×10^{12} @10 keV
Beam Size (HxV)	
Focused	23μm x 28μm
Unfocused	10mm x 3mm
Monochromator Type	Si 111
Energy Range	18-18 keV
Resolution (ΔE/E)	5×10^{-5}
Flux (photons/sec)	8×10^{11} @18 keV
Beam Size (HxV)	
Focused	26μm x 28μm
Unfocused	10mm x 3mm

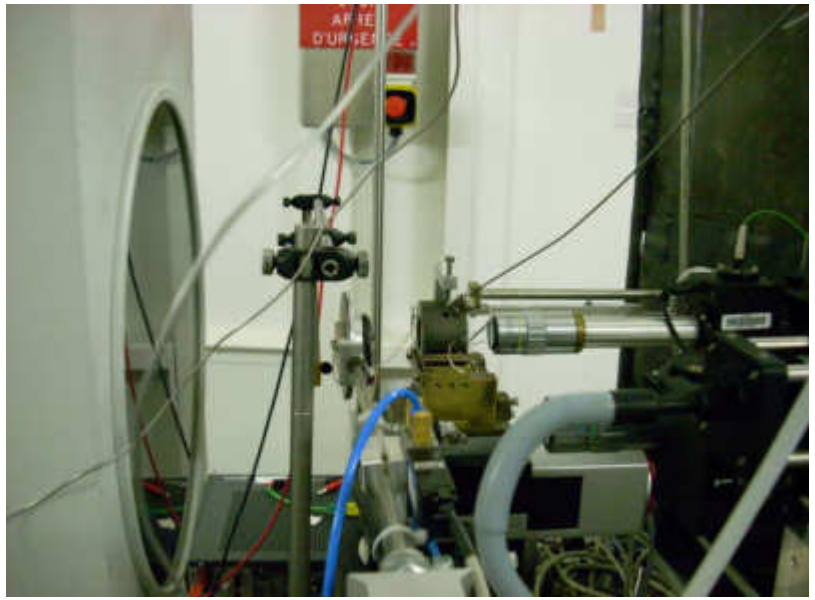

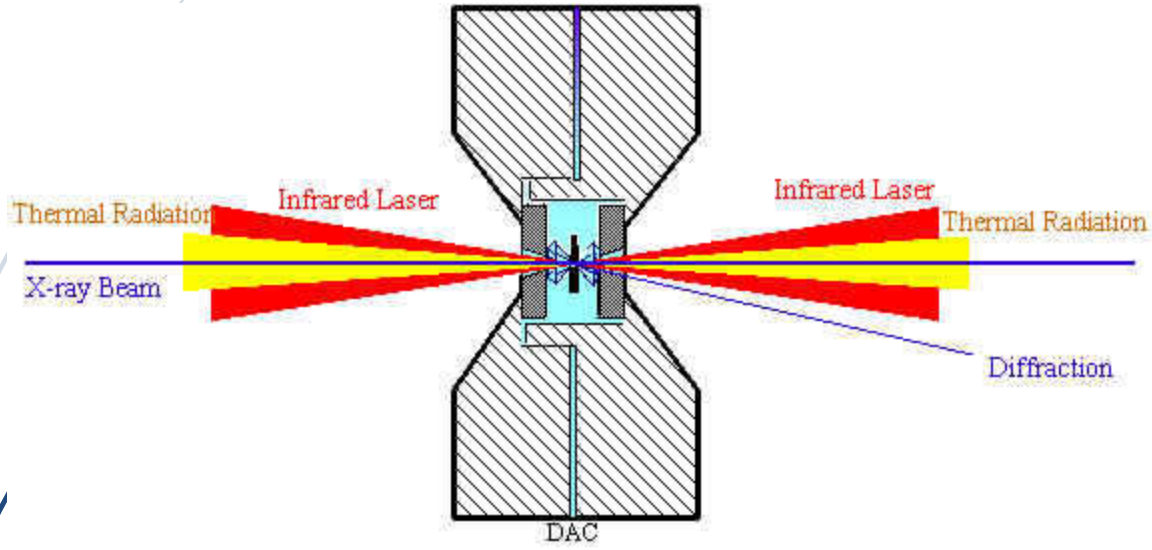

Double sided laser heated diamond cell for in-situ high P-T diffraction study. The double-sided heating approach allows one to combine different lasing modes to optimize temperature uniformity.

From GSECARS, APS web page

Multi- anvil with X-ray access = in situ sythesy and analysis of phase transformation

(BL04B1)

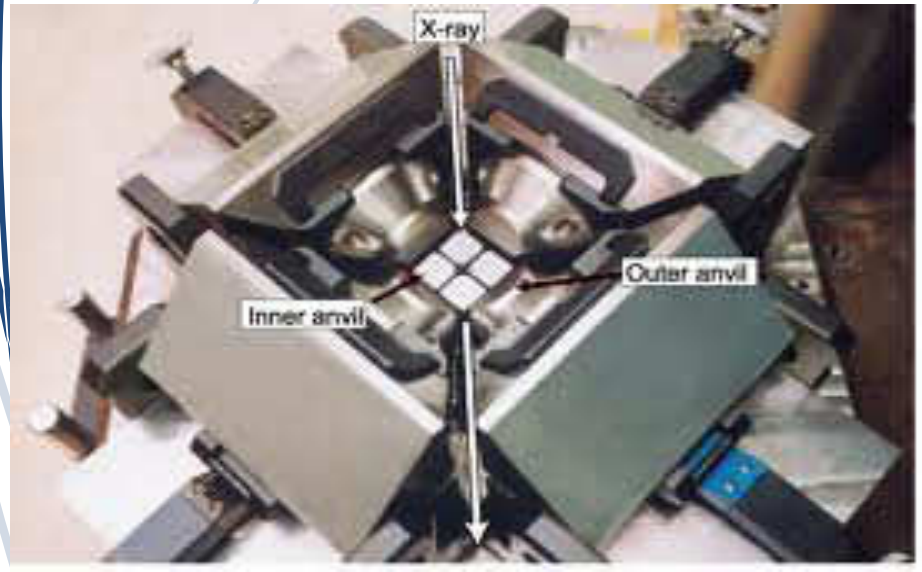

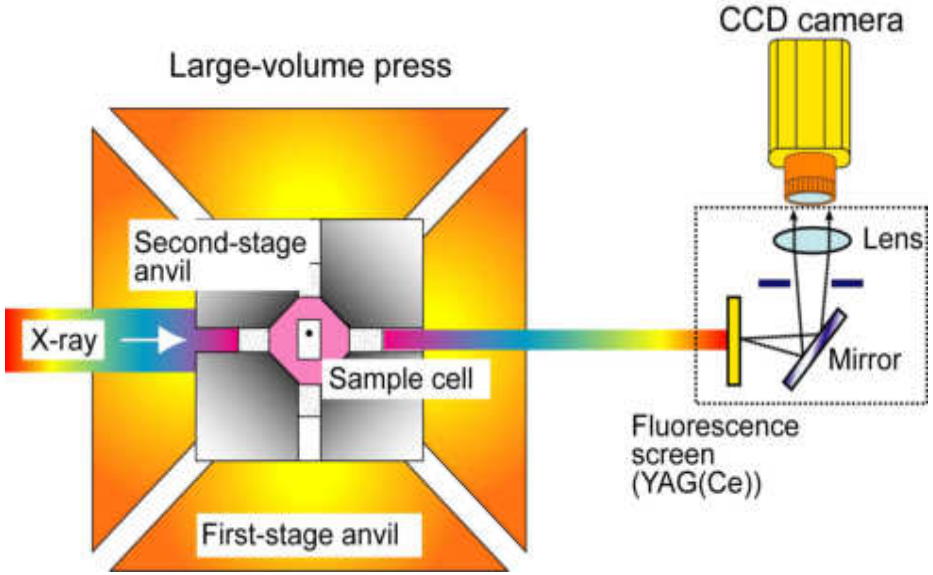

Why to determine physical properties?

1) To know the density changes

1) To know the structural changes (dehydration, phase transition….)

2) To know the physical properties changes (conducibility, seismic velocity,….)

Examples from my experience and from literature

a) Storage of deep water in the earth

b) Water in solar system

c) Phase transition and bad gap evolution

d) High spin-low spin transition: effects

e) Very deep earth

examples

1) 10 A e acqua all’interno della terra e terremoti
2) Solfosali e proprietà fisiche band gap
3) Bloedite planetologia

Deep water

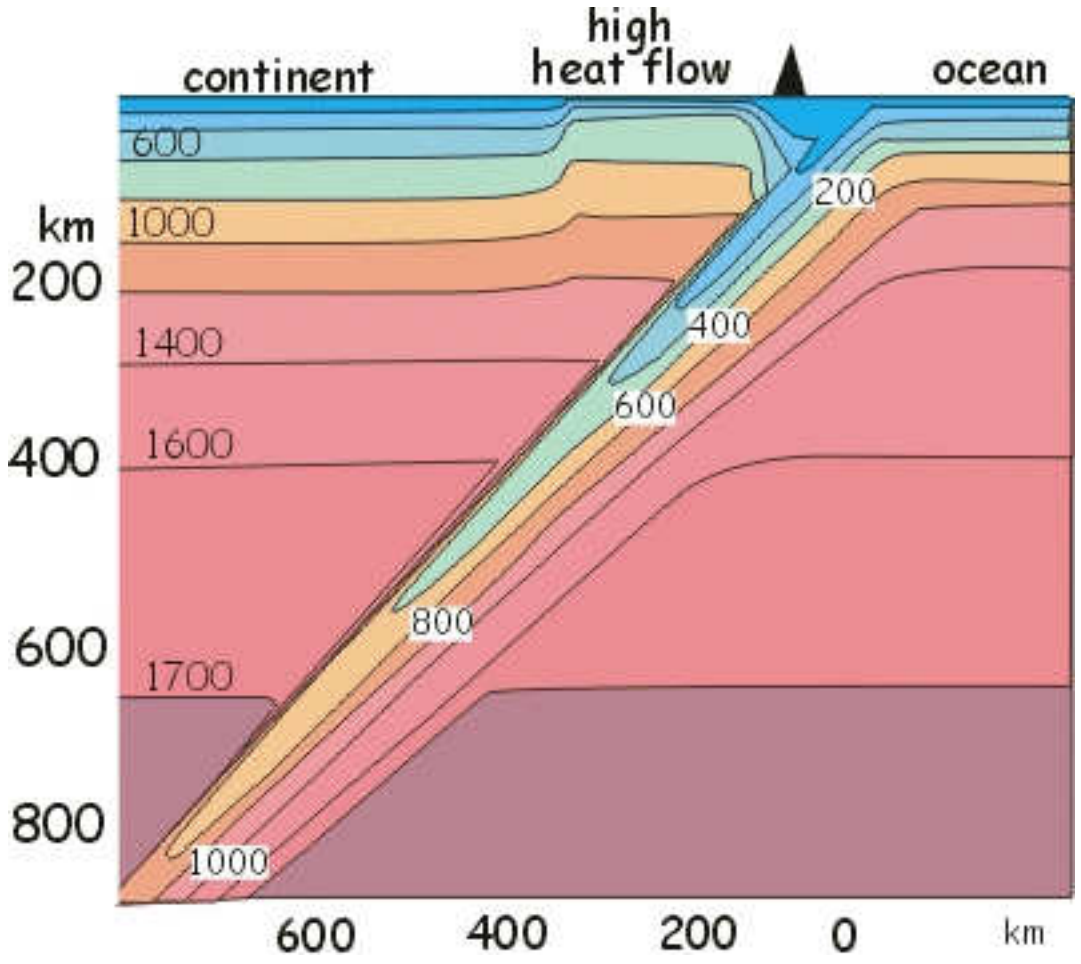

https://www.see.leeds.ac.uk/structure/dynamicearth/subduction/thermalbig.htm

Volatili in profondità

L'acqua l'influenza…
La solubilità
La miscibilità
Il calore di mixing
I coefficienti di ripartizione
Le proprietà elastiche
Le proprietà elettriche
Il punto di fusione
La viscosità
La velocità delle onde simiche
L'anisotropia
La resistenza sforzi di taglio

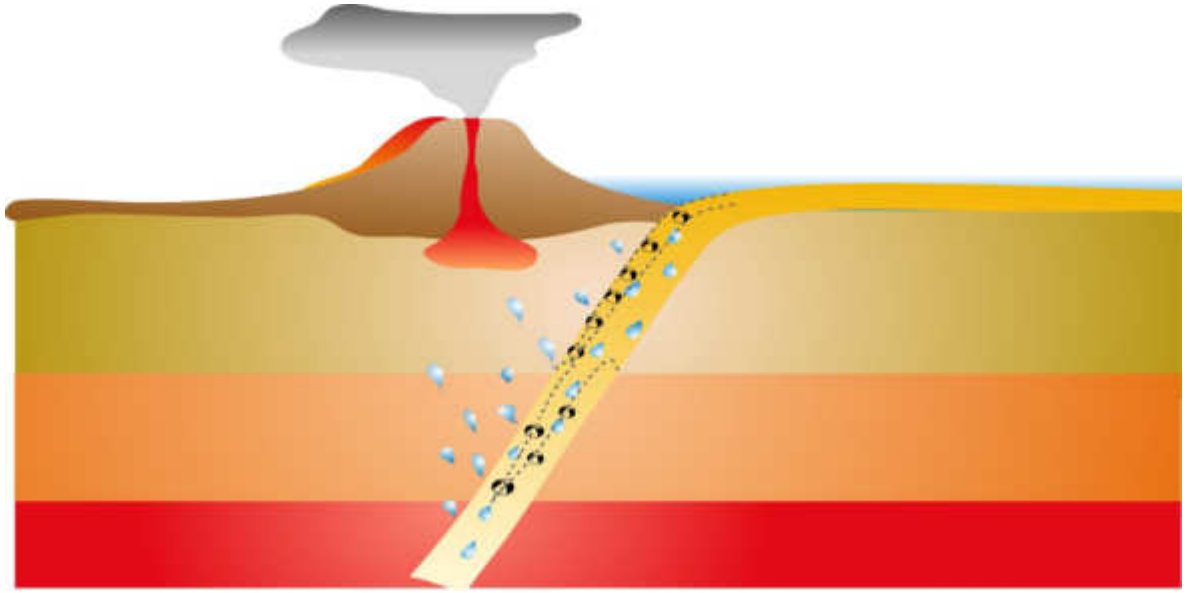

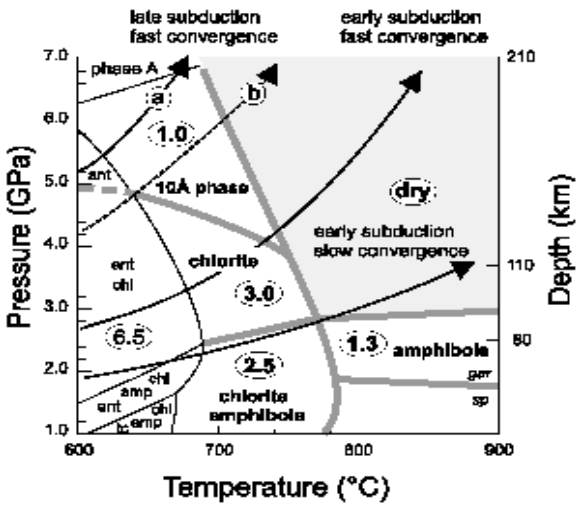

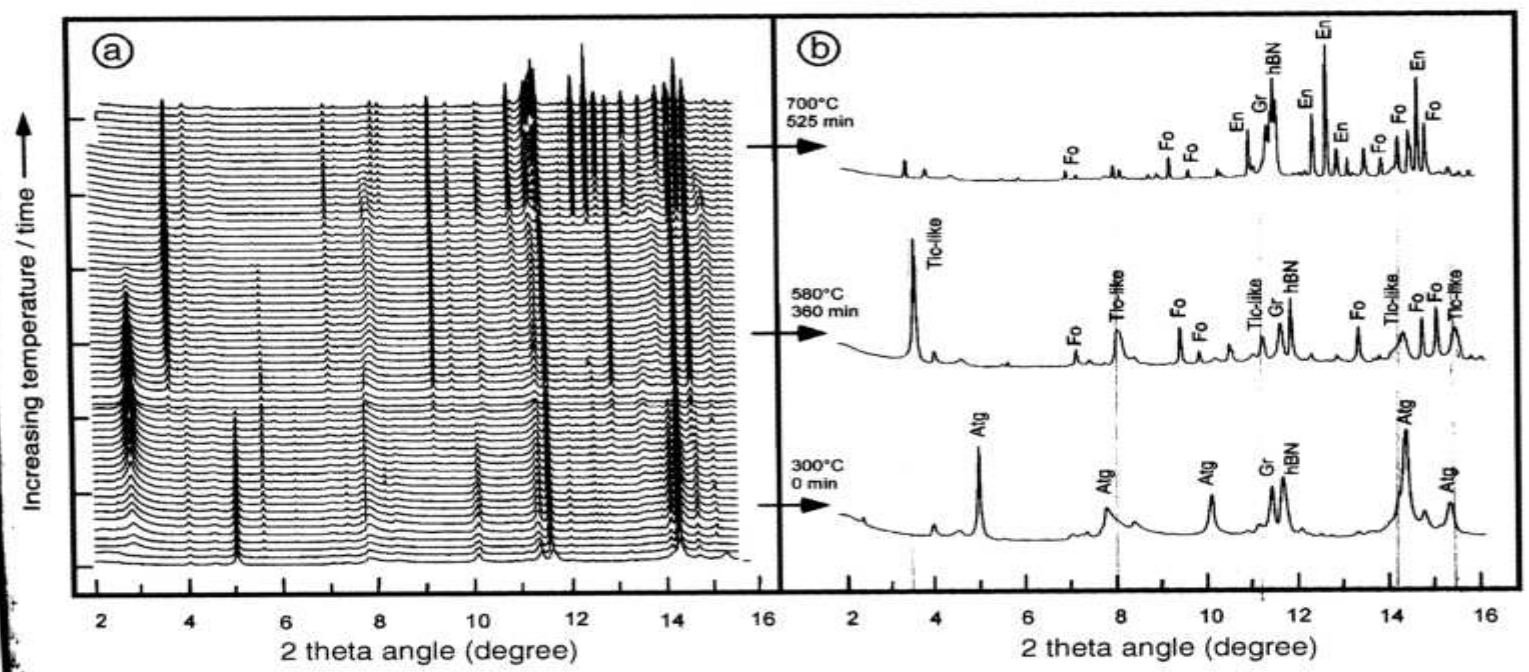

Fig. 1. (a) Time and temperature series of XRD spectra acquired during antigorite dehydration at 3.6 GPa (sample Antg11). (b) Selected patterns at 300, 580 and 700 °C. Diffraction peaks are labelled as Atg: antigorite, En: enstatite, Fo: forsterite, Gr: graphite, hBN: hexagonal boron nitride, Tlc-like: "talc-like" phase.

Crichton et al. 2002

DHMS = Dense Hydrous Magnesium silicates

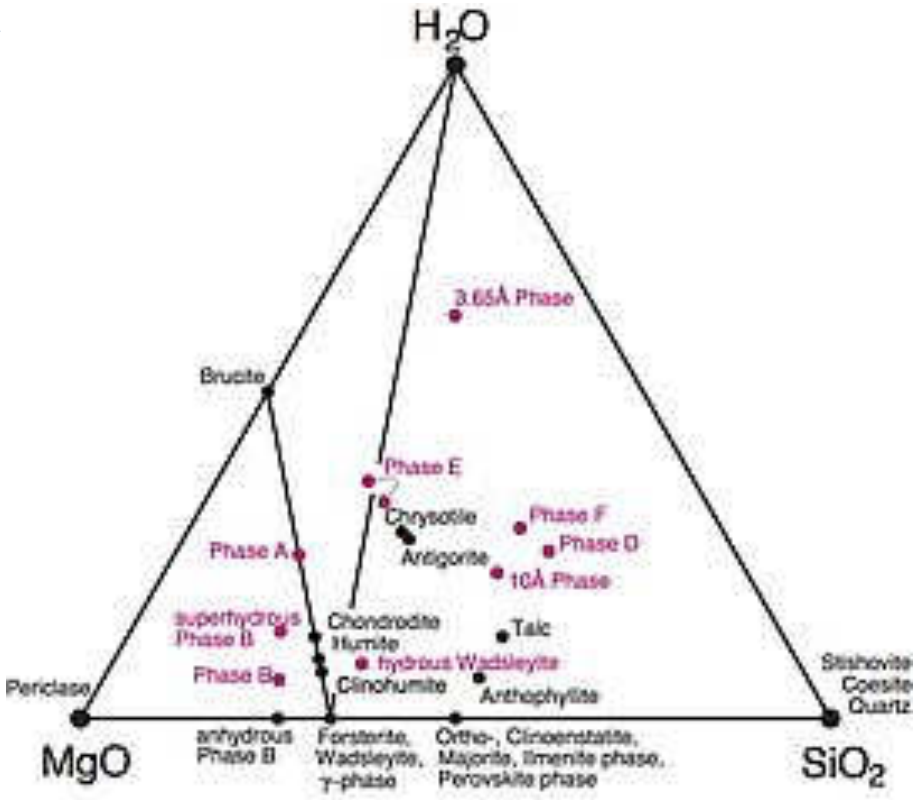

https://www.gfz-potsdam.de/en/section/chemistry-and-physics-of-earth-materials/projects/dense-hydrous-silicates/

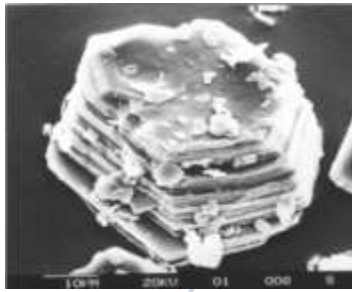

Fumagalli et al. 2001

American Mineralogist, Volume 90, pages 1012–1016, 2005

LETTER

The 10 Å phase: Crystal structure from single-crystal X-ray data

P. COMODI,[1] P. FUMAGALLI,[2] S. NAZZARENI,[1] AND P.F. ZANAZZI[1,*]

[1]Dipartimento di Scienze della Terra, Università di Perugia, Piazza Università, I-06100 Perugia, Italy
[2]Dipartimento di Scienze della Terra, Università di Milano, Via Botticelli 23, I-20133 Milano, Italy

Here we report the results of the first three-dimensional refinement of the 10 Å phase performed with single-crystal X-ray data.

The 10 Å phase, $Mg_3Si_4O_{10}(OH)_2H_2O$, is monoclinic, space group $C2/m$, a = 5.323(1)Å, b = 9.203(1)Å, c = 10.216(1)Å, β = 99.98(1)°, V = 492.9(2) Å^3; the calculated density, assuming Z = 2, is 2.676 g.cm^{-3}. The structure has been solved by direct methods and refined by least-squares method with anisotropic displacement parameters. The final agreement index (R_1) was 0.088 for 54 refined parameters and 499 unique observed reflections collected with a diffractometer with a CCD detector.

The structure of the 10 Å phase is very similar to that of a homo-octahedral, 1 M trioctahedral mica: it is a silicate consisting of 2:1 tetrahedral-octahedral layers parallel to (001). The mean Si-O, Mg1-O, and Mg2-O bond lengths are 1.626, 2.082, and 2.081 Å, respectively. The ditrigonal rotation angle α is 0.53°. The interlayer of the 10 Å phase is occupied by water molecules. According to the oxygen occupancy, 1 H_2O p.f.u. is assumed in the investigated sample. Although the average water oxygen position is in the mid-plane, structural refinement suggests disorder along **c***. Twelve hydrogen bonds are located between the water molecule and the 6 + 6 oxygen atoms of the basal rings of adjacent tetrahedral sheets (water-oxygen distances averaging 3.19 Å). Therefore there are six possible orientations for the water molecule, with six hydrogen bonds pointing toward the upper basal ring and six pointing toward the lower ring of tetrahedral sheets. The orientational disorder of water, in agreement with previous Raman spectroscopy data, is a feature relevant to the evaluation of thermodynamic functions and thermal stability of the 10 Å phase, which is a possible water carrier (9.1 wt%) in subducting slabs at high pressure.

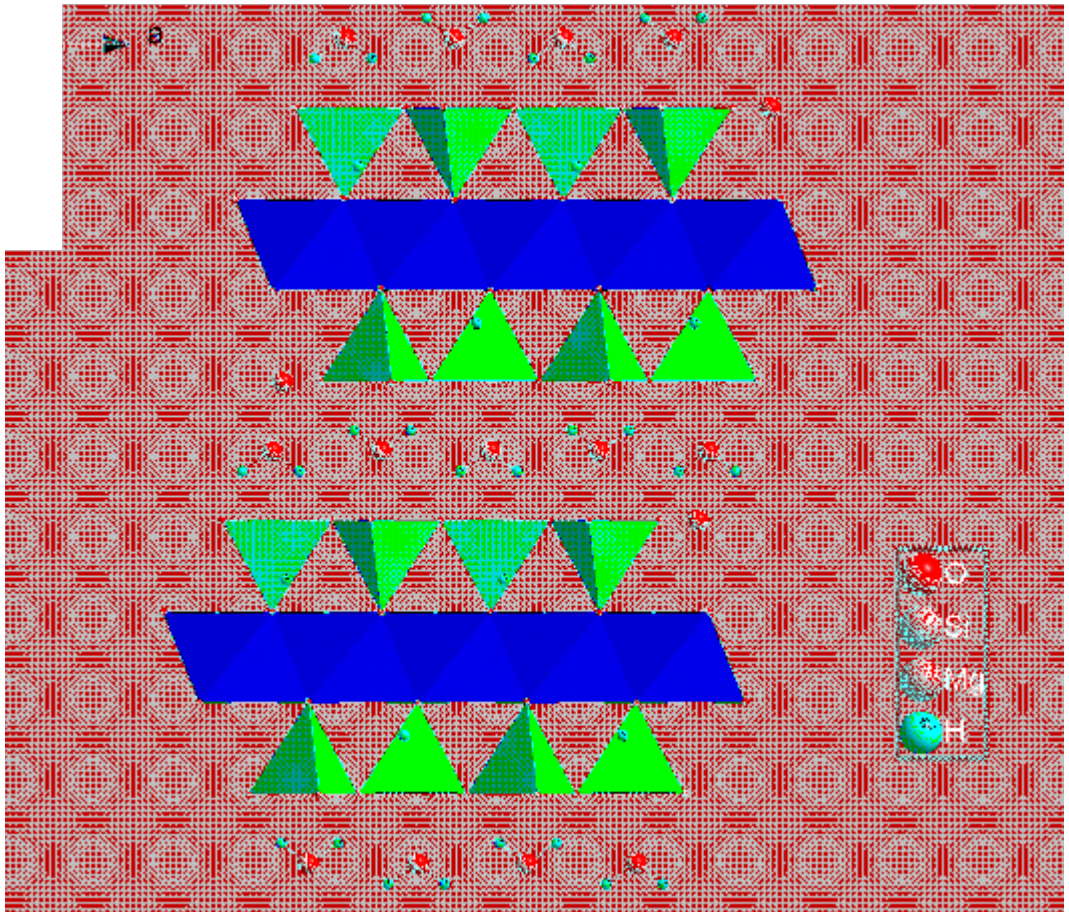

The 10Å in the $MgO-SiO_2-H_2O$ system
$Mg_3Si_4O_{10}(OH)_2 * H_2O$

C2/m , 1 H_2O p.f.u , 9.1 wt%

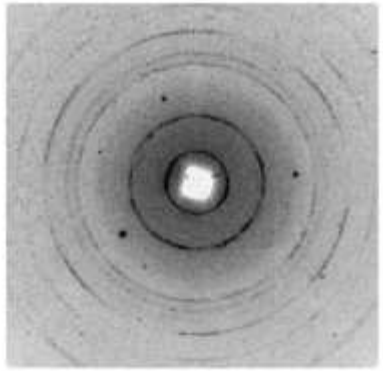

Fig. 1. X-ray diffraction image of the 10 Å phase inside the diamond anvil cell at 0.3 GPa.

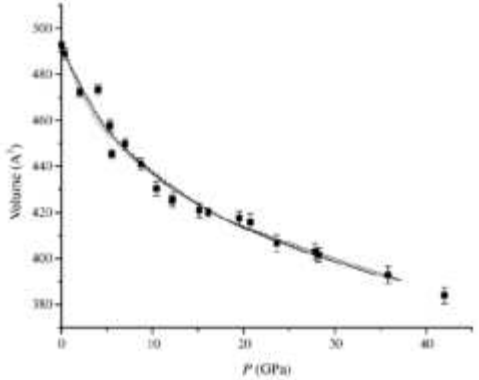

Fig. 5. Compression curve of the 10 Å phase using 3rd order Birch-Murnaghan (continuous line) and Vinet (dashed line) EoS. Measured data are also reported.

Available online at www.sciencedirect.com
SCIENCE DIRECT
ELSEVIER
Earth and Planetary Science Letters 246 (2006) 444–457
EPSL
www.elsevier.com/locate/epsl

The high-pressure behaviour of the 10 Å phase: A spectroscopic and diffractometric study up to 42 GPa

Paola Comodi [a,*], Fabio Cera [a], Leonid Dubrovinsky [b], Sabrina Nazzareni [a]

[a] Dipartimento di Scienze della Terra, Università di Perugia, Piazza dell'Università, I-06100 Perugia, Italy
[b] Bayerisches Geoinstitut, Universitat Bayreuth, D-95440 Bayreuth, Germany

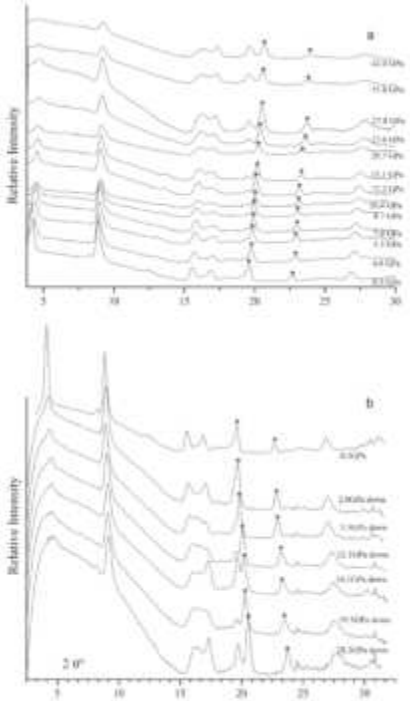

Fitting a third-order Birch-Murnghan equation of state to the P–V data yields values of V_0=492.9(3), K_0=39(3) GPa and K'=12.5(8). No significant

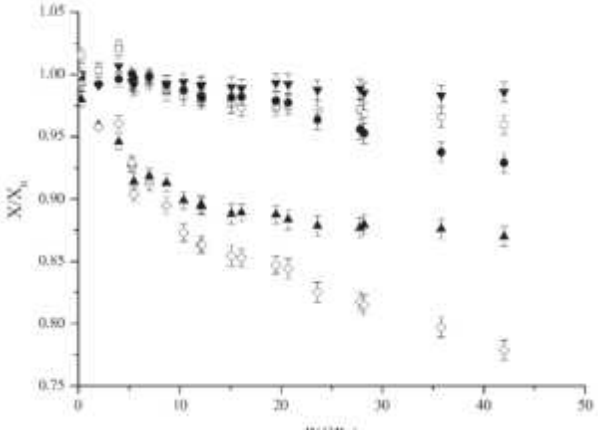

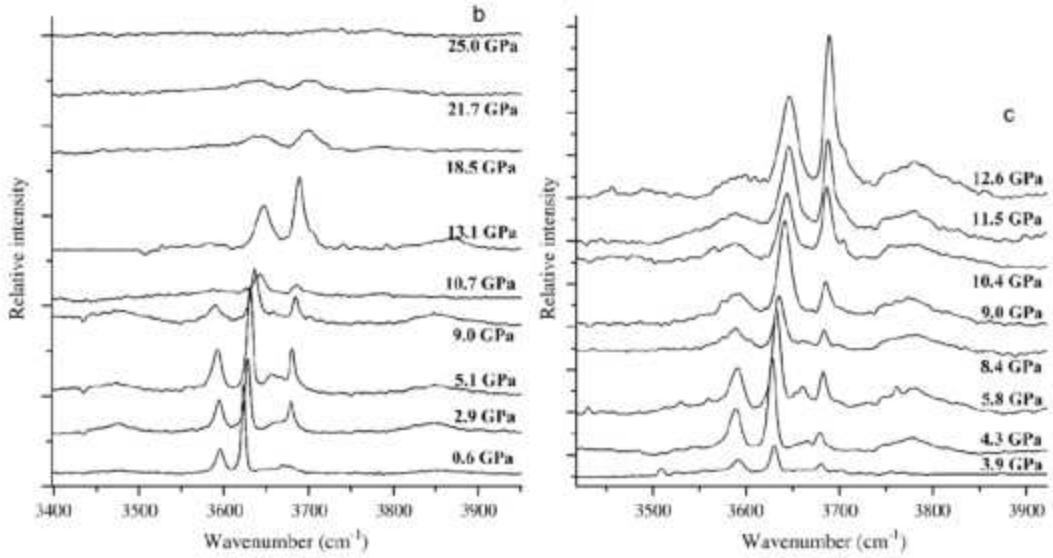

Fig. 8. High frequency region Raman spectra of the 10 Å phase in air (a) under increasing (b) and decreasing (c) pressures.

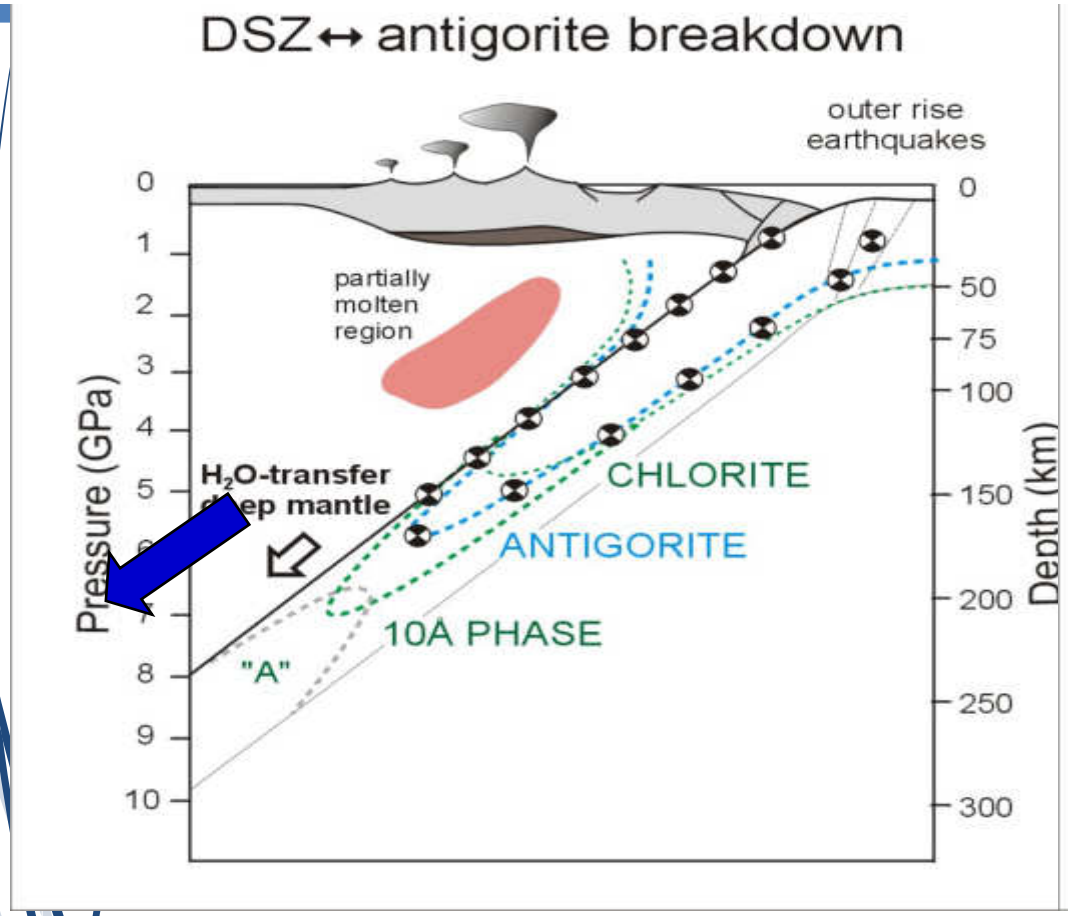

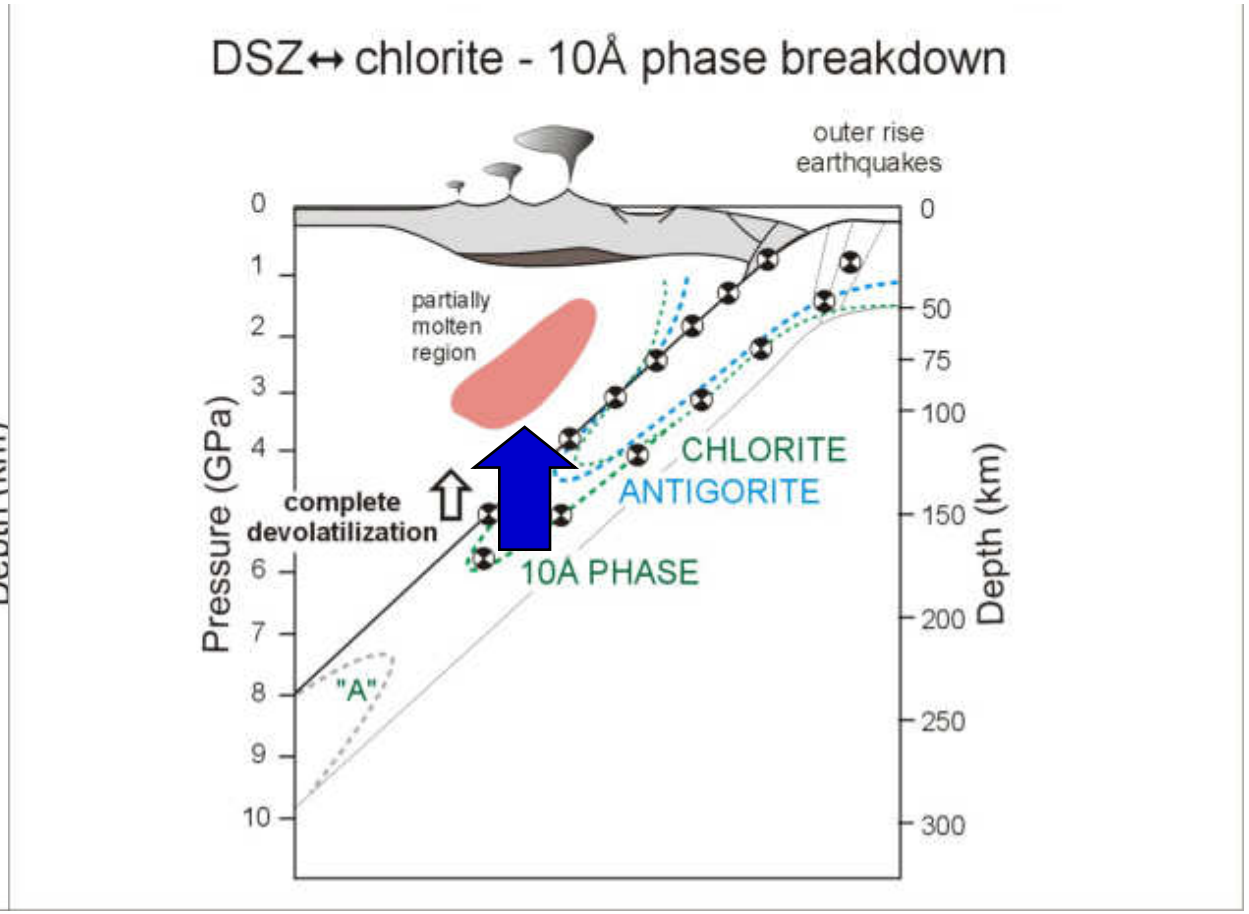

Modificata da Fumagalli and Poli, 2005

ehyond 10 A , phase A ,**phase D, phase H**

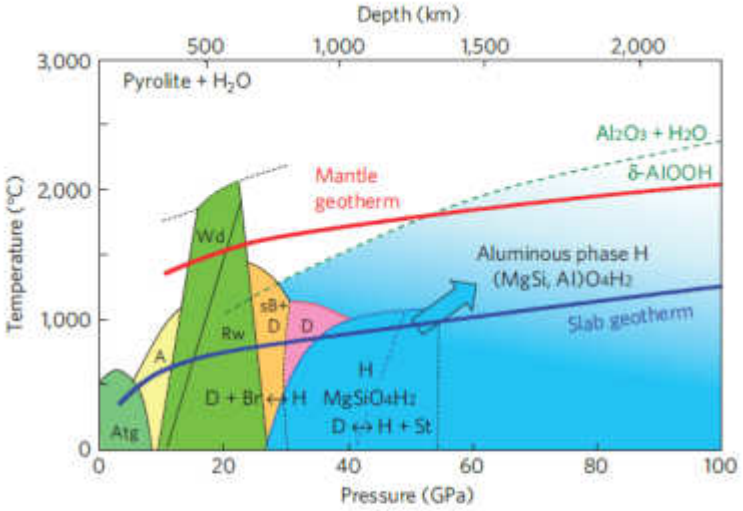

Figure 4 | Stability fields of major hydrous phases in the subducted slabs in a pyrolite +~2 wt% H_2O system. Those of δ-AlOOH (ref. 20) and aluminous phase H (H) are shown by a green dashed line and light blue region, respectively, for comparison. Coloured areas represent the regions where water is retained in the high-pressure phases. Typical in cold slabs[19] in the mantle geotherm[27] are shown by thick Atg, antigorite; A, phase A; Wd, wadsleyite; Rw, ringwoodite superhydrous phase B; D, phase D.

American Mineralogist, Volume 82, pages 651–654, 1997

Crystal structure of the dense hydrous magnesium silicate, phase D

HEXIONG YANG, CHARLES T. PREWITT, AND DANIEL J. FROST

Geophysical Laboratory and Center for High Pressure Research, Carnegie Institution of Washington, 5251 Broad Branch Road, NW, Washington, DC 20015, U.S.A.

ABSTRACT

Liu (1986, 1987) reported the diffraction pattern of a hydrous magnesium silicate resulting from the breakdown of serpentine at 22 GPa and 1000 °C and named this material "phase D." Since that time there have been several reports of the synthesis of phase D, but its confirmed composition and crystal structure have not yet been reported. We synthesized a new dense hydrous magnesium silicate at 20 GPa and 1200 °C and solved its crystal structure (R_w = 0.015 and R = 0.014). The single crystal has composition $Mg_{1.11}Si_{1.89}H_{2.22}O_6$ (ideal formula: $MgSi_2H_2O_6$), cell parameters a = 4.7453(4), c = 4.3450(5) Å, and V = 84.74(2) Å^3, and space group $P\bar{3}1m$. The crystal structure is relatively simple with all the Si occupying octahedral sites in a layer similar to that of brucite, but with one of every three octahedra vacant. The MgO_6 octahedra are located above and below each vacant octahedral site. All O-H bonding occurs between SiO_6 octahedral layers. This is the only high-pressure hydrous magnesium silicate structure reported to date that contains all octahedrally coordinated Si. The calculated density of phase D (d_{cal} = 3.50 g/cm^3) is substantially greater than any other high-pressure hydrous magnesium silicate phase.

Phase D

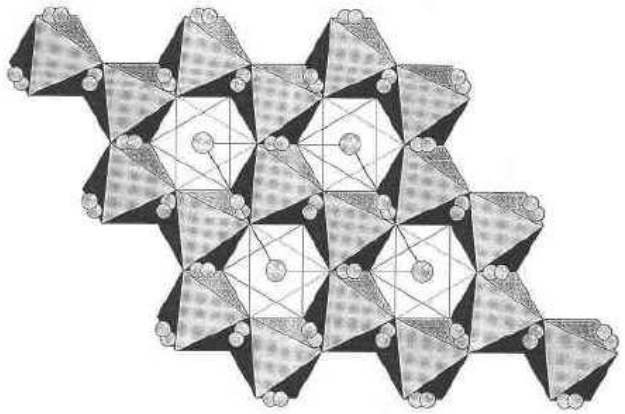

FIGURE 1. Crystal structure of phase D projected along c. Shaded and unshaded octahedra represent SiO_6 and MgO_6 octahedra, respectively. Large spheres represent Mg and small ones H.

mined by Frost and Fei (in preparation) from unit-cell volume compression data, is 200(4) GPa, the largest of all high-pressure hydrous magnesium silicates. Li and Jeanloz (1991) synthesized an assemblage of perovskite and phase D from a mixture of $Mg_{0.88}Fe_{0.12}SiO_3$ pyroxene with 4 wt% H_2O at ~40–60 GPa and ~1700 °C, which suggests that phase D is stable under lower mantle conditions. Given its large bulk modulus, high density, large

LETTERS
PUBLISHED ONLINE: 2 FEBRUARY 2014 | DOI: 10.1038/NGEO2074
nature geoscience

Stability of hydrous silicate at high pressures and water transport to the deep lower mantle

M. Nishi[1,2*], T. Irifune[1,2], J. Tsuchiya[1,2], Y. Tange[1,2], Y. Nishihara[1], K. Fujino[1] and Y.

The presence of water strongly influences the structure, composition and dynamics of the Earth's deep mantle[1–4]. Hydrous magnesium-rich silicates play an important role in transporting water into the deep mantle when oceanic plates subduct as slabs. The highest-pressure form of such hydrous silicates, phase D, was reported to dissociate into an assemblage of nominally anhydrous phases plus water at pressures of about 44 GPa, equivalent to 1,250 km depth[5]. In this way, free water would be released in the middle region of the lower mantle, which suggests that no water can reach the deeper regions of the lower mantle. Here we use *in situ* X-ray measurements in conjunction with a multi-anvil apparatus using sintered diamond anvils to show that hydrous phases are stable under lower mantle conditions up to 50 GPa. We found that phase D transforms to an assemblage with another hydrous silicate ($MgSiH_2O_4$), named phase H, at pressures above about 48 GPa. Our results suggest that phase H is the dominant hydrous silicate in descending slabs, and may be found at depths far deeper than 1,250 km. We conclude that a significant amount of water is retained in the descending slabs and may be delivered to the deepest part of the lower mantle.

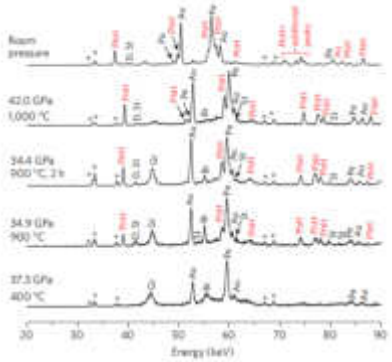

Figure 3 | Selected X-ray diffraction patterns of *in situ* observations (M1372). PhH, phase H; St, stishovite; Br, brucite; Pe, periclase; D, phase D; *, characteristic lines of Au, gold (67.0 and 68.9 keV) and La, lanthanum (33.0, 33.4 and 37.8 keV). Diffractions from the (Mg,Cr)O pressure medium (Pe, periclase) and capsule (Gr, graphite) overlap with those from the sample.

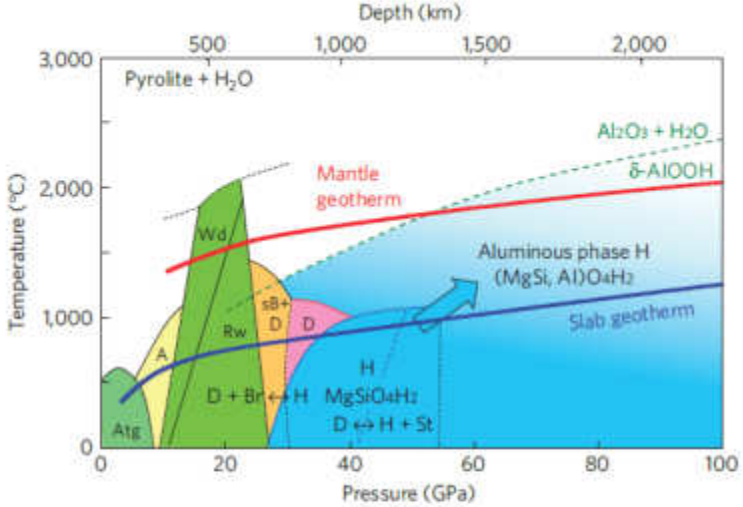

Figure 4 | Stability fields of major hydrous phases in the subducted slabs in a pyrolite +~2 wt% H_2O system. Those of δ-AlOOH (ref. 20) and aluminous phase H (H) are shown by a green dashed line and light blue region, respectively, for comparison. Coloured areas represent the regions where water is retained in the high-pressure phases. Typical temperatures in cold slabs[19] in the mantle geotherm[27] are shown by thick solid curves. Atg, antigorite; A, phase A; Wd, wadsleyite; Rw, ringwoodite; sB, superhydrous phase B; D, phase D.

Phase D trasform to Phase H at 48 Gpa

hydrous silicate, phase H, at pressures above ~48 GPa. Phase H in the descending slab may deliver a significant amount of water to the deepest part of the lower mantle thus influencing the structure and dynamics of the deep mantle.

Which the structure of phase H?

Phase X

American Mineralogist, Volume 99, pages 1802–1805, 2014

LETTER

Crystal chemistry of dense hydrous magnesium silicates: The structure of phase H, $MgSiH_2O_4$, synthesized at 45 GPa and 1000 °C

LUCA BINDI[1,2,*], MASAYUKI NISHI[3,4], JUN TSUCHIYA[3,4] AND TETSUO IRIFUNE[3,4]

[1]Dipartimento di Scienze della Terra, Università di Firenze, Via La Pira 4, I-50121 Firenze, Italy
[2]CNR, Istituto di Geoscienze e Georisorse, sezione di Firenze, Via La Pira 4, I-50121 Firenze, Italy
[3]Geodynamics Research Center, Ehime University, Matsuyama 790-8577, Japan
[4]Earth-Life Science Institute, Tokyo Institute of Technology, Tokyo 152-8550, Japan

The crystal structure of the dense hydrous magnesium silicate phase H, $MgSiH_2O_4$, synthesized at 45 GPa and 1000 °C, was investigated by single-crystal X-ray diffraction. Although showing a deterioration process under the X-ray beam, the compound was found to be orthorhombic, space group *Pnnm* ($CaCl_2$-type structure), with lattice parameters $a = 4.733(2)$, $b = 4.3250(10)$, $c = 2.8420(10)$ Å, $V = 58.18(3)$ Å^3, and $Z = 1$. The structure was refined to $R_1 = 0.0387$ using 53 observed reflections [$2\sigma(I)$ level]. Magnesium and silicon were found to be disordered at the same octahedral site (with a mean bond distance of 1.957 Å). Hydrogen was not located in the difference Fourier maps, but it is very likely disordered at a half-occupied 4*g* position. The centrosymmetric nature of the structure of phase H is examined in relation to that reported for pure δ-AlOOH at ambient conditions (non-centrosymmetric, $P2_1nm$), and the possibility that these two compounds can form a solid solution at least at high pressure is discussed.

Keywords: Phase H, dense hydrous magnesium silicates, lower mantle, crystal structure, synthesis

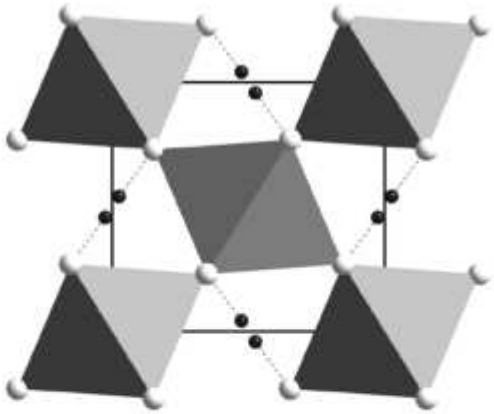

FIGURE 3. The crystal structure of phase H down [001]. The horizontal direction is the *a* axis. Gray polyhedra refer to (Mg,Si)-O octahedra; white circles refer to oxygen atoms, whereas the hydrogen atoms (small black circles) have been tentatively drawn at the Wyckoff position 4*g* (0.475, 0.042, 0) and bonded (dashed lines) to oxygen. The fact that hydrogen is half occupied does impede the formation of the unrealistic H–H distance of 0.43 Å.

t it crystallizes with the $CaCl_2$-type structure, *Pnnm* space

Struttura tipo diasporo delta

SCIENTIFIC REPORTS

OPEN

Crystal structure, equation of state, and elasticity of phase H ($MgSiO_4H_2$) at Earth's lower mantle pressures

Received: 23 March 2015
Accepted: 18 September 2015
Published: 23 October 2015

Jun Tsuchiya[1,2] & Mainak Mookherjee[3,4]

Dense hydrous magnesium silicate (DHMS) phases play a crucial role in transporting water in to the Earth's interior. A newly discovered DHMS, phase H ($MgSiO_4H_2$), is stable at Earth's lower mantle, i.e., at pressures greater than 30 GPa. Here we report the crystal structure and elasticity of phase H and its evolution upon compression. Using first principles simulations, we have explored the relative energetics of the candidate crystal structures with ordered and disordered configurations of magnesium and silicon atoms in the octahedral sites. At conditions relevant to Earth's lower mantle, it is likely that phase H is able to incorporate a significant amount of aluminum, which may enhance the thermodynamic stability of phase H. The sound wave velocities of phase H are ~1–4% smaller than those of isostructural δ-AlOOH. The shear wave impedance contrast due to the transformation of phase D to a mixture of phase H and stishovite at pressures relevant to the upper part of the lower mantle could partly explain the geophysical observations. The calculated elastic wave velocities and anisotropies indicate that phase H can be a source of significant seismic anisotropy in the lower mantle.

P (GPa)	ρ (g/cm³)	a (Å)	b (Å)	c (Å)	γ (°)	r_{O-H} (Å)	$r_{O\cdots O}$ (Å)	MgO_6 (Å³)	SiO_6 (Å³)
0	3.338	4.786	4.328	2.948	93.3	1.039	2.580	12.1	8.1
10	3.547	4.689	4.230	2.797	92.9	1.071	2.481	11.3	7.8
20	3.720	4.620	4.157	2.754	92.6	1.115	2.419	10.7	7.5
25	3.797	4.590	4.126	2.735	92.8	1.168	2.394	10.8	7.4
30	3.865	4.567	4.100	2.718	92.7	1.182	2.382	10.2	7.3
40	3.986	4.523	4.042	2.686	92.4	1.183	2.365	9.8	7.2
50	4.098	4.484	4.027	2.658	92.2	1.175	2.350	9.5	7.0
60	4.202	4.449	3.996	2.632	92.0	1.169	2.338	9.2	6.9
70	4.300	4.418	3.968	2.609	92.0	1.163	2.325	9.0	6.7
80	4.393	4.389	3.943	2.587	92.7	1.157	2.314	8.7	6.6
90	4.481	4.362	3.919	2.567	93.4	1.152	2.303	8.5	6.5
100	4.565	4.338	3.897	2.548	93.5	1.146	2.293	8.4	6.4

Table 1. Cell parameters, hydroxyl (r_{O-H}) bond distances, oxygen-oxygen ($r_{O\cdots O}$) bond distances, and polyhedral volumes of phase H (model-1) as a function of pressure.

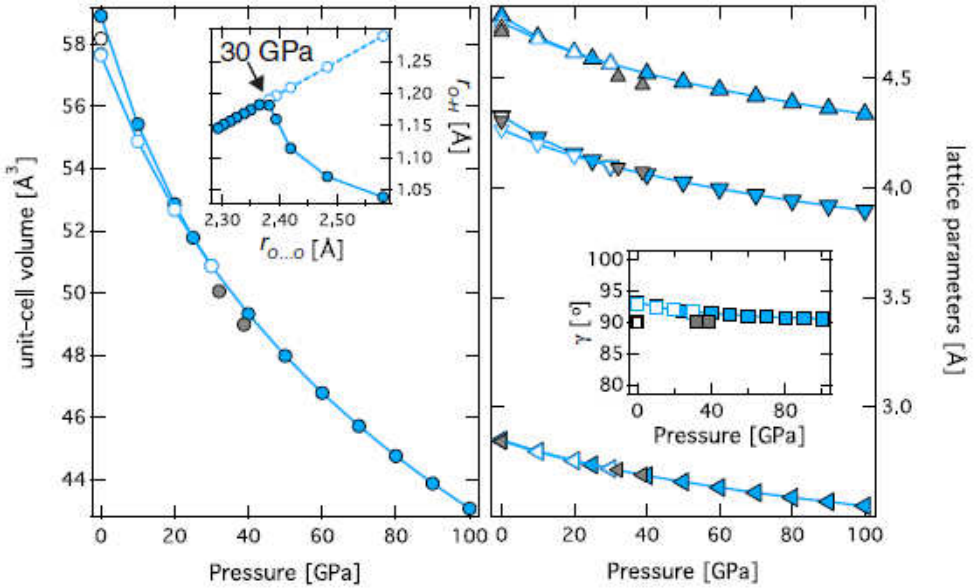

Figure 2. Pressure dependence of unit-cell volume and lattice parameters. The left panel shows the plot of unit-cell volume as a function of pressure for phase H with ordered Mg and Si atoms (model-1) (light blue filled symbol). Also, shown are the metastable extensions of unit-cell volume for the symmetric hydrogen bonded structure (light blue open symbols). Inset shows the plot of r_{O-H} as a function of $r_{O\cdots O}$, at around 30 GPa, r_{O-H} becomes (1/2) of $r_{O\cdots O}$, i.e., hydrogen bond symmetrizes. The right panel shows the plot of the ***a***-, ***b***-, and ***c***-axes as a function of pressure. Inset shows the plot of γ as a function of pressure. For comparison, the experimental results are also plotted (open symbols)[18] and (grey filled symbols)[19].

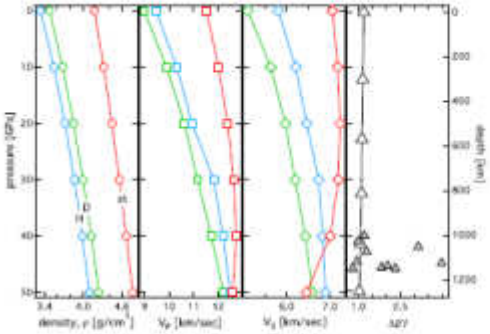

Figure 5. Density, velocity, and impedance contrast. Plot of (a) density, (b) primary wave velocity (V_P), and (c) shear wave velocity (V_S) vs. pressure for phase H (model-1) (H: light blue open symbols), phase D (D: light green open symbol), and stishovite (st: red open symbols). (d) plot of impedance contrast (ΔI/I) (open triangles) defined as the sum of shear velocity contrast and density contrast[44] across the reaction phase D = phase H + stishovite. Also shown are the depth dependent impedance contrasts from seismological observations (filled grey triangles)[11].

Sulfosalts

Complex salts:
(analogue of oxysalts = simple cation + complex anion $(MeO_m)^{n-}$

$$(Me^{+}, Me^{2+}, etc.)_x\ [(Bi, Sb, As)^{3+}, Te^{4+}]_y\ [(S, Se, Te)^{2-}]_z$$

Important for:

Extraction of (Cu, Pb, Ag, Fe) metals

Photovoltaic cell

Photo-voltaic materials beyhod c-Si

CdTe and CIGS($CuIn_{1-x}Ga_ySe_yS_{2-y}$) absorber systems hav been developed for thin-film PV (photovoltaic) devices, instead of silicon because they absorb light more strongly (directly instead of indirectly) but…

They are limited in the long-term by the scarsity of Te,Ga, In.

Cd is toxic

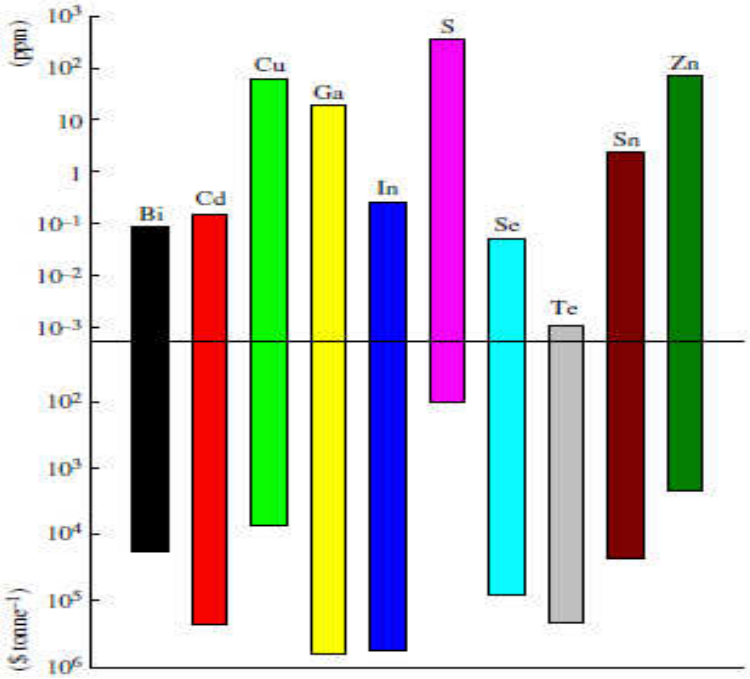

Figure 1. Occurrence in the Earth's crust and current costs of some of the elements relevant to thin-film photovoltaics. Note that logarithmic scales have been used for both y axes. Current technologies include copper indium gallium diselenide (CIGS) and cadmium telluride (CdTe). Promising alternatives include copper zinc tin sulphide (CZTS). (Online version in colour.)

http://rsta.royalsocietypublishing.org/content/369/1942/1840.figures-only

New photovoltaic generation characteristics:

Optimal band gap (E_g = 1.4-1.5 eV)
High absorption coefficient in the visible range (about 10^4 cm^{-1})
High power conversion efficiency (theoretical limit 30%)
Earth-abundant
Low cost
Non toxic costituent

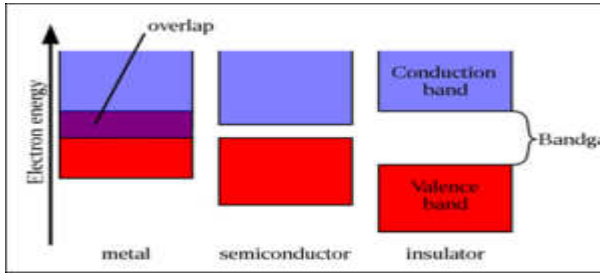

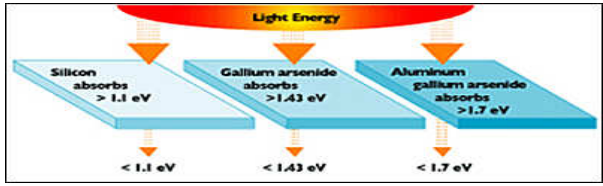

http://energyeducation.ca/encyclopedia/Conduction_band

New materials

quaternary semiconductor -CZTS

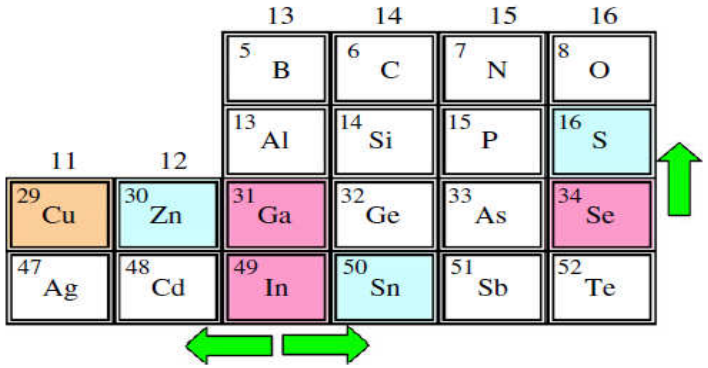

Figure 13. Section of the periodic table showing the logic of changing from CuIn(Ga)Se; Cu_2ZnScS_4 by moving from group 13 to groups 12 and 14. (Online version in colour.)

CZTS = Kesterite = Cu_2ZnS

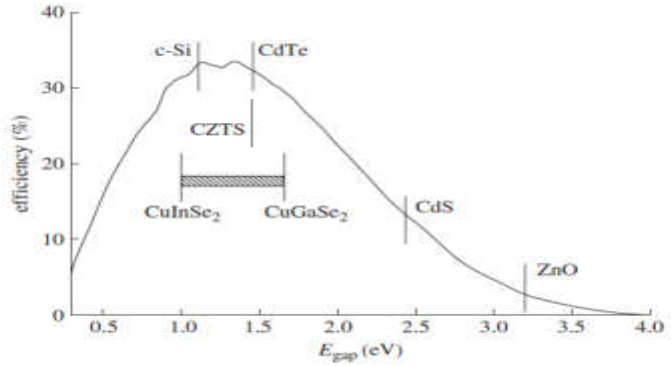

Figure 5. Maximum theoretical efficiency (Shockley–Queisser limit) for solar cells under AM illumination without concentration. The bandgaps of absorber materials (c-Si, CdTe, CIGS, CZ and window materials (CdS, ZnO) are shown for comparison. Note that the bandgap of the CI system can be tuned by controlling the In/Ga ratio.

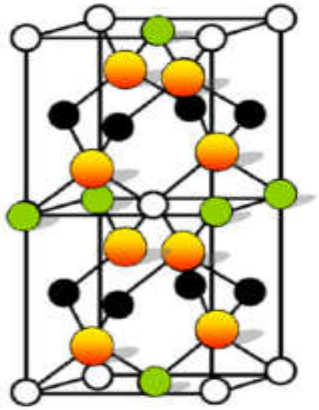

Figure 14. Crystal structure of copper zinc tin sulphide (CZTS), which is a promising sustainable alternative to CIGS [31]. Black filled circles, Cu; open circles, Sn; green circles, Zn; orange circles, S. (Online version in colour.)

http://rsta.royalsocietypublishing.org/content/369/1942/1840.figures-only

Alternative ……..ternary copper sulfides based on Cu-Bi-S or Cu-Sb-S type materials

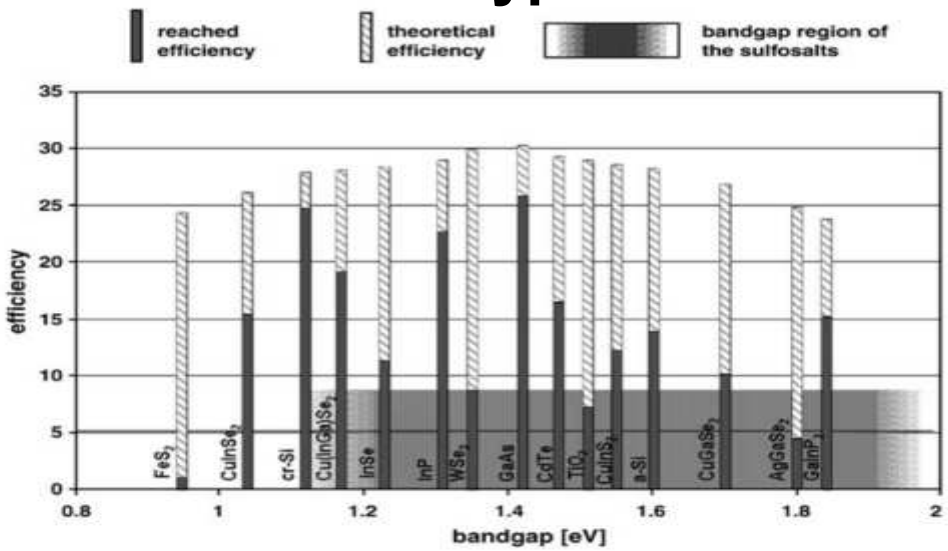

Fig. 2. Bandgap region of sulfosalts compared to standard photovoltaic materials.

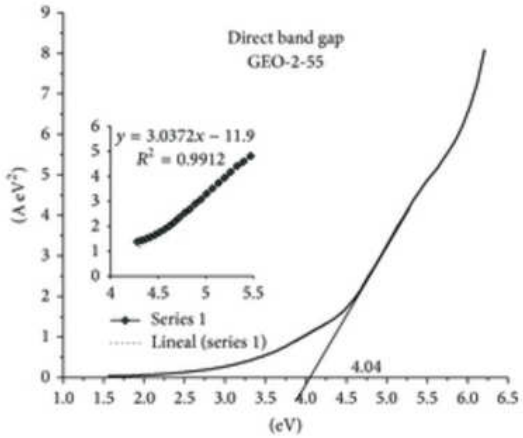

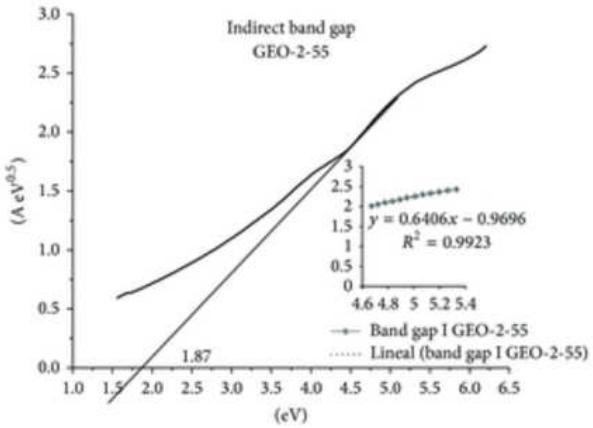

Cite this: *Phys. Chem. Chem. Phys.*, 2012, **14**, 7229–7233

www.rsc.org/pccp **PAPER**

Structural and electronic properties of $CuSbS_2$ and $CuBiS_2$: potential absorber materials for thin-film solar cells

Jesse T. R. Dufton, Aron Walsh, Pooja M. Panchmatia, Laurie M. Peter, Diego Colombara and M. Saiful Islam*

Received 19th January 2012, Accepted 27th March 2012
DOI: 10.1039/c2cp40916j

ELSEVIER

Available online at www.sciencedirect.com
ScienceDirect

Thin Solid Films 515 (2007) 5745 – 5750

www.elsevier.com/locate/tsf

Sulfosalts — A new class of compound semiconductors for photovoltaic applications

Herbert Dittrich *, Anna Bieniok, Uwe Brendel, Michael Grodzicki, Dan Topa

Department of Materials Science, Div. of Mineralogy, University of Salzburg, Hellbrunnerstr. 34, A-5020 Salzburg, Austria

Available online 1 February 2007

https://www.researchgate.net/publication/277348515_Photocatalytic_Activity_in_Phenol_Removal_of_Water_from_Graphite_and_Graphene_Oxides_Effect_of_Degassing_and_Chemical_Oxidation_in_the_Synthesis_Process/figures?lo=1

Lone electron pair

a **lone pair** refers to a pair of valence electrons that are not shared with another atom and is sometimes called a **non-bonding pair**.

As^{3+}, Sb^{3+},Bi^{3+},Sn^{2+},Ge^{2+} required an usually asymmetrically situated structural space for their non bonding s^2 pair.
The degree of sterochemical activity of the lone pair (namely the influence of the lone pair in the relative spatial arrangement of atoms in a structure) varies with the species (decreasing with increasing Z, lower with Bi and higher with Sb) and with structure type

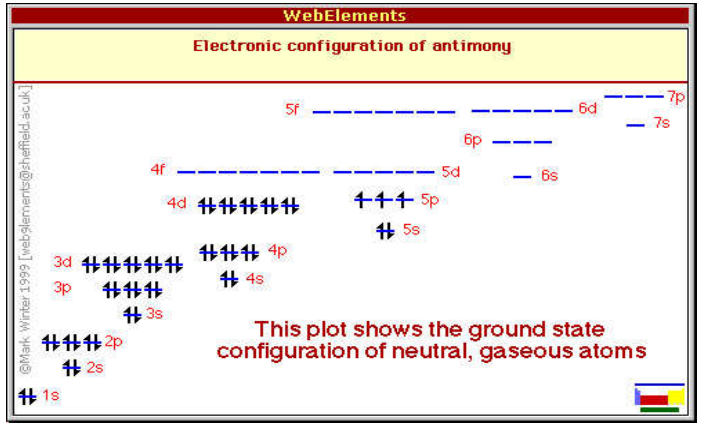

Chalcostibite $CuSbS_2$

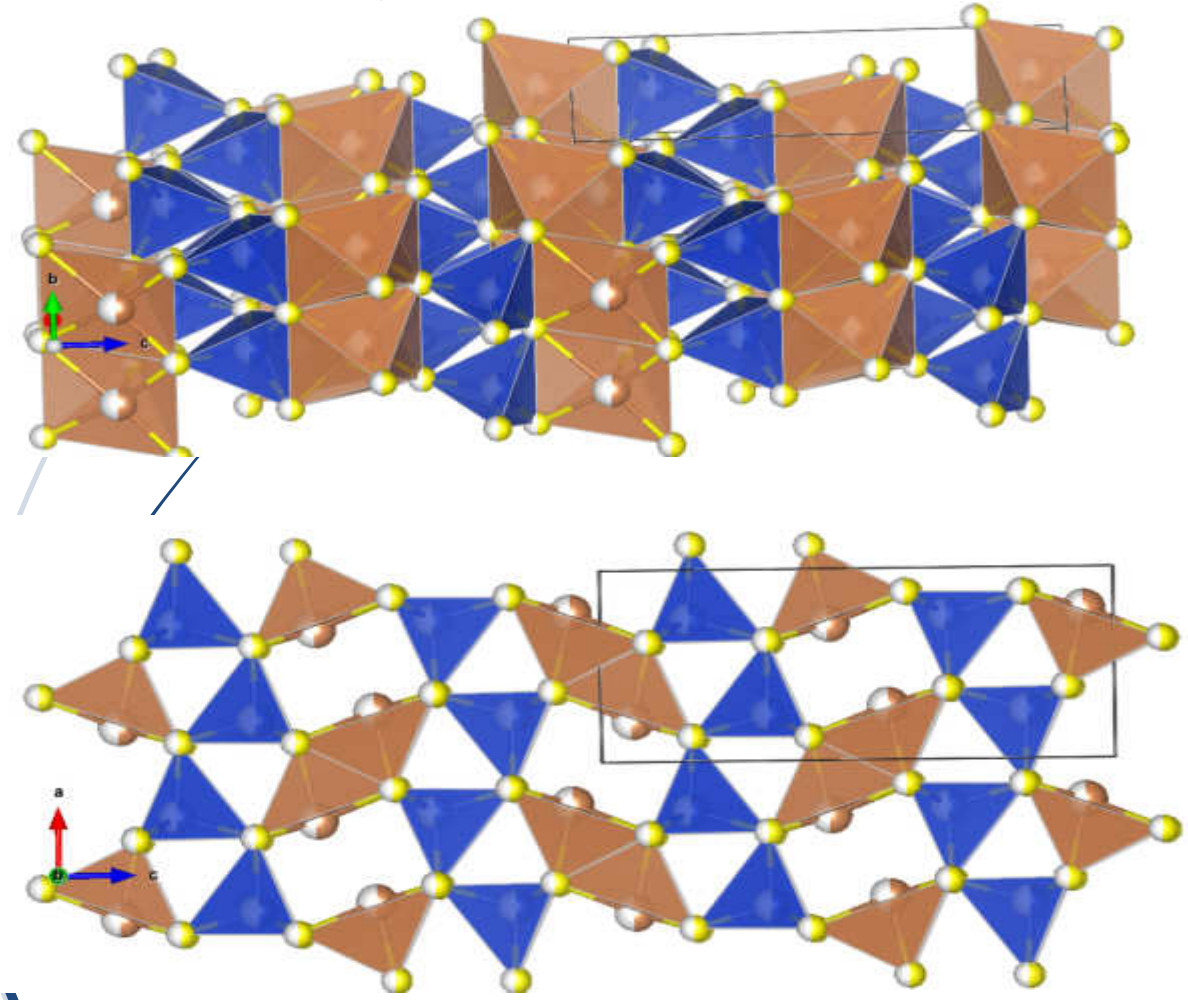

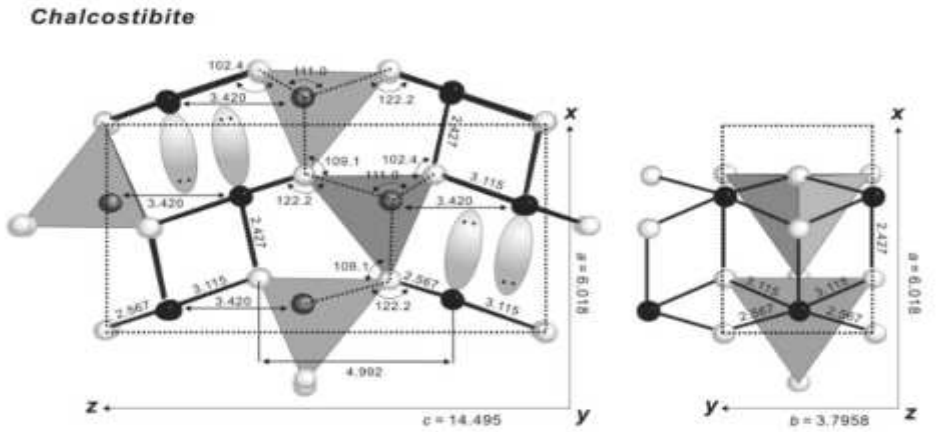

FIGURE 1. Projection of the crystal structure of chalcostibite parallel to [010] and [001] showing CuS_4 tetrahedra (gray) and Sb-S bonds in the SbS_5 square pyramid (bold stick). The white and black spheres represent S and Sb atoms, respectively. Lone-pair electrons are shown schematically. Interatomic distances and angles are given in Å and degrees, respectively.

Emplectite $CuBiS_2$

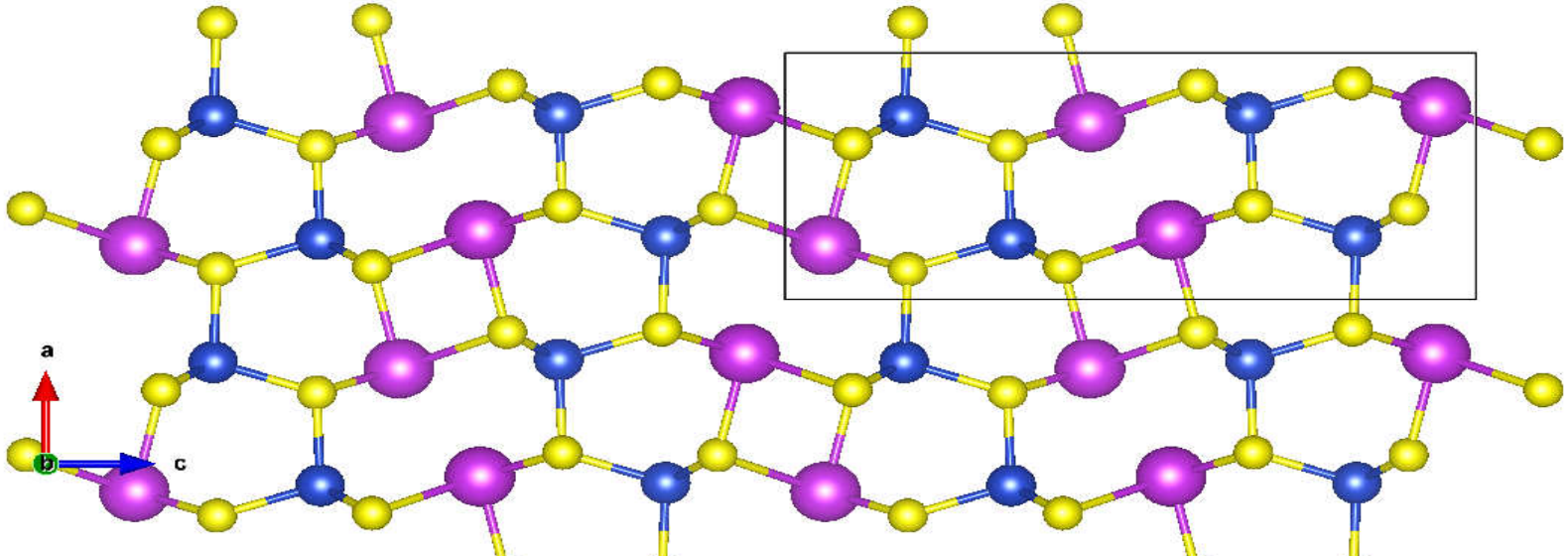

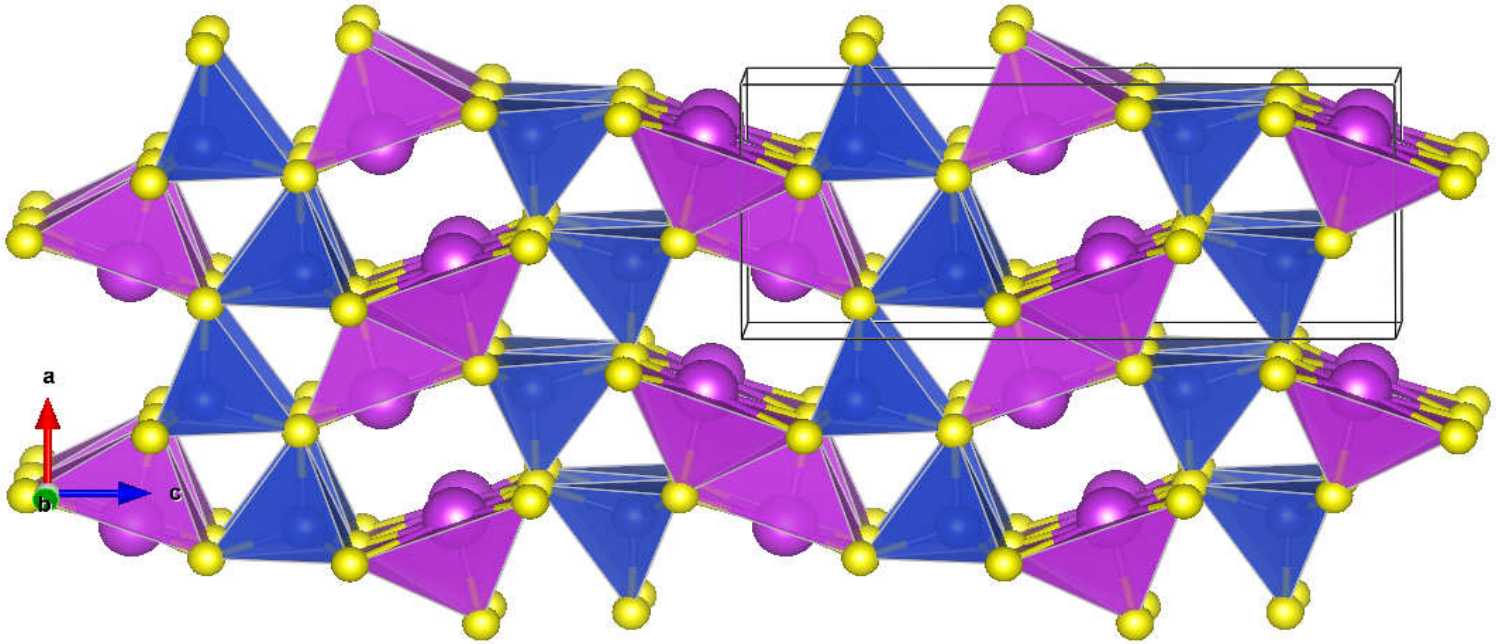

SnS- archetype
Herzenbergite (mineral)

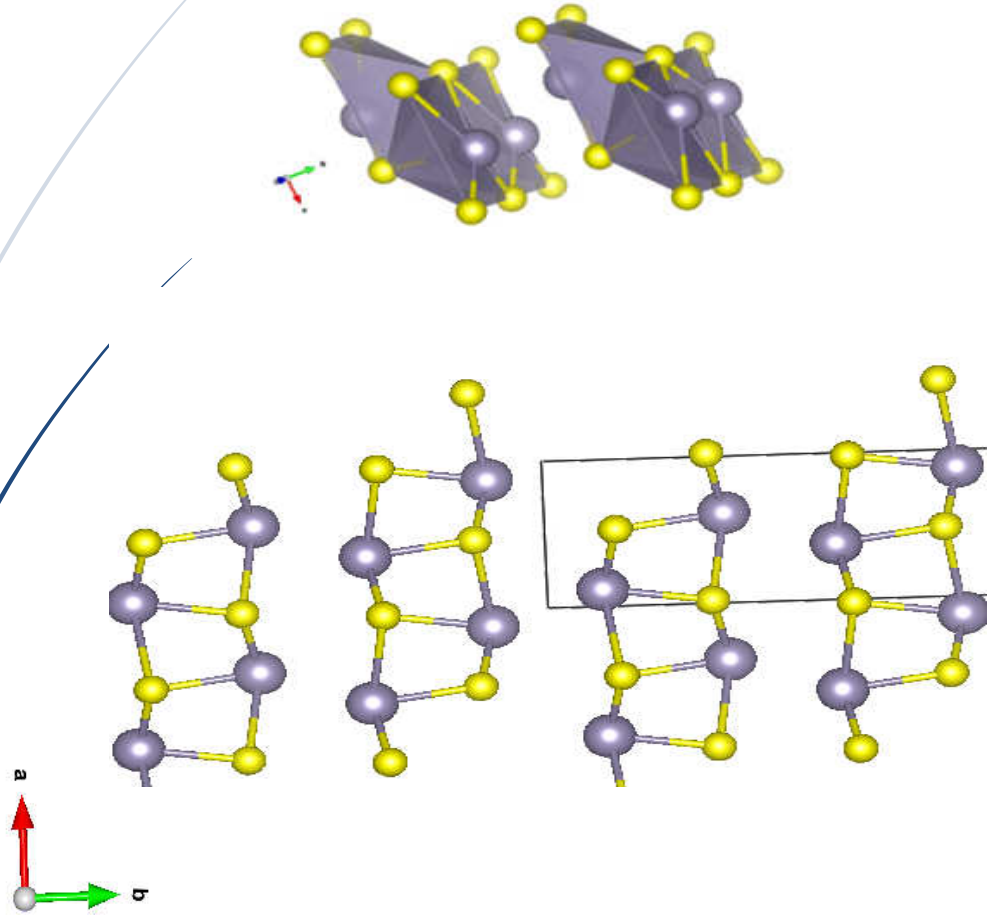

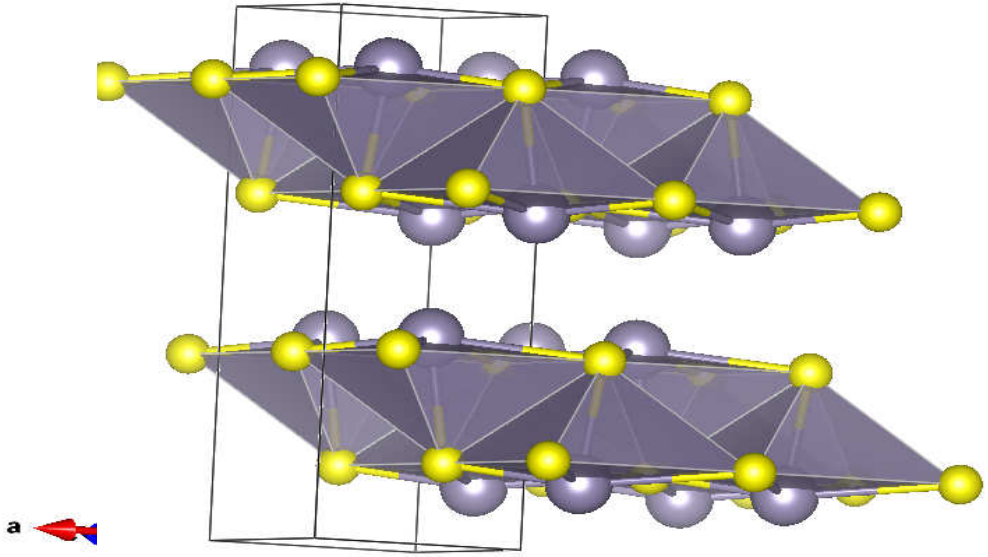

Table 1. Coordination numbers and hybridization types for the cations commonly occurring in chalcogenides.

CN	Type of Hybridization	Category
2	sp; p^2	Cu^+, Cu^{2+}, Ag^+, Hg^{2+}
3	sp^2	Cu^+, Ag^+
3	p^3	As^+, Sb^{3+}, Bi^{3+}, Pb^{2+}
4	sp^3	Cu^+, Ag^+, Au^+; Zn^{2+}, Cd^{2+}, Hg^{2+}; Ga^{3+}, In^{3+}, Tl^{3+}; Ge^{4+}, Sn^{4+}; As^{5+}, Sb^{5+}; Mn_H^{2+}, Fe_H^{2+}
4 (sq)	dsp^2	Fe_H^{3+}, Co_H^{3+}, Ni_H^{2+}, Ni_H^{3+}, Pd^{2+}, Pt^{2+}, Cu^{2+}
5	dsp^3 p^3d^2	Ni_L^{2+} Sb^{3+}, Bi^{3+}; Pb^{2+}
6	d^2sp^3 sp^3d^2 p^3; d^2sp^3	Fe_L^{2+}, Fe_L^{3+}, Co_L^{3+}, Ni_L^{4+}, Pt_L^{4+} Sn^{4+} Pb^{2+}; Bi^{3+} (Sb^{3+})

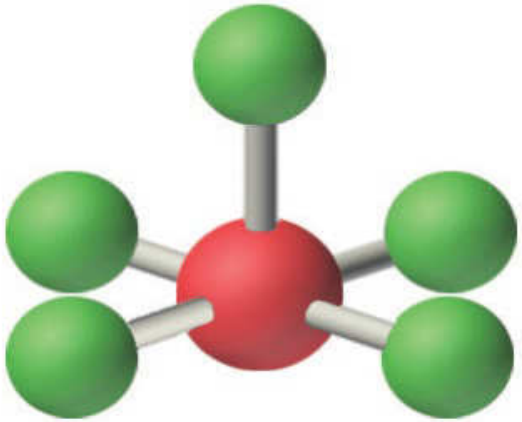

High pressure study of chalcostibite: **why**

-Pressure can change structure and structural properties

- LEP evolution with P
-LEP effect on the baric behaviour

-Pressure is an important parameter which could be used to tune
-the thermoelectric properties of materials

Thermoelectric efficiency
Seebech effect = converting T to current
Peltier effect = converting current to T
Thomson effect = conductor heating/cooling
All material have a non zero thermoelectric effect, but quite small to be useful.

explore the physical prorperties as a means of improving its photovoltaic performance

Journal of Materials Chemistry A

ROYAL SOCIETY OF CHEMISTRY

PAPER

View Article Online
View Journal | View Issue

CrossMark

Cite this: *J. Mater. Chem. A*, 2017, 5, 3249

The impact of lone-pair electrons on the lattice thermal conductivity of the thermoelectric compound $CuSbS_2$

Baoli Du,[*ab] Ruizhi Zhang,[b] Kan Chen,[b] Amit Mahajan[b] and Mike J. Reece[*b]

High pressure study of chalcostibite: **where**

Experiment @GSECAR-BM13

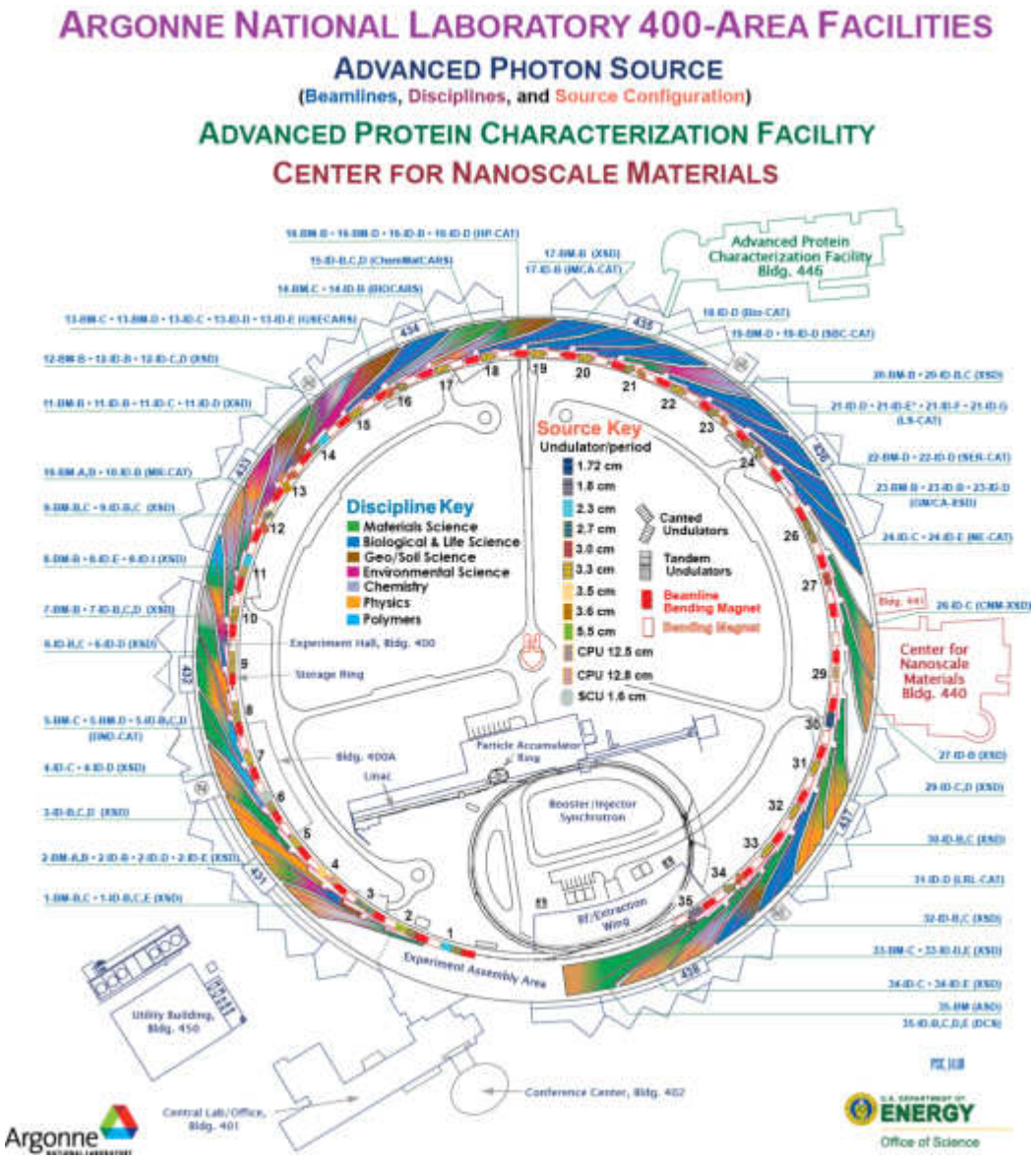

http://comptech.compres.us

High pressure study of chalcostibite: **how**

ETH-type DAC with diamond backing plates

600 μm diamond culet

pre-indented rhenium gasket with a 250 μm hole

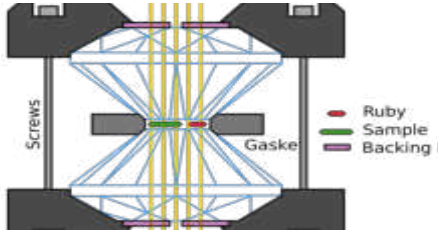

ruby chip and a gold crystal as internal pressure calibrants.

Ne as P trasmitting medium

Multi-samples mounting

High pressure study of chalcostibite: **how**

fixed wavelength of 0.3344 *Å*

MarResearch Mar165 detector calibrated for sample-to
detector distance, tilting and distortion by the

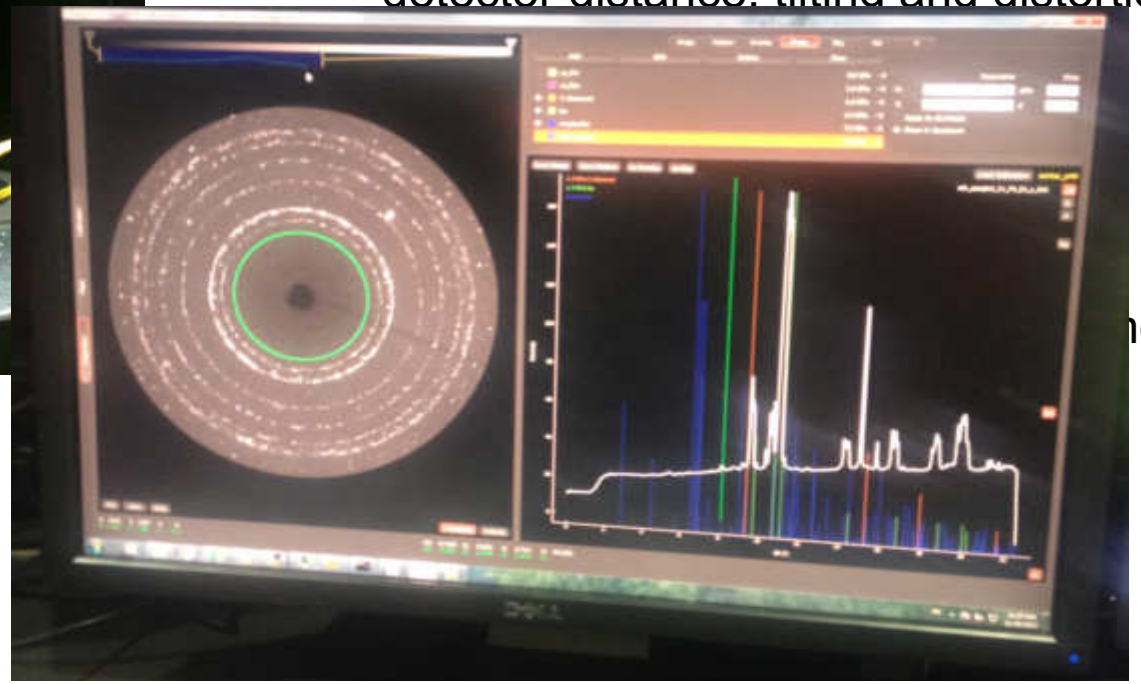

nega-axis

Atrex –RSV software

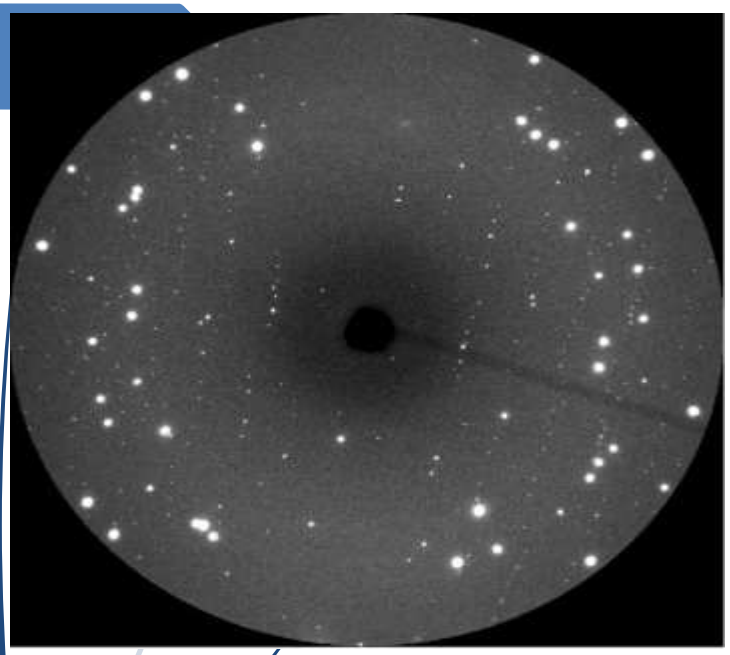

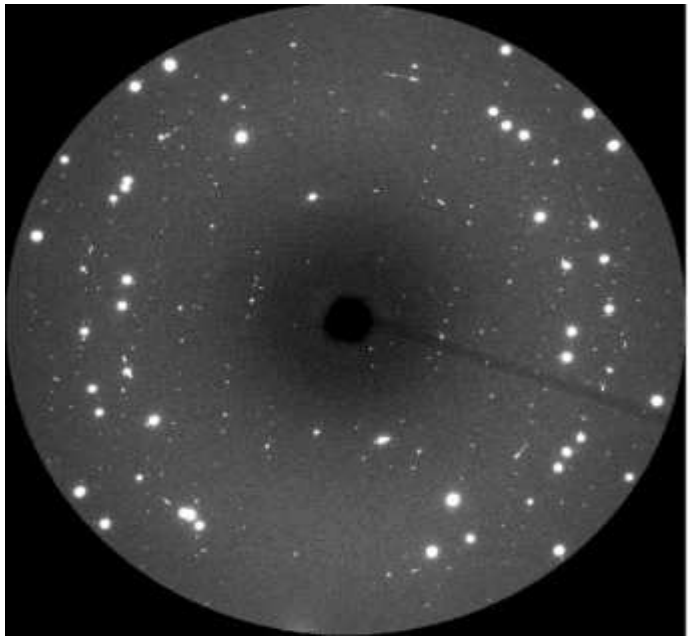

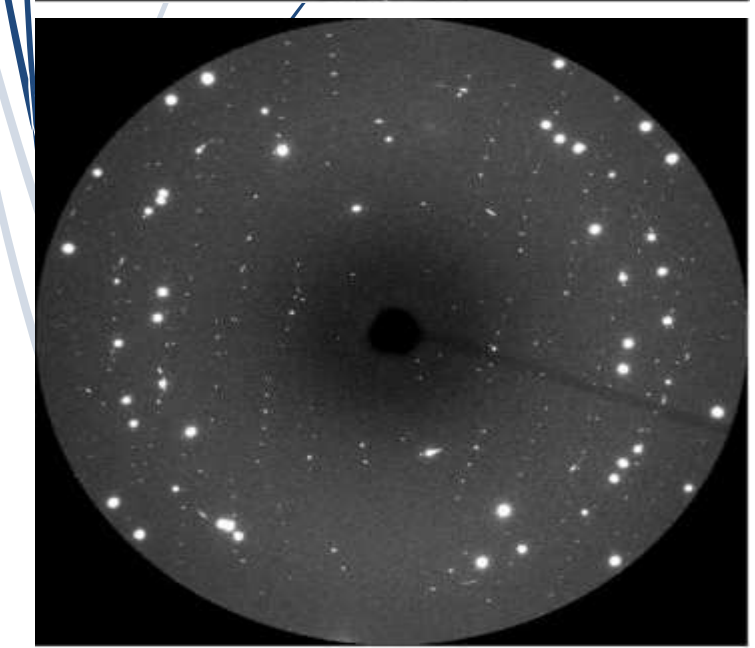

GSE_ADA/RSV is a free software package for custom analysis of single-crystal micro X-ray diffraction (SCμXRD) data,

samples enclosed in diamond anvil cells

The package has been in extensive use at the high pressure beamlines @ APS

The software is optimized for processing of wide-rotation images and includes a variety of peak intensity corrections to make data management from SCμXRD easier and more reliable.

Results - EOS

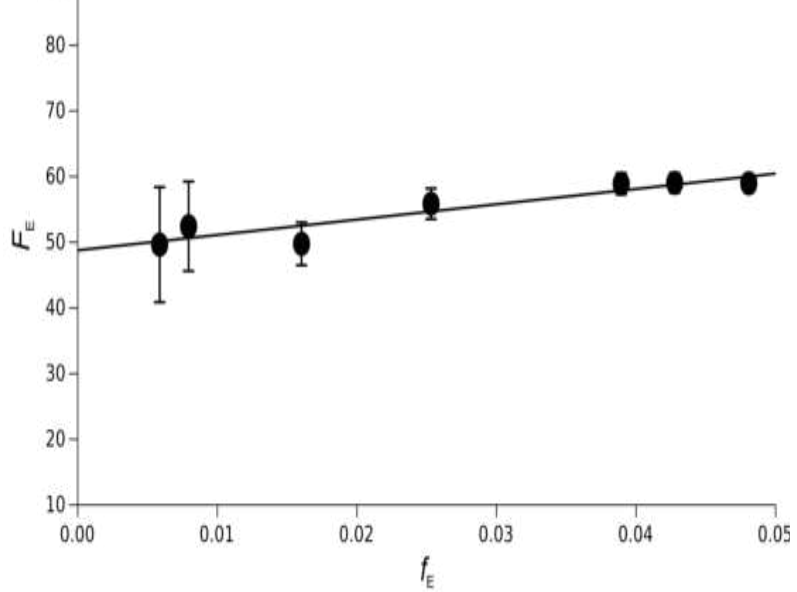

Figure 3d

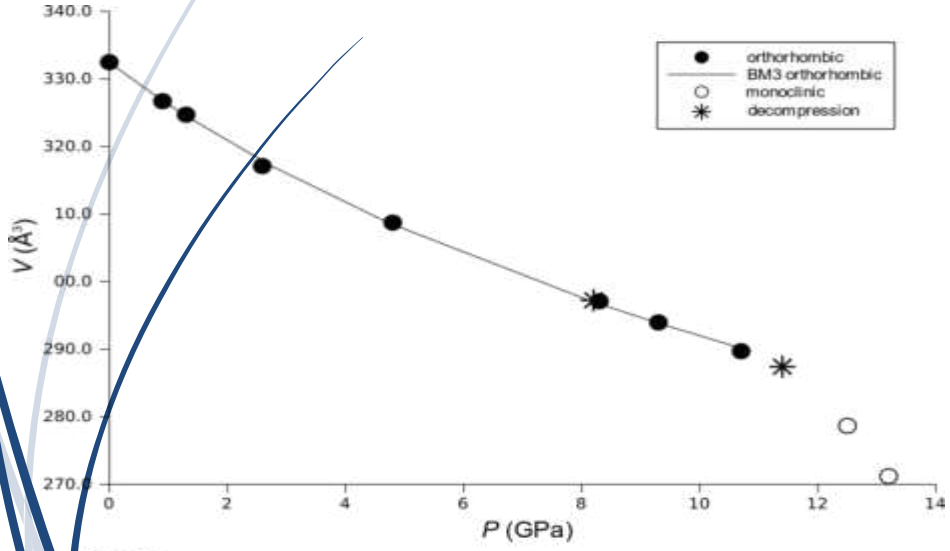

Figure 2b

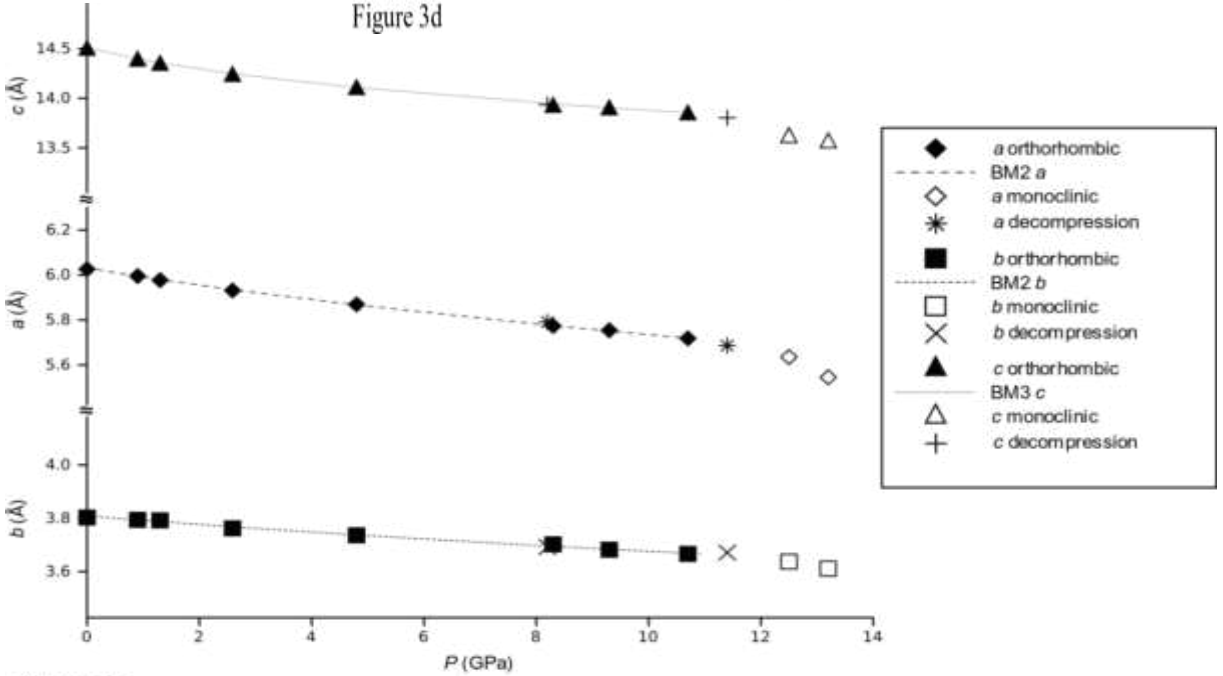

Figure 2a

Evolution of Sb eccentricity with pressure

(Ivton software, Balic-Zunic, 2007)

Sb-coordination polyhedron = 5+2
At HP:
 short distance stay constants
Long distance decreasing

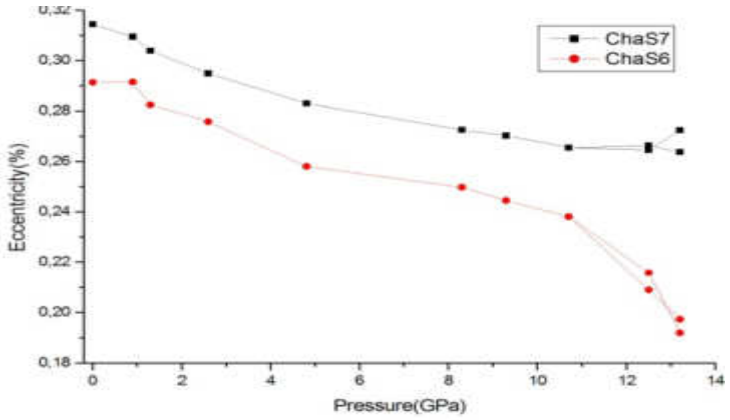

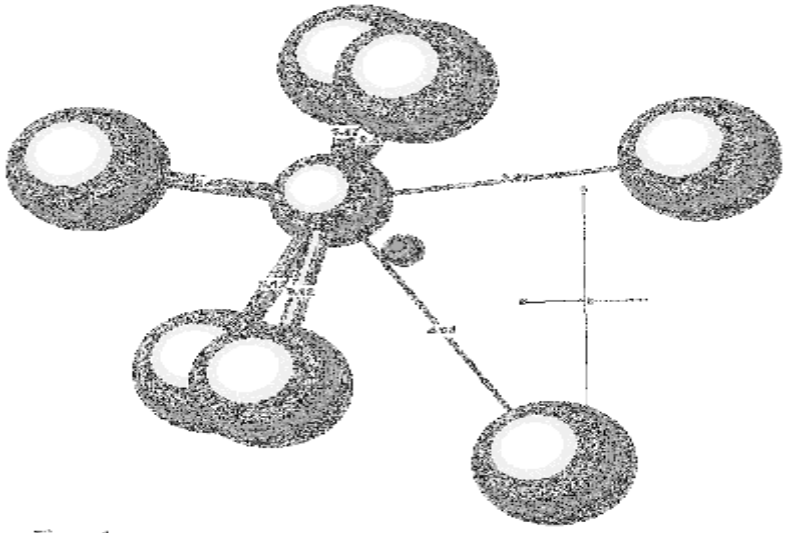

Figure 4a

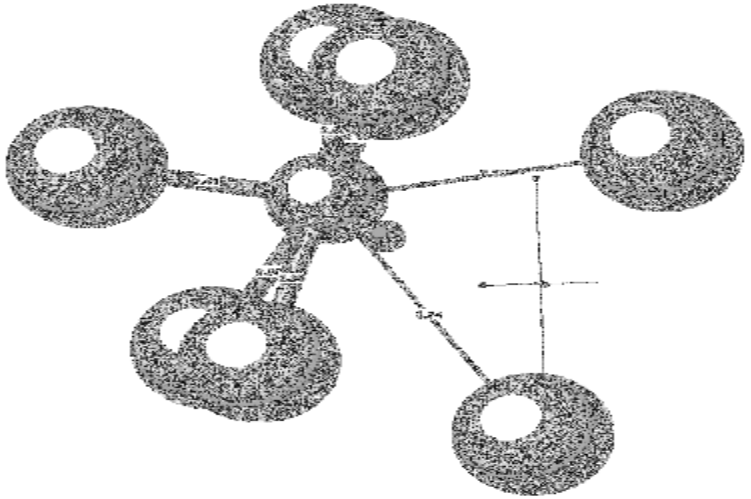

Figure 4b

Sphericity evolution with P

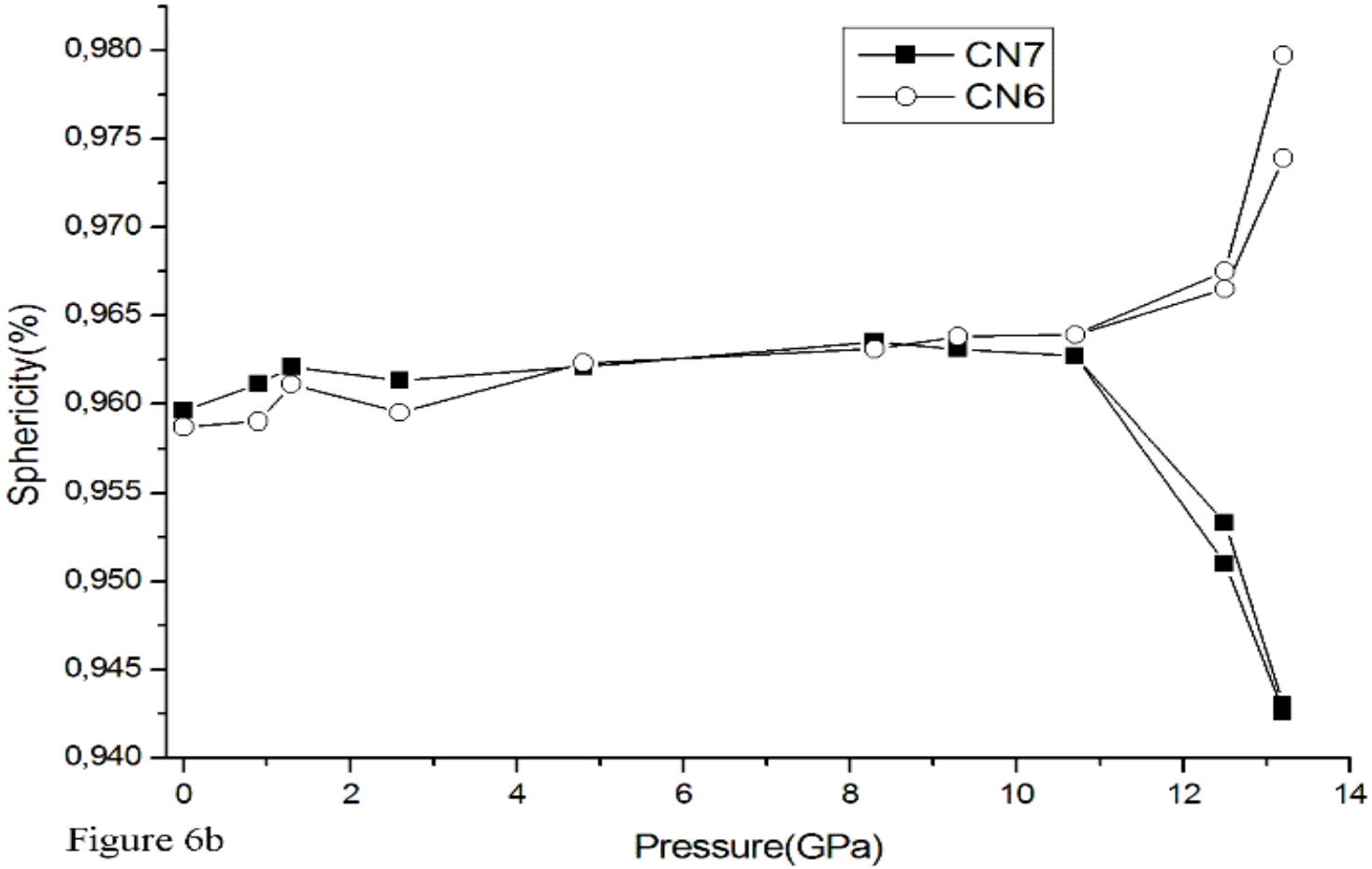

Figure 6b

Movement of LEP of Sb closer to the parent atom with P up to 12 GPa

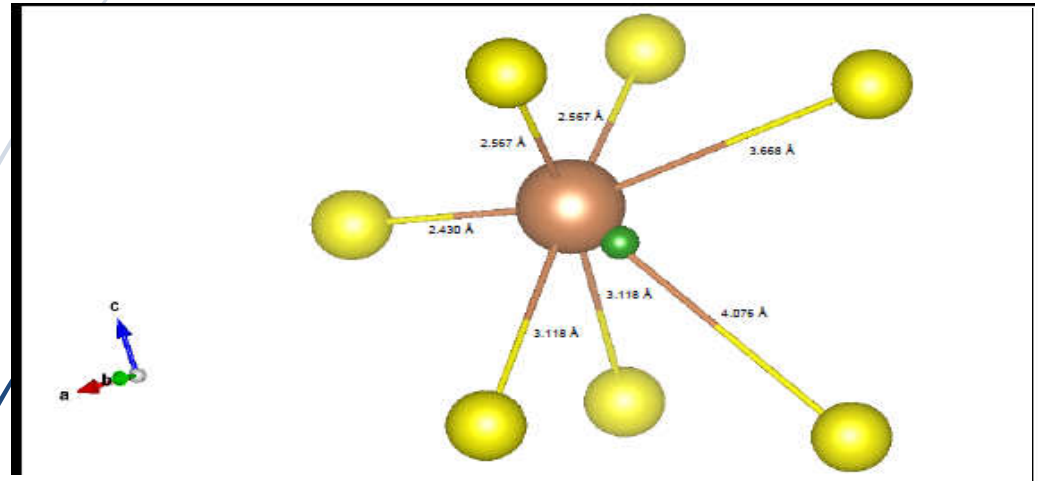

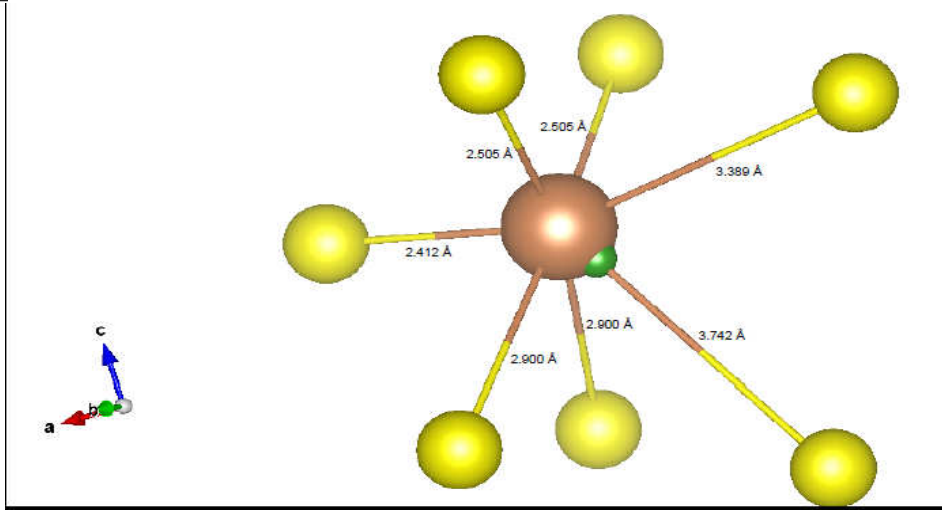

✓-chalcostibite

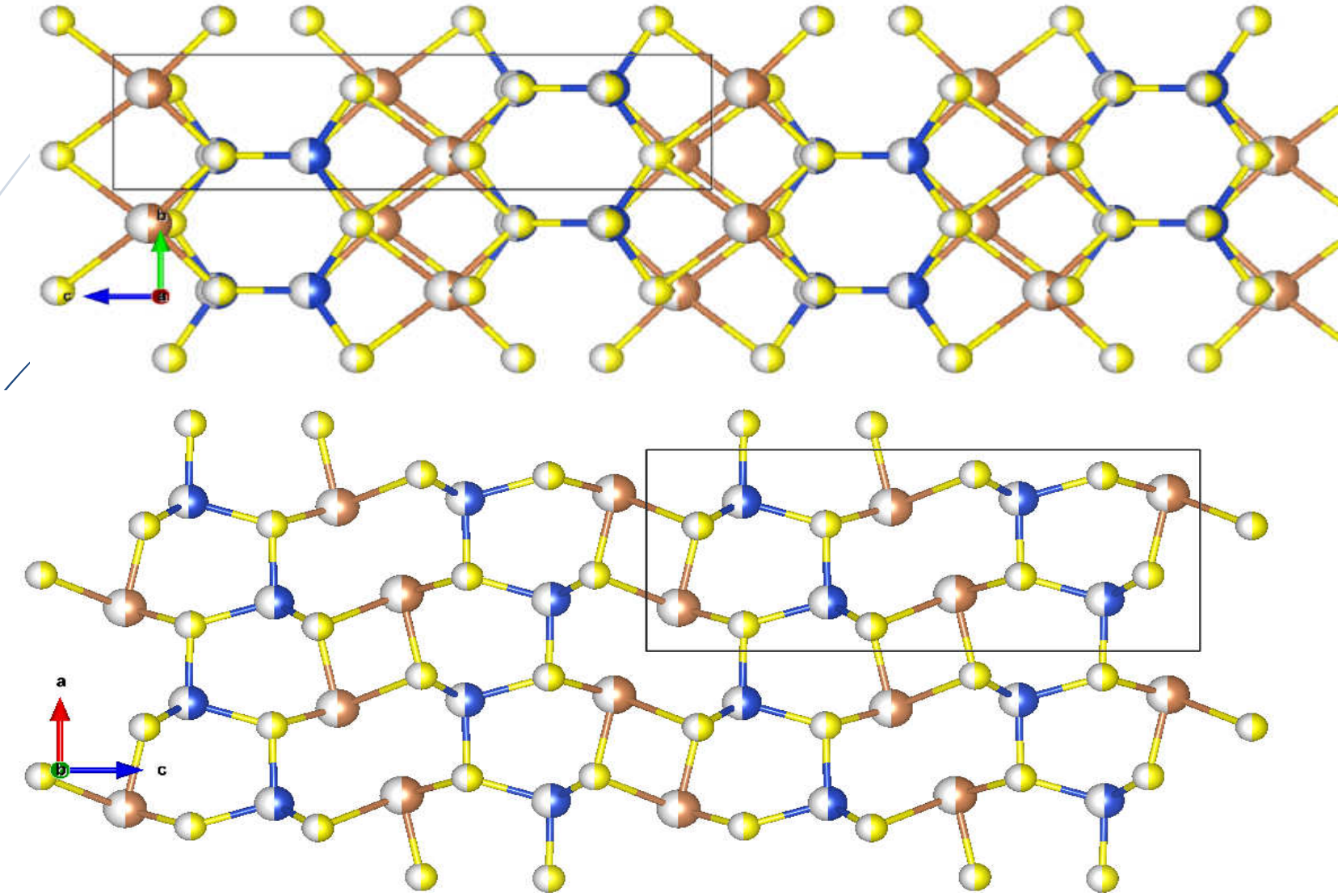

✓-β transition Sb CN from 5 + 2 to 6

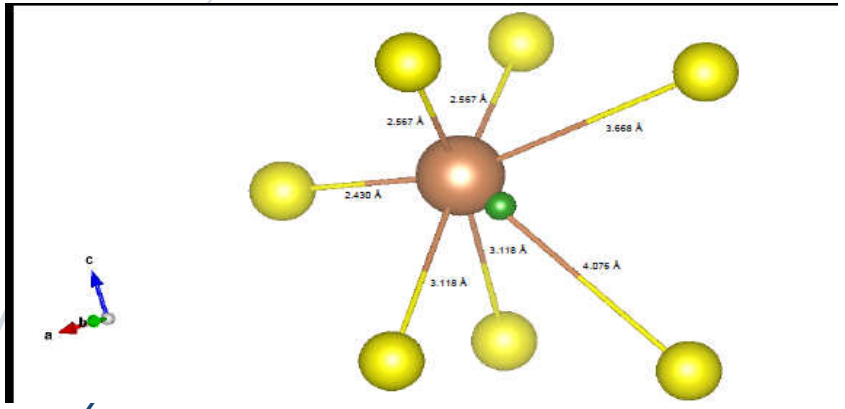

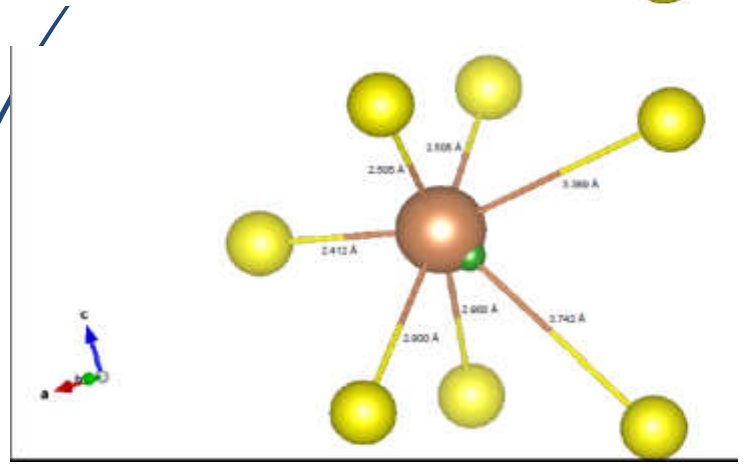

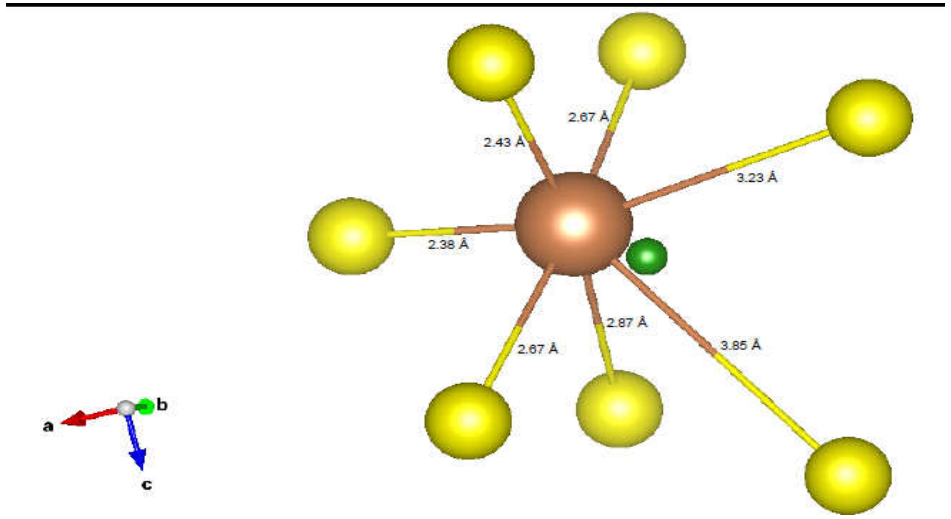

Along [100]

Cu^{+1} change coordination from IV to V

at the transition relative displacement of SnS-like slabs paraller to (001), at 13.5 the dispacemement is about 2 A.

This way the Cu change coordination from 4 to 5 , note the change of distance in red

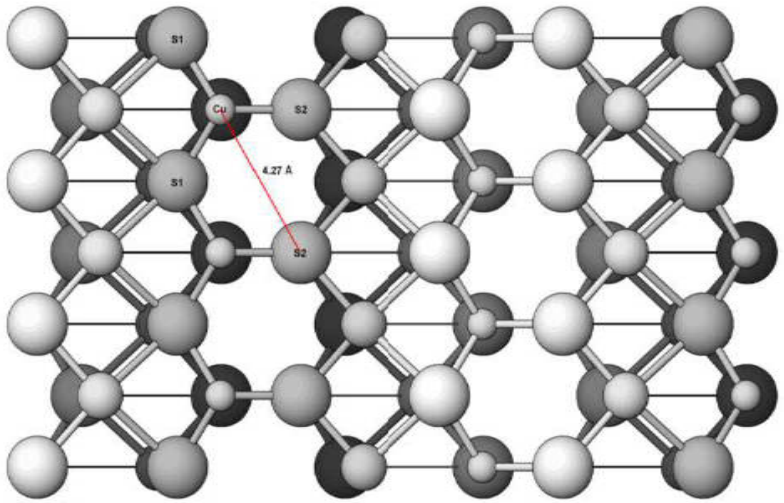

Figure 5a

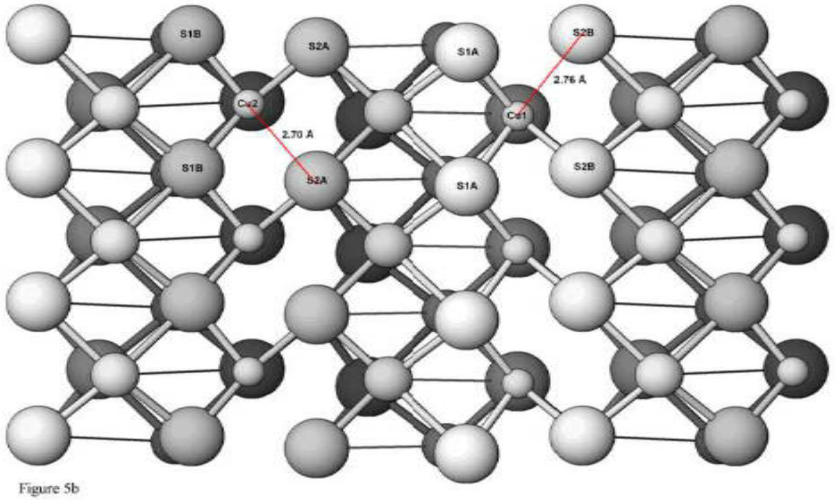

Figure 5b

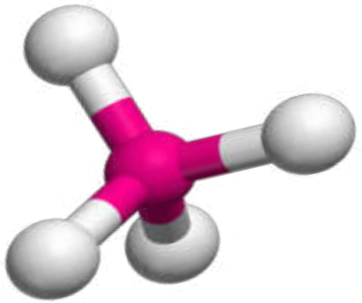

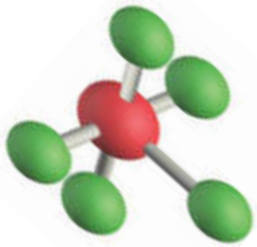

b

c

@ the transition increases the Sb coordination from 5+2 to 6+1

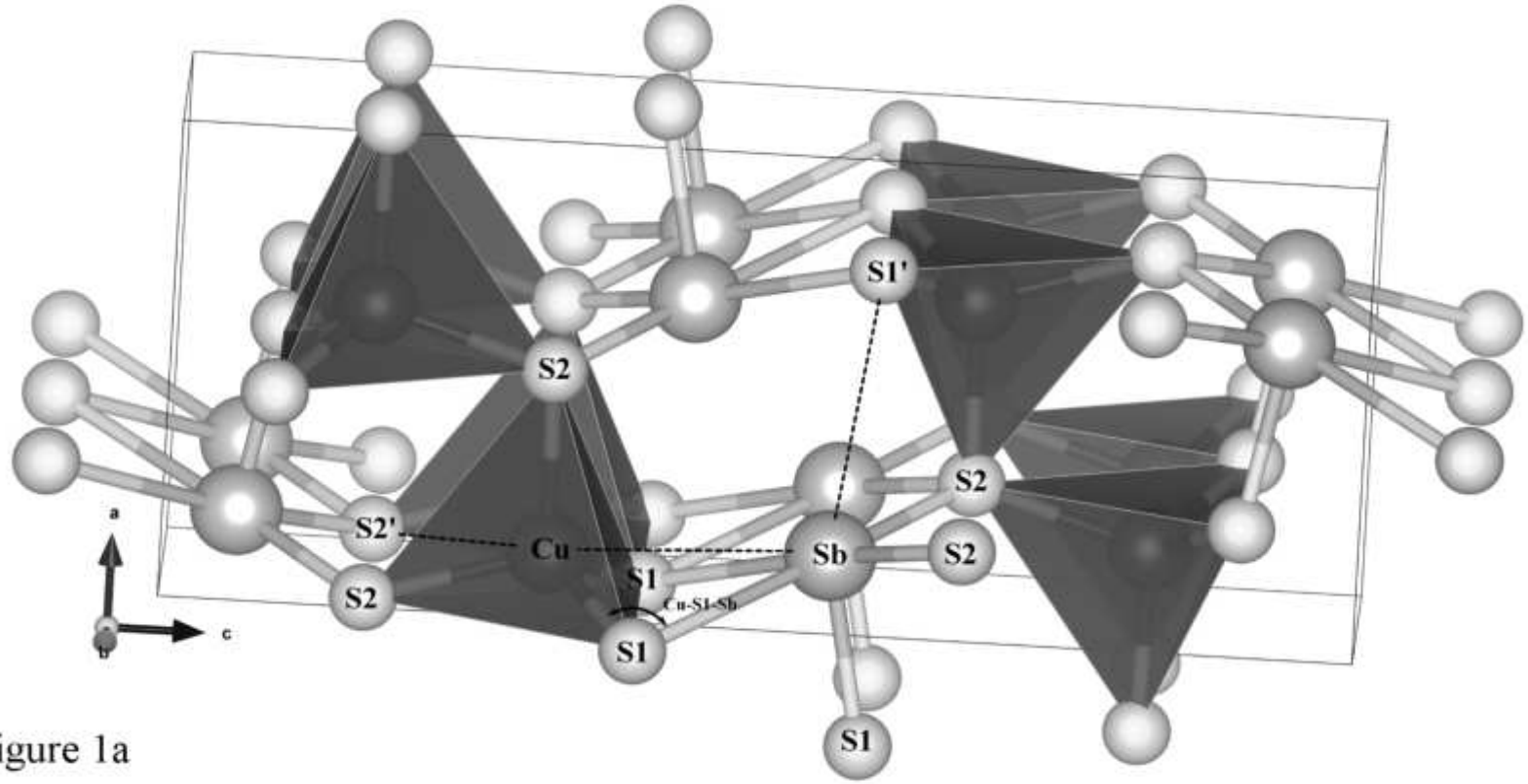

Figure 1a

α - β transition

Moving toward the coordination of Sb from 5+2 to 6+1

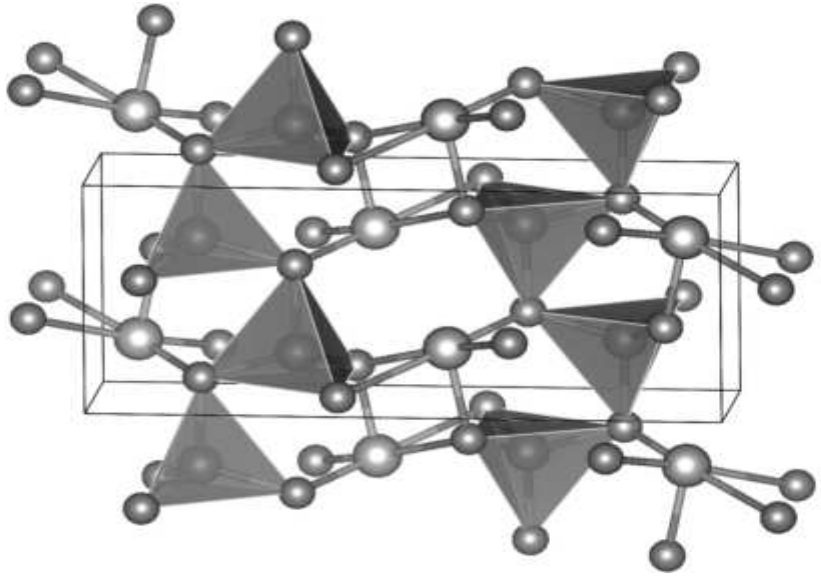

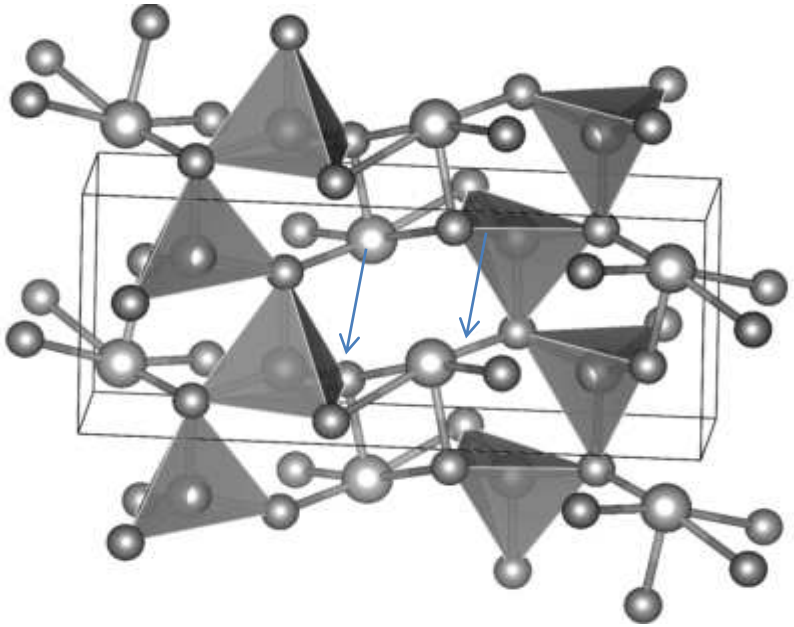

α - β transition

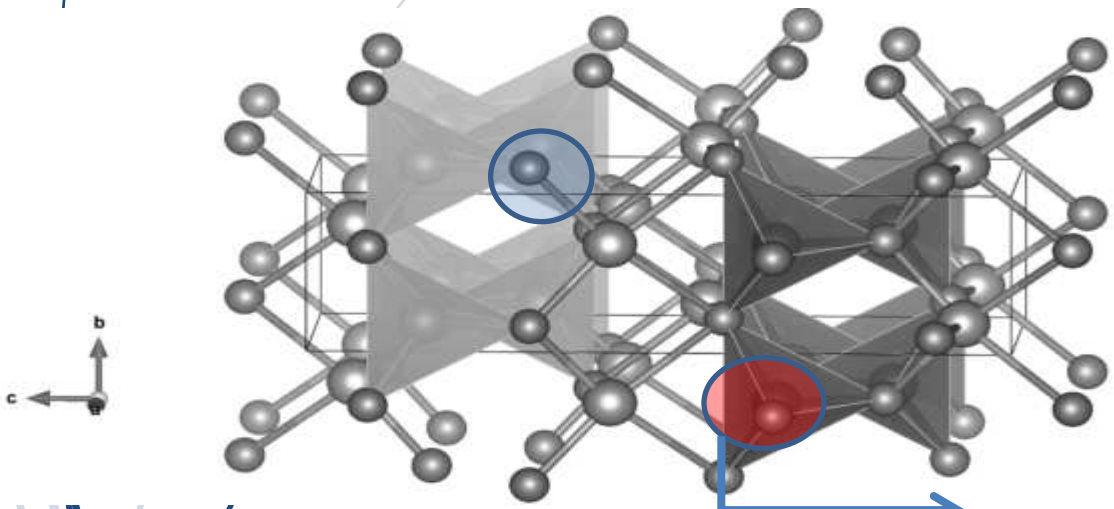

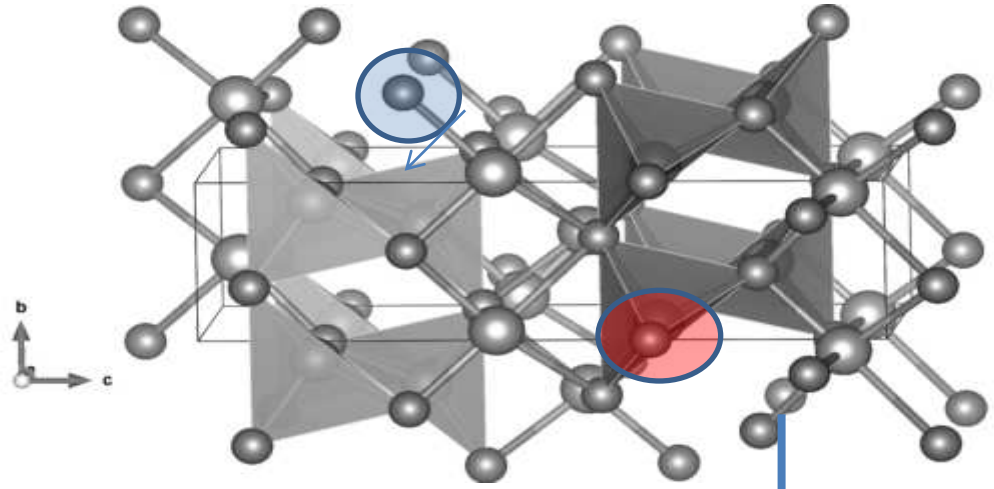

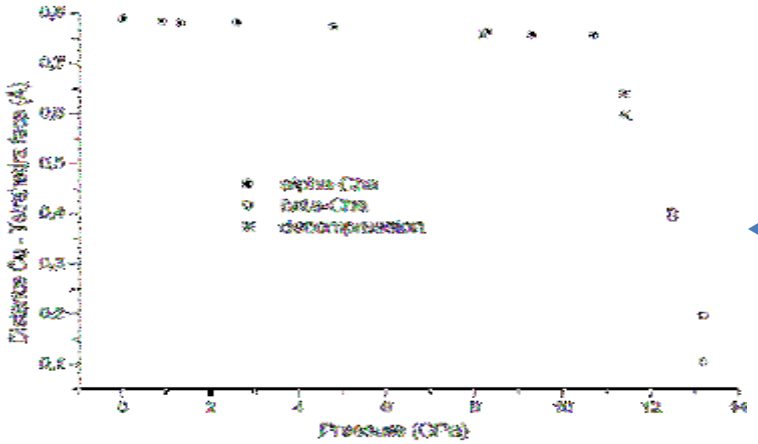

β-Chalcostibite

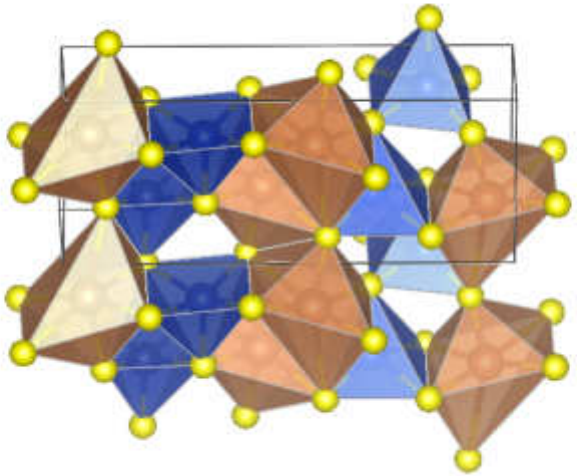

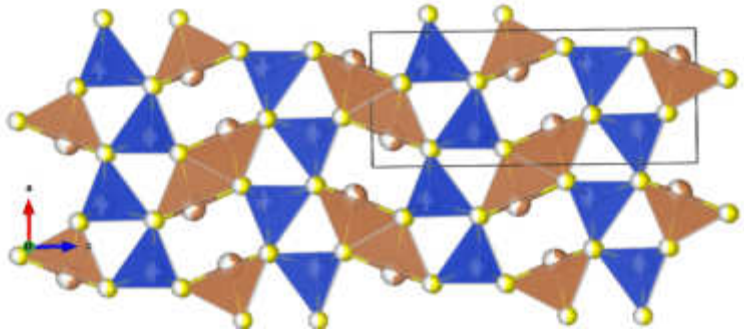

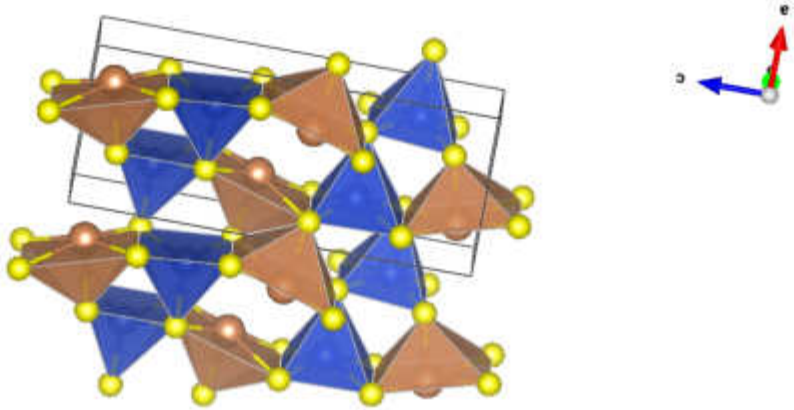

FT-NIR @ HP @LENS

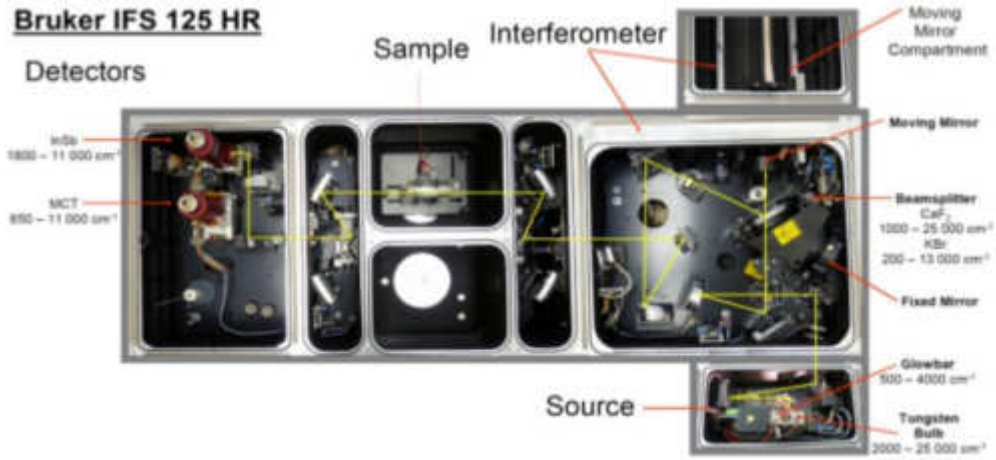

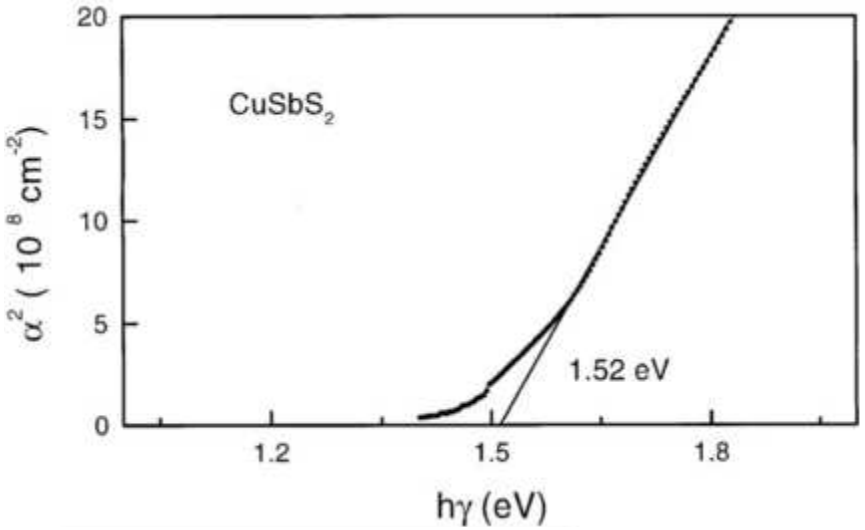

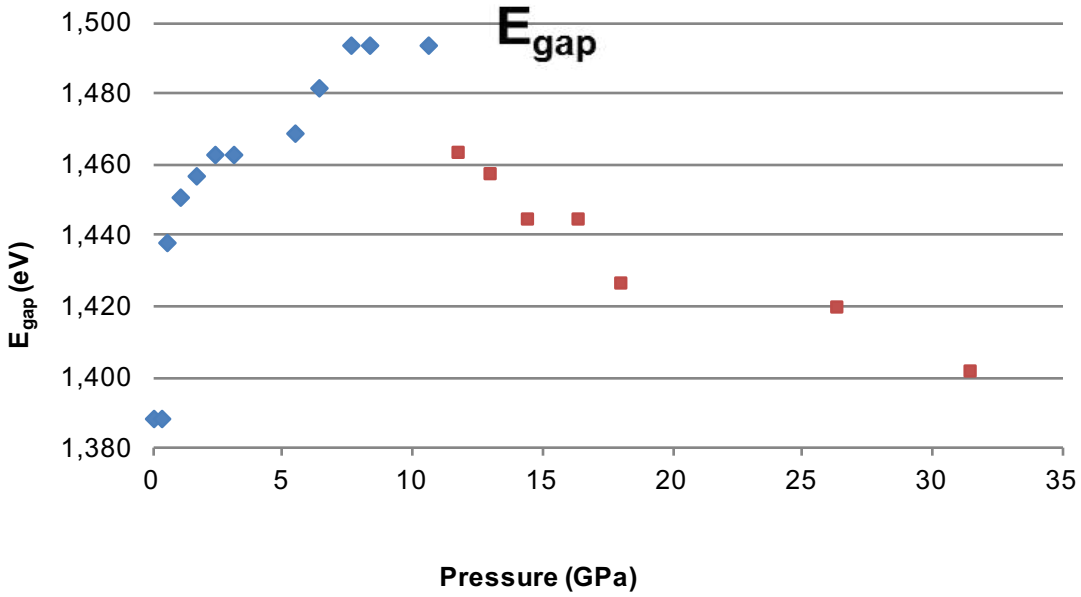

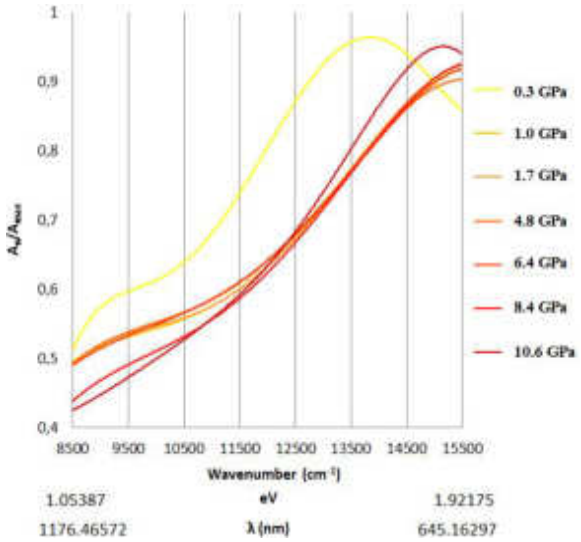

Conclusion

Cu change coordination from 4 to 5 (unknown Cu coordination!!!)

Square coordination and square pyramid coordination (found in the nickel sulfide millerite) has the same geometry as conventional octahedral coordination with one or two atoms removed.

Tetragonal pyramidal coordination with Cu^{++} for example in Azurite ($Cu_3(CO_3)_2(OH)_2$)

Sb change coordination from 5 plus 2 to 6 plus 1

LEP stereo chemistry – activity reduced with P, allowing a better structural packing…really

Density increase of about 2.2 %

Reversible transition

High pressure and planetology

Remote-sensing infrared spectroscopy is the principal field of investigation for planetary surfaces composition. Past, present and future missions to the solar system bodies include in their payload, instruments measuring the emerging radiation in the infrared range. Apart from measuring the reflected radiance, more and more spacecrafts are equipped with instruments measuring directly the emitted radiation from the planetary surface. The emitted radiation is not only a function of the composition of the material but also of its texture and especially the grain size distribution.

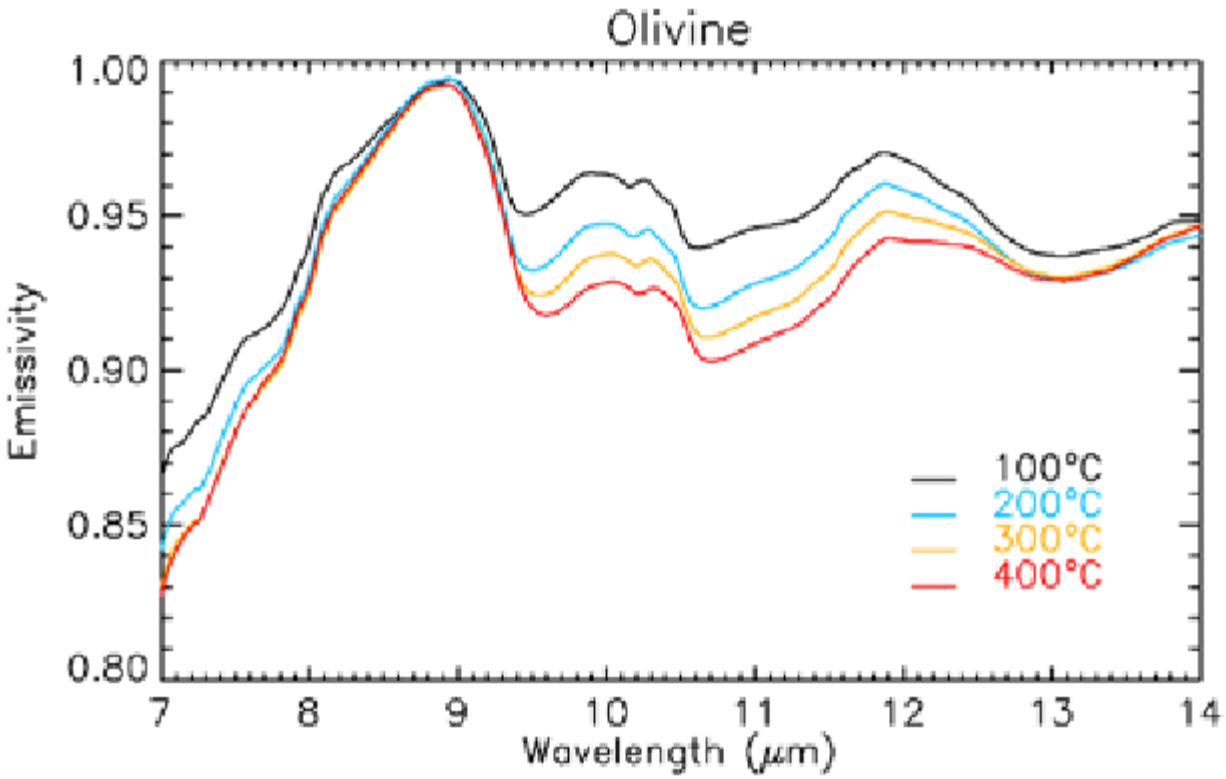

https://www.researchgate.net/project/Surface-Mineralogy-of-Planet-Mercury/figures

Ganymede	3,274
Callisto	2,986
Io	2,256
Europa	1,945

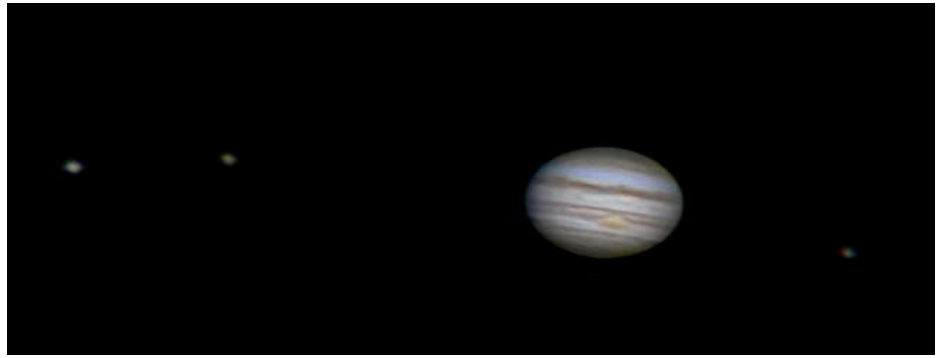

The Galilean Satellites

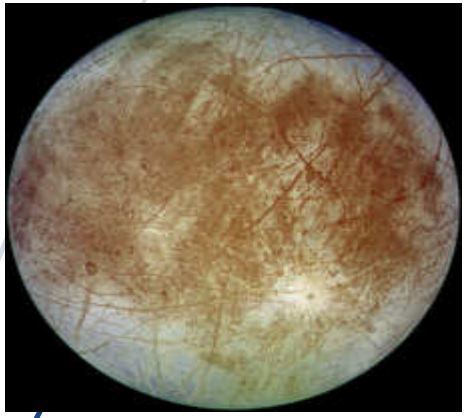

http://faculty.virginia.edu/skrutskie/ASTR1210/notes/galsat.html

Europa probably has a layered crust composed of anhydrous Mg-Na sulfates near the base and a frozen or partially molten eutectic mixture of ice and hydrated Mg and Na sulfates near the surface.

Ganymede may have a crust about 300 km thick composed of a l0:1 ratio of ice:mirabilite, and a mantle 500 km thick composed of 50% ice phases plus 50% hydrated Mg and Na sulfates.

https://skeptoid.com/blog/2013/06/07/jupiters-galilean-satellites-europa/

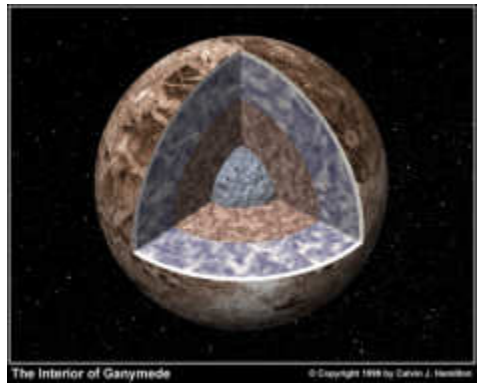

Do Ganymede and/or Europa have water?

The possible internal structures of Ganymede and Callisto are shown in Fig. 7. The interior of Ganymede has been modeled from gravity data, and appears to be differentiated into an outermost ~800-km-thick ice layer and an underlying silicate mantle. A central iron core might also be present, which would explain the existence of a magnetic field. Ganymede has internal mass anomalies, perhaps related to topography on the ice-rock interface [24], [25]. Results from the magnetometer onboard the Galileo probe may indicate the presence of an internal ocean within 100–200 km of Ganymede's surface, but inference is less robust than at Europa and Callisto [26]. The Ganymede surface is more cratered and ancient than Europa's, consistent with a much thicker outer shell of solid ice. The role of icy volcanism in modifying the surfaces of outer planet moons is an outstanding question about which little is truly understood. Like many other icy moons, there is ambiguous evidence for cryovolcanic processes modifying the surface of Ganymede.

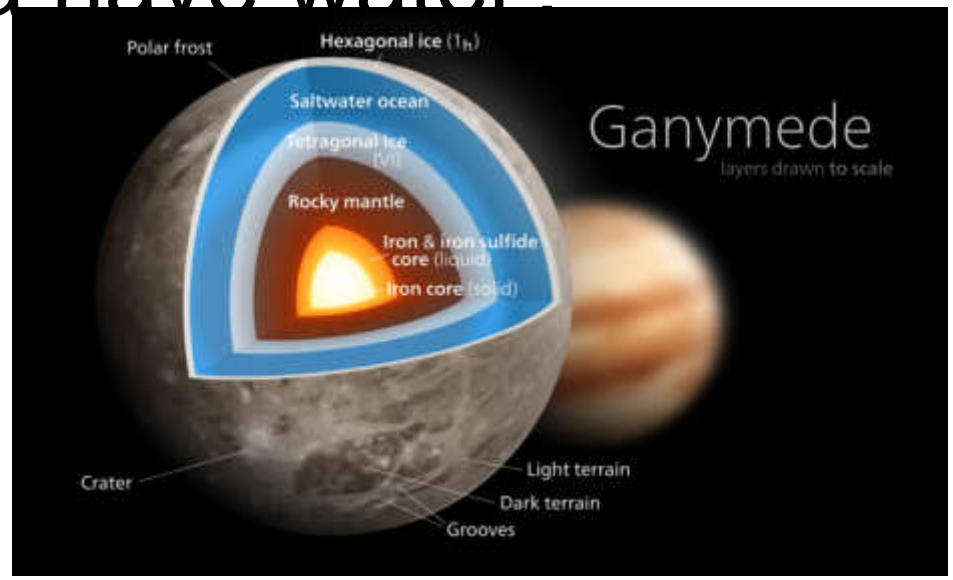

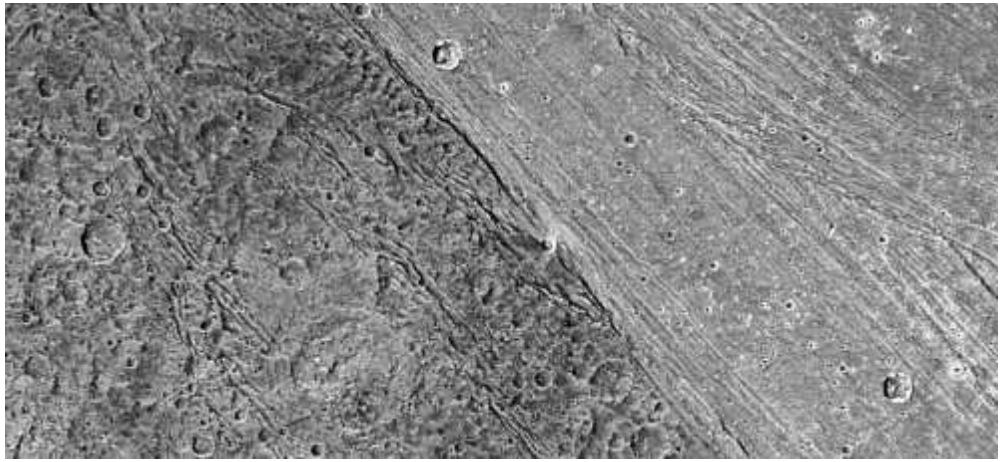

https://en.wikipedia.org/wiki/Ganymede_(moon)

Which are the P-T stability conditions of the $MgSO_4$-Na_2SO_4-H_2O phases ?

At which condition hydrated minerals become anydrous minerals?

At which T and P we have free water?

How do evolve the density of the phases with P-T?

Bloedite

$(Na_2Mg(SO_4)_2 \cdot 4H_2O)$

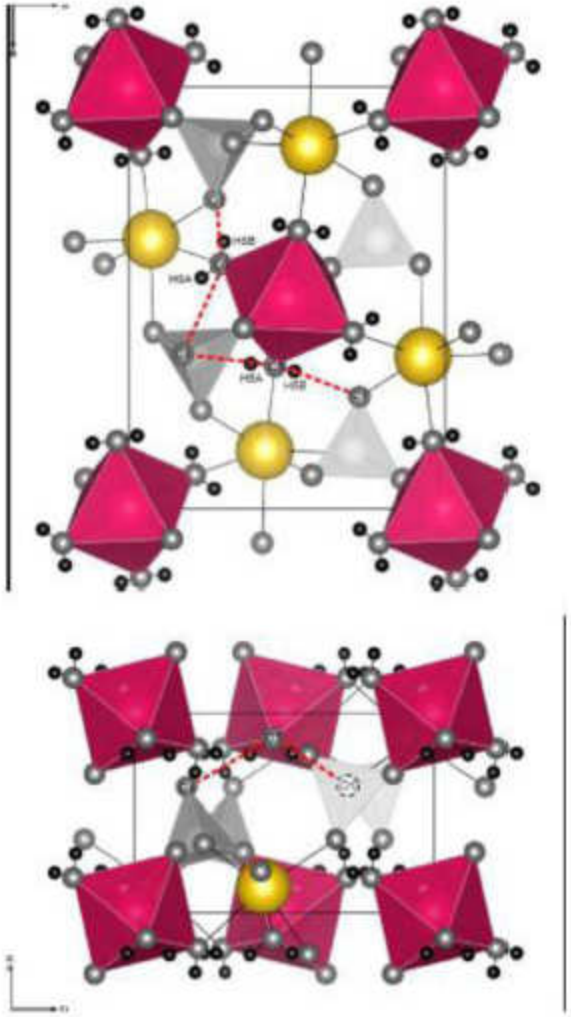

Fig. 1. Shown is the crystal structure of blödite projected along a) (001) and b) (100) axes, respectively. Mg coordination polyhedra are represented by pink octahedra, S coordination polyhedra are represented by gray tetrahedra. Yellow, bright gray and dark gray spheres represent Na, O and H atoms, respectively. Dashed red lines indicate the hydrogen bonds.

ID-09 @ ESRF

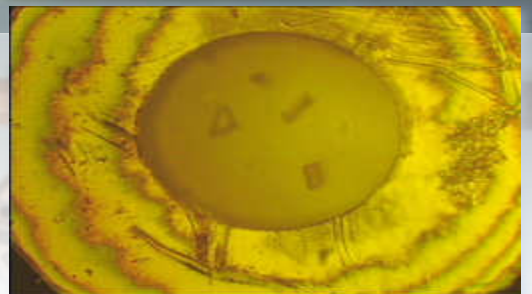

https://www.gettyimages.it/detail/foto/the-storage-ring-building-of-esrf-at-dusk-fotografie-stock/57199980

Beamline ID09A is dedicated to the determination of structural properties of solids at HP using angle-dispersive-diffraction with DACs.

Energy 30 keV flux of 10^{11} photons/s at 200 mA.
Sample dimensions up to **10x10 μm^2** for megabar experiments

The scattered radiation is collected by an **image-plate detector**, an on-line **Mar555 reader,** which has a 430 x 350 mm (555mm diagonal) active area.

A laser spectrometer is available for pressure determination by the ruby fluorescence method. It is also possible to perform **Raman scattering** experiments simultaneously.

The beamline is equipped with several membrane-type diamond anvil cells (0-40 GPa), a Liquid He cooled cryostat to perform HP

experiments at low temperatures (**down to 50 K**), and external resistive heating equipment for high temperatures up **to 600 K**.

A Nd-YAG laser system is available externally for high temperature annealing of samples inside the diamond anvil cell.

Lattice parameters vs P

P(GPa)	a	b	c	beta	V
0.0001 *	5.5406	8.248	11.141	100.92	
0	5.539	8.242	11.126	100.84	498.87
0.166	5.518	8.23	11.09	100.7	494.9
0.58	5.4901	8.189	11.051	100.59	488.4
1.3	5.461	8.14	11.002	100.57	480.8
2.1	5.428	8.091	10.947	100.49	472.7
3.4	5.372	7.996	10.843	100.45	458
5.1	5.315	7.917	10.784	100.45	446.2
6	5.283	7.891	10.734	100.29	440.3
8.2	5.207	7.812	10.657	100.44	426.3

* Collected @ PG

Equation of state

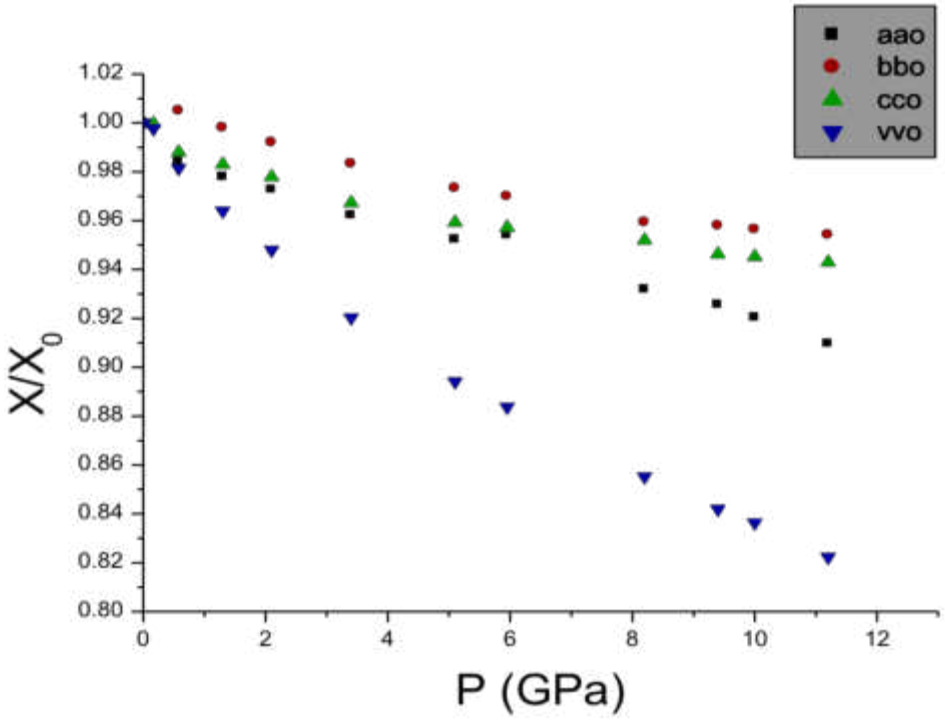

EoS BM2

K_0 = 39.7(7)
V_0 = 496.1 (9)

EoS BM3

K_0 = 34.1 (10)
K' = 5.5 (4)
V_0 = 497.9(8)

EoS Vinet3

K_0 = 33.9 (14)
K' = 5.7 (4)
V_0 = 497.9 (8)

β_a = 0.0073(4) (GPa^{-1})
β_b = 0.0046(3) (GPa^{-1})
β_c = 0.0049(4) (GPa^{-1})

bloedite structure resulted most incompressible along [010], the direction perpendicular to open sheet.

Icarus 285 (2017) 137–144

Contents lists available at ScienceDirect

Icarus

journal homepage: www.elsevier.com/locate/icarus

The compression behavior of blödite at low and high temperature up to ~10 GPa: Implications for the stability of hydrous sulfates on icy planetary bodies

Paola Comodi[a,*], Vincenzo Stagno[b], Azzurra Zucchini[a], Yingwei Fei[c], Vitali Prakapenka[d]

[a] Department of Physics and Geology, University of Perugia, Italy
[b] Department of Earth Sciences, Sapienza University of Rome, p. le A. Moro, 5, 00185 Roma, Italy
[c] Geophysical Laboratory, Carnegie Institution of Washington, Washington, DC 20015, USA
[d] Argonne National Laboratory, University of Chicago, US

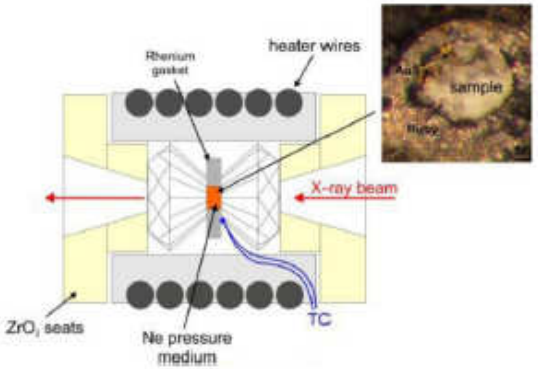

Fig. 2. a) Cross-section of the used diamond anvil cell with resistive heating (Antonangeli et al., 2012); b) the inset shows the recovered sample chamber with gold and ruby used as pressure markers (see main text).

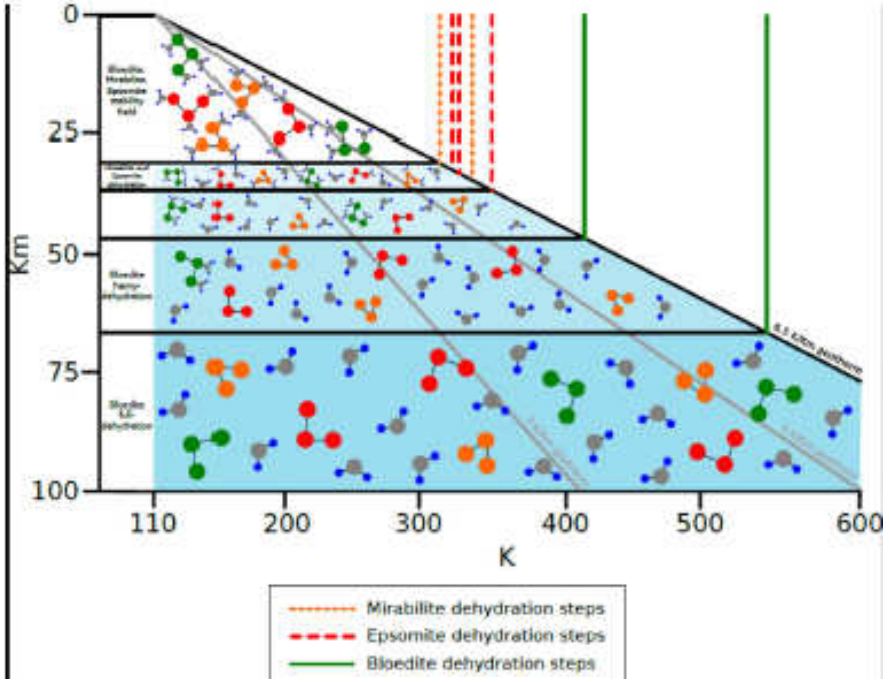

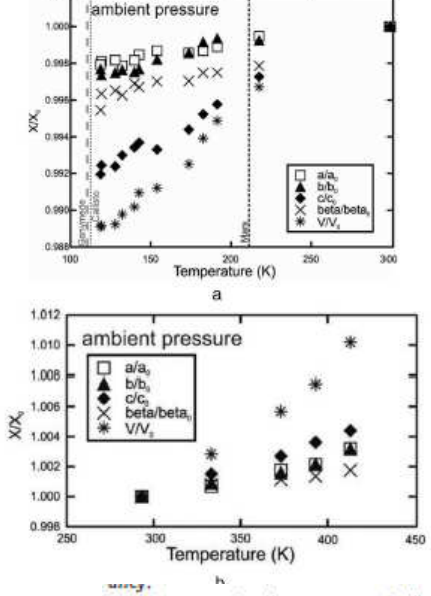

Fig. 5. Reciprocal l
> 250 K. Dashed lin
listo, and Mars.

Moreover, the data presented allowed to determine the depth of the dehydration of Na and Mg salts as well as that of mixed Na-Mg salts in planetary bodies when the thermal model is known. Fig. 8 shows a cartoon reporting a scenario of the different depths for the dehydration of simple and mixed Na-Mg salts in Ganymede, where an average surface temperature of 110 K, and a constant thermal gradient of 6.5 K/km are estimated (Montesi and Collins, 2005). Whereas the dehydrations of mirabilite and epsomite occur in a narrow temperature range, between 310 and 347 K (determined with thermogravimetric analyses by Prieto et al., 2000) namely at around 30 Km, our data for blödite indicate that the dehydration condition starts at 413 K (with a limited effect of pressure) forming a hemydrated phase, and it is complete at 570 K (Balic-Zunic et al., 2015) between 50 and 70 km of depth.

Because the dehydration temperatures of blödite are higher with respect those of mirabilite and epsomite, the liquids beyond 65 Km as showed in Fig. 8 should increase in volume due to blödite dehydration from the brines. As consequence, perched oceans, increasing in salinity with depth, can exist as some planetological models hypothesized (Vance and Brown, 2013).

Moreover, the fluid phase formed at different depths may determine dramatic rheological changes, and a contrast in material properties with different viscosity which affects the complex structure observed on Galilean satellites surface. For example, features on Europa and Ganymede related to cryovolcanic activity (Prockter et al., 1998), as eruption of aqueous solution or partly crystallized slurry derived from partial melting of ice-bearing materials, may be associated to different dehydration conditions of the deeply stored hydrous sulphate phases. This and other possible implications deriving from high pressure investigations require more focused systematic studies on the stability of hydrous sulfates at relevant conditions for the interior of icy planets.

Conclusion

To know elastic properties of materials,

You need collect data *in situ*

Poor but not bad quality of data

Several times you have to collect data with different tecniques

Eos and phase transitions are important tools to know in deep the material behavior

Sometime they reprent unique data for earth and material sciences

Thank you for your attention